Generation and Characterization of a *Dmd*^{EGFP} Reporter Mouse as a Tool to Investigate Dystrophin Expression

Inaugural-Dissertation
to obtain the academic degree
Doctor rerum naturalium (Dr. rer. nat.)

Submitted to the
Department of Biology, Chemistry and Pharmacy
of the Freie Universität Berlin
and
in cotutelle to the
Ecole Doctorale 515 "Complexité du vivant"
of Université Pierre et Marie Curie Paris

by

Mina Petkova

from Sofia, Bulgaria

2015

The research presented in this thesis was conducted from October 2011 until December 2015 in the followng laboratories:

Department of neuropediatrics and NeuroCure, Charité Cross Over, Charité Universitätmedizin, Berlin, Germany.

Biothérapies des maladies neuromusculaires, UFR des sciences de la santé Simone Veil, Université de Versailles Saint-Quentin-en-Yvelines, France.

THESIS COMMITTEE:

Thesis supervisor and reviewer Freie Universität Berlin: Prof. Dr. Markus Schuelke

Thesis supervisor Université Pierre et Marie Curie Paris: Prof. Dr. Helge Amthor

Representative Université Pierre et Marie Curie Paris: Dr. Gillian Butler-Browne

Reviewer Freie Universität Berlin: Prof. Dr. Sigmar Stricker

External reviewer: Prof. Dr. Volker Straub

External reviewer: Prof. Dr. Ketan Patel

Postdoctoral fellow Freie Universität Berlin: Dr. Annemarie Hofmann

Date of defense: 05.02.2016

STATUTORY DECLARATION

I hereby declare that I wrote the presented dissertation *"Generation and characterization of a Dmd^{EGFP} reporter mouse as a tool to investigate dystrophin expression"* independently and used no other aids than those cited. In the written paragraphs, I have clearly identified the source of the passages that are quoted or paraphrased from other works. I also hereby declare that I have conducted my scientific work according to the principles of good scientific practice in accordance with the current "Richtlinien der Freien Universität Berlin" (Guidelines of the Free University of Berlin) and "Charte du doctorat à l'UPMC" (Charter of PhD students at UPMC). I, Mina Petkova, received assistance in the writing of this thesis with respect to grammar and syntax, which was provided by Markus Schuelke and Helge Amthor.

Berlin, 6.01.2016

_____

(Signature)

The most beautiful thing we can experience is the mysterious.

It is the source of all true art and science.

(Albert Einstein)

TABLE OF CONTENTS

1. SUMMARY

Dystrophin is a rod-shaped cytoplasmic protein that physically links the cytoskeleton to the ECM through the dystrophin-associated protein complex (DAPC), thereby providing sarcolemmal stability. Mutations in the dystrophin encoding *DMD* gene cause the severe X-linked disorder Duchenne muscular dystrophy (DMD). DMD is characterized by progressive muscle wasting and fibrosis, impairing notably skeletal and heart muscle function as well as to various degrees cognitive, visual and gastrointestinal function due to missing dystrophin in the respective tissues. In this work a novel *Dmd^EGFP* reporter mouse that expresses a fluorescently labelled endogenous dystrophin – EGFP fusion protein was generated and characterized. The protein was tagged at the C-terminus that is present in the most dystrophin isoforms. To date, no dystrophin reporter mice exist, thus imaging is only possible by indirect antibody-mediated processing *ex vivo*. For the generation of transgenic mice a targeting vector containing a FLAG-EGFP coding sequence inserted in-frame after the last modified exon 79 of the murine *Dmd* gene was constructed. Following the EGFP sequence a lox*P* flanked *neomycin* cassette was inserted into the 3'UTR. The vector was used for modification of the X-chromosomal *Dmd* locus in embryonic stem cells and germline transmission of the modified allele. After removal of the *neomycin* selection cassette in the F1 generation *Dmd^EGFP* mice and their wildtype littermates were characterized.

Strong natural EGFP expression was observed in skeletal and smooth muscles, heart, brain and the eye and EGFP fluorescence co-localized with dystrophin at all sites suggesting proper tagging of the major dystrophin isoforms. In skeletal muscle, dystrophin as well as other proteins of the DAPC were expressed in normal quantity at correct sarcolemmal/subsarcolemmal localization. Skeletal muscle maintained normal tissue architecture, suggesting a correct function of the dystrophin-EGFP fusion protein. Isolated myofibers as well as satellite-cell derived myotubes expressed EGFP *in vitro*. Thus, the novel dystrophin reporter mouse provides a valuable tool for direct visualization of dystrophin expression.

Furthermore, the model can be used to investigate dystrophin re-expression *in vivo* or *ex vivo* after various gene therapy protocols that are aimed at the reestablishment of the dystrophin open reading frame or in naturally occurring revertant fibers.

2. ZUSAMMENFASSUNG

Dystrophin ist ein zytoplasmatisches Protein, welches wesentlich für den Aufbau des Dystrophin-assoziierten Proteinkomplexes (DAPC) ist. Der Komplex vernetzt das Zytoskeleton mit der extrazellulären Matrix, wodurch das Dystrophin entscheidend zur Stabilisierung des Sarkolemmas und zur Erhaltung der Muskelfaserintegrität während der Muskelkontraktion beiträgt. Mutationen im Dystrophin kodierenden *DMD* Gen, verursachen die schwere X-chromosomal vererbte Muskeldystrophie Duchenne (DMD). DMD ist gekennzeichnet durch eine fortschreitende Muskeldegeneration und Fibrose, welche die Skelettmuskel- und Herzmuskelfunktion beeinträchtigt. Darüber hinaus sind zu einem gewissen Grad auch kognitive, visuelle und gastrointestinale Funktionen gestört. Ursache für die Krankheit ist das Fehlen des Dystrophin-Proteins in dem jeweiligen Gewebe. In der vorliegenden Arbeit habe ich ein neues Mausmodel, die *Dmd^{EGFP}* Reportermaus, generiert und charakterisiert. Das Model ist gekennzeichnet durch die Expression eines Fluoreszenz-markierten Dystrophin-EGFP Fusionsproteins. Bislang existiert keine Reportermaus für Dystrophin, so dass die Visualisierung der Dystrophin-Expression bisher nur mittels indirekter Antikörperfärbung *ex vivo* möglich war. Für die Herstellung der transgenen Maus habe ich einen Targeting-Vektor entwickelt, welcher die FLAG-EGFP Gensequenz downstream des letzten Exons (Exon 79) des *Dmd* Gens der Maus einfügt. Weiter 3' downstream habe ich noch eine lox*P* flankierte Neomycin Selektionskassette eingebracht, welche später nach homologer Rekombination und Blastozysteninjektion durch Verpaarung der F1-Generation mit einer ubiquitär exprimierenden Cre-Maus wieder entfernt werden konnte. Zum Nachweis der Dystrophin Expression und zum Ausschluss einer möglichen Induktion einer Dystrophinopathie durch das EGFP-markierte Fusionsprotein habe ich die *Dmd^{EGFP}* Mäuse und ihre wildtyp Wurfgeschwister histologisch charakterisiert. Dabei konnte ich eine starke natürliche EGFP Fluoreszenz sowohl in den Skelett- Herz-, und glatten Muskeln, als auch im Gehirn und Auge beobachten. Das EGFP-Signal kolokalisierte mit dem immunhistologisch nachgewiesenen Expressionsmuster des Dystrophins, was die korrekte Markierung der Mehrheit der Dystrophin Isoformen bestätigt. Im Skelettmuskel wurden Dystrophin sowie andere Proteine des DAPCs in normaler Menge am Sarkolemma exprimiert. Der Muskel bewahrte seine normale Gewebestruktur, was die korrekte Funktion des Dystrophin-EGFP Fusionsproteins impliziert. Sowohl isolierte Muskelfasern als auch aus Satellitenzellen generierte Myotuben exprimierten das EGFP-

Fusionsprotein *in vitro*. Somit ist die neue Reportermaus ein nützliches und wertvolles Model für die direkte Visualizierung der Dystrophin Expession.

Darüber hinaus kann man das Model benutzen, um *in* oder *ex vivo* die Dystrophin-Reexpression nach Gentherapie oder in natürlich vorkommenden „*revertant fibers*" zu studieren.

3. RÉSUMÉ

La dystrophine est une protéine cytoplasmique qui lie physiquement le cytosquelette à la matrice extracellulaire par le biais du complexe dystrophine-protéines associées (DAPC), assurant ainsi la stabilité du sarcolemme. Des mutations dans le gène *DMD* codant pour la dystrophine, conduisant à l'absence de la protéine, sont à l'origine de la dystrophie musculaire de Duchenne (DMD) qui est une maladie liée au chromosome X. La DMD est caractérisée par une atrophie et fibrose musculaire progressive, affectant les fonctions musculaires squelettiques et cardiaques. Les fonctions cognitives, visuelles et gastro-intestinales peuvent aussi être atteintes à différents niveaux. Pour mes travaux de thèse, j'ai généré et caractérisé un nouveau modèle de souris transgéniques rapportrices, dénommé *Dmd^EGFP*, qui exprime une protéine dystrophine endogène fusionnée avec la protéine fluorescente EGFP. La protéine dystrophine est liée dans sa région C-terminale qui est présente dans la majorité des isoformes.

A ce jour, il n'existe aucune souris rapportrice pour la dystrophine et le marquage de la dystrophine doit se faire de manière indirecte par le biais d'anticorps. Pour la construction du vecteur de ciblage génique, la séquence codante pour FLAG-EGFP a été insérée après le dernier exon 79 du gène *Dmd* murin en respectant son cadre de lecture et dans lequel le codon de terminaison était enlevé. En aval de la séquence EGFP, une cassette ayant une séquence codante d'un gène de résistance à la *néomycine,* lui-même flanqué de sites lox*P*, était insérée afin de sélectionner les cellules ES. La recombinaison homologue dans le locus *Dmd* du chromosome X était vérifiée par la technique du Southern blot et les cellules ES étaient injectées dans des blastocystes. Après la transmission germinale, des animaux *Dmd^EGFP* de la génération F1 étaient croisés avec des souris exprimant la Cre recombinase dans le but d'enlever la cassette *néomycine*. Le génotypage des souris était effectué par PCR.

Une expression forte et naturelle de l'EGFP était observée dans les muscles squelettiques, lisses, le cœur, le cerveau et l'œil, ce qui suggère un étiquetage correct de tous les isoformes de la dystrophine. La fluorescence de l'EGFP co-localisait exactement avec la dystrophine dans tous les sites. Dans le muscle squelettique, la dystrophine ainsi que d'autres protéines de la DAPC étaient exprimées dans des quantités normales et dans la bonne localisation subsarcolemmale. De plus, l'architecture du tissu musculaire squelettique était normale, suggérant que la fonction de la protéine de fusion dystrophine-EGFP était maintenue. Par

ailleurs, in vitro, l'EGFP est également exprimée dans les fibres musculaires isolées, ainsi que dans les myotubes dérivés des cellules satellites. Par conséquent, cette nouvelle souris rapportrice de la dystrophine devient un outil important pour la visualisation directe et *in vivo* de l'expression de la dystrophine.

De plus, le modèle peut être utilisé pour étudier la dystrophine ré-expression *in vivo* ou *ex vivo* après différents protocoles de thérapie génique qui visent à le rétablissement du cadre de lecture ouvert de la dystrophine ou en fibres révertantes d'origine naturelle.

4. INTRODUCTION

Dystrophin is large rod-like cytoskeletal protein that is primarily found at the inner surface of muscle fibers. It is expressed in all types of muscles as well as in the nervous system. Dystrophin was identified as the protein which is absent in patients suffering from Duchenne muscular dystrophy (DMD), a severe neuromuscular disorder. Most of our knowledge on the function of dystrophin is derived from studies on DMD patients as well from animal models of the disease. No cure for DMD has been found yet. Prevously unknown functions of dystrophin have been discovered recently leading the research on DMD into new directions. Hence there are still many questions to be answered in order to better understand the role of dystrophin in the normal and in the context of disease.

4.1. Pathology of Duchenne muscular dystrophy

Duchenne muscular dystrophy (DMD; OMIM#310200) is the most common form of muscular dystrophies in childhood, a group of diseases characterized by progressive muscle degeneration, loss of the ability to walk, the impairment of repiratory and cardiac function and early death. Due to its transmission in families it was known that the disease is hereditary and X-linked, but the precise mechanism remained a mystery until 1986, when the causative genetic defect in DMD was discovered (Koenig *et al.*, 1987; A. P. Monaco *et al.*, 1986) and its protein product, named dystrophin from then on, was identified (Hoffman *et al.*, 1987). It is either absent in or nearly absent DMD patients or truncated and reduced in the milder disease form, called Becker muscular dystrophy (BMD) (Worton, 1995).

Duchenne muscular dystrophy was first described by Guillaume-Benjamin-Amand Duchenne (de Boulogne) (Duchenne, 1868) and William Richard Gowers (Gowers, 1878). It is the most common and severe form of an X-linked, recessive neuromuscular disorder, affecting 1 in 3,500 boys (Emery, 1998). Initial symptoms in DMD start in early childhood and include difficulties in running, in climbing stairs and a waddling gait. A characteristic sign of proximal muscle weakness is the so-called Gowers' phenomenon by which the child climbs up his thighs when trying to rise from the floor (Gowers, 1878). Typical features of the disease are the hypertrophy of the calf muscles, a progressive weakness and wasting of the proximal skeletal muscles (Figure 1). Ambulation is lost in most DMD patients by the age of 12 years and only a few patients survive until the third decade of life. Respiratory and/or cardiac failure are the

main causes of death in DMD patients. Other organs being affected besides the skeletal muscles and myocardium are the smooth muscles as well as the central nervous system (CNS) (Barohn *et al.*, 1988; Bresolin *et al.*, 1994; Nigro *et al.*, 1990; Zellweger and Niedermeyer, 1965).

Further features of the disease include a high elevation of serum creatine phosphokinase, myopathic pattern during electromyography, and histological changes including myofiber degeneration, regeneration with fibrosis and fatty infiltrations as well as necrosis accompanied by immune cell infiltrations (Emery and Muntoni, 2003; McDouall *et al.*, 1990).
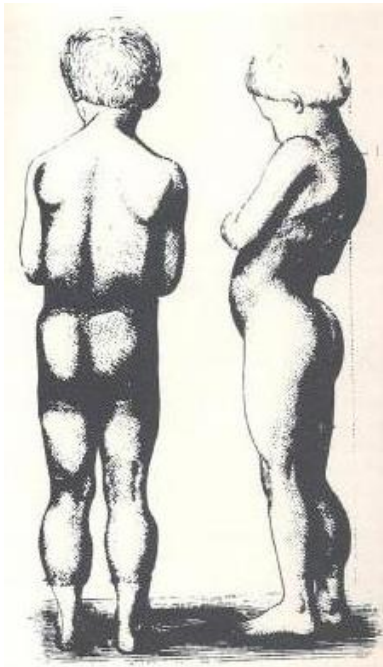
Figure 1: Duchenne's original case showing marked calf enlargement and lumbar lordosis. From (Emery and Muntoni, 2003, p14).

Milder forms of DMD exist and the most common one is the Becker-type muscular dystrophy (BMD, OMIM#300376) (Becker and Kiener, 1955). The clinical presentation of BMD patients is much more diverse then in DMD, and walking ability might be lost in the late teens, but in some patients symptoms may occur very late, so that they experience no significant physical impairment. The distribution of muscle wasting and weakness are very similar to DMD (Bushby and Gardner-Medwin, 1993).

The dystrophin protein, discovered more than 100 years after the first documented cases of DMD as well as its coding dystrophin gene *(DMD)*, which bears the causative mutations, have been subjects to extensive investigations and analysis in the past decades. In DMD patients

mutations disrupt the open reading frame and prevent the expression of dystrophin, whereas in BMD dystrophin is expressed, but in a shorter, internally truncated versions due to in-frame mutations (Koenig *et al.*, 1989), however there are exceptions to this reading frame rule.

The long period between the publication of first case reports and the discovery of the disease cause might be due to the fact that the skeletal muscle as the main affected tissue is complex with regard to its development, physiological function and regulation.

4.2. The *mdx* mouse: a naturally occurring animal model for DMD

Animal models are indispensable to study and understand the function of dystrophin in normal and disease states as well as for the development of therapies against DMD. Until present, more than 50 animal models have been described, both laboratory made and naturally occurring ones. Studies have been done using murine, canine and feline models but also small model organisms like the zebrafish *Danio rerio (D.rerio)* and the nematode *Caenorhabditis elegans (C.elegans)* (McGreevy *et al.*, 2015).

The most widely used and best characterized model for DMD is the *Dmd^{mdx}* mouse, which will be referred to from here on as *mdx*- mouse*,* <u>m</u>urine <u>d</u>ystrophy <u>X</u>-linked (Bulfield *et al.*, 1984). It has largely contributed to our general knowledge about muscle biology and dystrophin.

The *mdx* mouse carries a spontaneous nonsense point mutation in exon 23 (CAA→TAA) at nucleotide position 3185 of *Dmd* leading to a premature translation termination, (p.Gln1062*) and a subsequent absence of dystrophin expression (Sicinski *et al.*, 1989). The *mdx* mouse displays some hallmarks of DMD-such as muscle degeneration, cardiomyopathy and the elevation of activity of muscle specific enzymes in the serum. However, in contrast to human DMD, those symptoms manifest much later and in milder form if refered to the entire life span of a mouse (Quinlan *et al.*, 2004; Stedman *et al.*, 1991). The life span of the *mdx* mouse is reduced by only 25%, as compared to >50% for DMD patients (McGreevy *et al.*, 2015). The dystrophic changes begin to apprear in the animals between 3-6 weeks of life with a rapid muscle fiber degeneration followed by a regeneration phase, typically characterized by the presence of central nuclei in regenerating fibers and an inflammatory reaction. Unlike in humans, where the condition turns rapidly into muscle atrophy, mice maintain hypertroph troughout much of their life span. Only the diaphragm muscle of *mdx* mice displays the muscle wasting and degeneration observed in DMD boys. (Chamberlain *et al.*, 2007; Dupont-

8

Versteegden and McCarter, 1992; Pastoret and Sebille, 1995; Stedman *et al.*, 1991). The less severe murine phenotype has been partially attributed to an increased expression and probable compensation by utrophin, which is a shorter dystrophin homologue, and will be discussed in more detail in section 4.4.4 (Matsumura *et al.*, 1992; Rybakova *et al.*, 2006). Consequently, it has been shown that dystrophin/utrophin double mutant mice have a much more severe phenotype than *mdx* mice (Deconinck *et al.*, 1997). Another explanation for the difference between human and mouse might be a different muscle load and mechanical stress that both organisms are exposed to. If examined under conditions of exhaustion or of physical work, which enhances the *in vivo* and *ex vivo* mechanical load, the clinical course of the *mdx* mouse was shown to be aggravated (Danialou *et al.*, 2001; Nakamura *et al.*, 2001). Furthermore, the body size between man and mouse differ considerably, as do the processes by which such difference is achieved and maintained throughout life (Partridge, 2013).

To characterize and understand DMD as a disease process, the function of the dystrophin protein in the muscles and in other tissues has to be understood. In the next sections I thus describe the organization of the muscle and the function which dystrophin has therein. Moreover, I discuss the current knowledge about the role of dystrophin in non-muscle tissue.

4.3. The structure and function of the muscle

The muscle is a specialized organ with various functions and locations throughout the body and is characterized by its ability to contract. Based on its histological appearance, we distinguish between smooth and striated muscle, the latter being further subdivided into skeletal and cardiac muscle.

4.3.1. Skeletal muscle

The skeletal muscle is a voluntary controlled muscle and the largest organ of the human body. In humans, a total of ≈640 skeletal muscles account for ≈38% of total body mass in males and ≈30% in females (Janssen *et al.*, 2000). It is characterized mainly by its mechanical activity required for posture, movement and breathing, which depends on the ability of muscle fibers to contract. The skeletal muscle is composed of parallel bundles of myofibers, which are organized in fascicles while a network of collagen fibers surrounds each fascicle (*perimysium*) and extends into the space between individual muscle fibers (*endomysium*). Each myofiber,

9

also called muscle cell, is a multinucleated syncytium generated by fusion of numerous dividing mononucleated myoblasts. After fusion and generation of the fiber, the myonuclei do not divide anymore and remain in the subsarcolemmal space of the sarcoplasm. The muscle stem cells, also called "satellite cells", are mononucleated cells located between the plasma membrane (*sarcolemma*) and the basement membrane (Mauro, 1961). Satellite cells have myogenic potential and the capability to self-renew. They are responsible for postnatal muscle growth, repair and regeneration (Emery and Muntoni, 2003).

A single myofiber is composed of many myofibrils containing the contractile proteins actin and myosin, which represent the thin and thick filaments respectively. The myofibrils are organized into sarcomeres, the functional contractile units of the skeletal muscle. The sarcomeres are demarkated by their Z-discs that provide a scaffold for the thin actin filaments and anchor the center of the actin filament bundles. Near the Z-discs thin actin filaments form the I-band. Additional proteins of the Z-discs provide a link to the *sarcolemma via* the dystrophin-associated protein complex, which plays a central role in the mechanical and contractile properties of the muscle. The region containing the thick myosin filaments is called the A-band and in its center, a dense zone called the M-band is located. Structures called T-tubules are transversely arranged and interconnected tubular extensions of the plasma membrane into the sarcoplasm (Figure 2) (Emery and Muntoni, 2003).

Contraction of the skeletal muscle is initiated through an action potential traveling down its supplying nerve (α-motoneuron) leading to a release of the neurotransmitter acetylcholine (ACh) from the presynaptic terminus of the neuromuscular junction (NMJ). In the synaptic cleft of the NMJ, ACh binds to the acetylcholine receptors (AChR) that are densely clustered in the postsynaptic membrane of the NMJ (Pratt *et al.*, 2015). This results in the depolarization of the skeletal muscle membrane and a downstream release of calcium from the sarcoplasmic reticulum into the cytosol. Calcium causes binding of myosin to actin, which subsequently leads to a contraction of the myofibers as an adenosine triphosphate (ATP) consuming process by which the bundles of myosin filaments slide onto the actin filaments (e.g. the "sliding filament" theory), (Huxley and Niedergerke, 1954). This entire process is called "Excitation-contraction coupling".

Myofibers differ in their ability to resist fatigue and produce muscle force. Their fiber type can be determined immunohistochemically *via* the subtype of its myosin heavy chain. Type I fibers

are fatigue resistant and provide little force (also named "slow-twitch", oxidative fibers), type IIa and IIx fibers produce higher force, are less resistant to fatigue and are also called "fast-twitch" and may be either oxidative or glycolytic (Schiaffino and Reggiani, 2011). Fast IIb fibers are identified in other mammals but not in humans (Gorza, 1990).
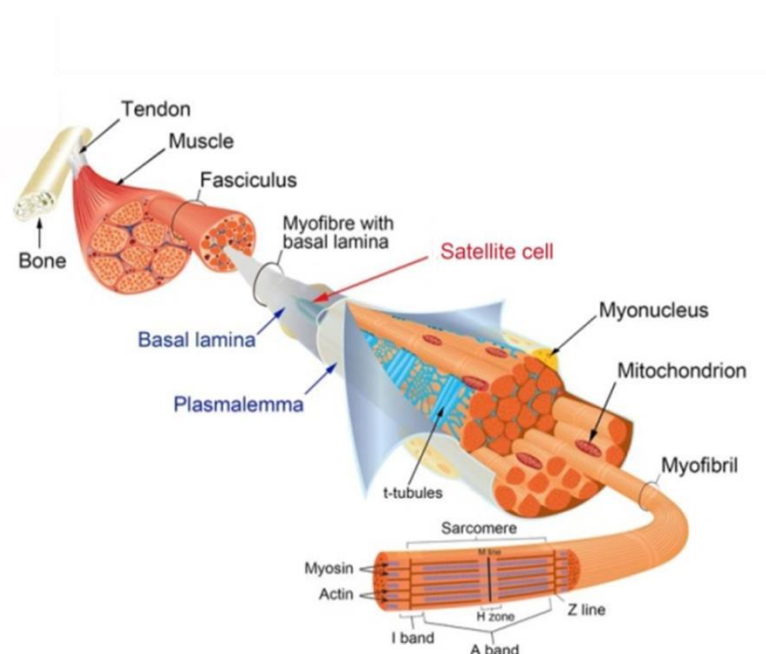
Figure 2: Structure of the skeletal muscle.
The skeletal muscle is attached to the bone *via* a tendon and composed of myofibers that are organized into *fasciculi*. Each myofiber, a multinucleated muscle cell, is surrounded by the plasmalemma and the basal lamina. Sandwiched between these two layers reside the skeletal muscle stem cells, also called the "satellite cells". The myofiber contains numerous myofibrils, actin and myosin filaments which are organized into the sarcomeres. The contractile units consist of actin and myosin filaments. The sarcomeres are divided into alternating I- and A-bands giving the fiber their "striated" appearance. Modified from (Relaix and Zammit, 2012)

4.3.2. Cardiac and smooth muscle

Cardiac muscle is also striated but an involuntary muscle. Similar as in the skeletal muscle, actin and myosin filaments are organized into sarcomeres, but the contractile tissue has a different structure and is regulated in different manner. The individual cardiomyocytes remain oligonucleated cells, which are connected through the intercalated disc, a highly specialized structure providing mechanical as well as electric coupling. Three different cell-cell junctions exist in the intercalated discs: (i) gap junctions, responsible for the electrical coupling, (ii) intermediate filament anchoring desmosomes, and (iii) adherent junctions which anchor actin (Perriard *et al.*, 2003).

Smooth muscles are involuntary as well and their contraction is mostly non-conscious. They are lining the walls of hollow organs like the gastrointestinal tract, uterus, urinary bladder,

and blood vessels. The structure of the smooth muscle differs largely from that of skeletal muscle; the muscle cells are thin, elongated and arranged in parallel, which accounts for their smooth appearance. Smooth muscle tissue is primarily under the control of the autonomic nervous system and single cells are connected with each other mechanically through adherens junctions and chemo-electrically through gap junctions.

4.3.3. Myogenesis

The process by which muscles are generated is called "myogenesis". Thereby, we distinguish three phases which are (i) embryonic and fetal development, (ii) postnatal muscle growth, and (iii) re-establishing homeostasis after regeneration. Different factors orchestrate the complex process of myogenesis. All three above mentioned processes are fueled by precursor cells with myogenic potential. Such myocyte-generating cells differ between different muscles, but also between the myogenic phases of the same muscle type.

Skeletal muscles have a remarkable capacity for regeneration after injury, a function attributed to the presence of dormant adult muscle stem cells, the satellite cells, which are also responsible for the postnatal muscle growth. The process of regeneration plays an important role in the pathophysiology of muscle dystrophy, which in itself can be considered a state of chronic injury.

4.3.4. The satellite cell and skeletal muscle regeneration

The satellite cells were first described in 1961 based on their location under the basal lamina of the myofiber (Katz, 1961; Mauro, 1961). During postnatal growth, the satellite cells proliferate and give rise to myoblasts that differentiate and fuse with each other to form the new myofibers (Bischoff, 1975; Konigsberg *et al.*, 1975; Lipton and Schultz, 1979). When the muscle matures, satellite cells become postmitotic and remain quiescent at their location on the muscle fibers. In the adult muscle, myoblasts are required for normal homeostasis as well as for hypertrophic growth or myofiber repair and regeneration. In those cases, satellite cells are activated, start to proliferate and differentiate thereby supplying the muscle with the necessary myoblasts. As satellite cells have also stem cell properties, they have the ability to self-renew and to replenish their own pool (Zammit *et al.*, 2006).

12

The differentiation of the early myoblast through the myogenic program into a mature muscle cell is characterized by a distinct gene expression program. The paired box transcription factor 7 (Pax7) is considered a satellite cell marker, and has been shown to be expressed in mice as well as in many other species including humans (Yablonka-Reuveni, 2011). Ablation of Pax7 leads to the inability of the muscle to regenerate thus demonstrating the essential role of satellite cells in this process.

Activation of satellite cells is controlled by proximal signals from the muscle niche and microvasculature and through an inflammatory response (Bischoff, 1989; Carlson *et al.*, 2008; Christov *et al.*, 2007; Gopinath and Rando, 2008; Shavlakadze *et al.*, 2009; Yablonka-Reuveni *et al.*, 1999). Furthermore, systemic factors like hepatocyte growth factor, neuronal nitric oxide synthase (nNOS) and Notch-ligands can activate satellite cells (Yablonka-Reuveni, 2011). In a states of muscle degeneration such as in DMD, denervation, advanced age, or wasting syndromes, the satellite cell number and their proliferative capacity decreases. The system becomes exhausted thus reducing the regenerative capacity of the muscle (Jejurikar and Kuzon, 2003). In DMD, lack of dystrophin and the sarcolemmal instability induce new cycles of degeneration and the satellite cells fail to repair the muscle after unsuccessful rounds of regeneration, which ultimately results in necrosis. The exact mechanism of reduced regenerative capacity due to satellite cells exhaustion is not clear yet and different theories exist. In *mdx* mice, it has been shown that the capability to regenerate is not an endogenous quality of satellite cells, but depends on extracellular cues from the stem cell niche (Boldrin *et al.*, 2012; Brack *et al.*, 2007; Conboy *et al.*, 2005). Boldrin and colleagues demonstrated that satellite cells from young and aged *mdx* mice can regenerate *in vivo* in the same manner as wildtype satellite cells (Boldrin *et al.*, 2015). Other studies show that cell-autonomous factors (satellite cell intrinsic functions) are responsible for the changes in their regenerative capacity (Cosgrove *et al.*, 2014; Dumont *et al.*, 2015). In a recent study Dumont and colleagues suggested that the impaired regeneration in *mdx* mice was the result of defective asymmetric division of satellite cells and generation of myogenic progenitors due to intrinsic dysfunction resulting from dystrophin loss (Dumont *et al.*, 2015). The aforementioned work described for the first time a functional role of dystrophin in satellite cells and is discussed in section 4.4.7. Another recent study showed in mice that, unlike previously assumed, loss of satellite cell-dependant regenerative capacity had no direct

impact on sarcopenia, the state of age-related loss of muscle mass and strength. However, the satellite cell loss contributed to the increased fibrosis observed in aged skeletal muscle (Fry *et al.*, 2015). These studies highlight the necessity of a broader research approach, which should be aimed to unravel the interplay of cell intrinsic and extrinsic factors that influence the satellite cell fate in normal state and conditions of degeneration. Such understaning could be exploited for the development of satellite cell centered regenerative therapies.

4.4. Dystrophin

4.4.1. The *DMD* gene

Dystrophin is a large, rod-shaped protein which is expressed in all types of muscle (i.e. skeletal, cardiac, and smooth muscles) as well as in neurons (Hoffman *et al.*, 1987, 1988; Uchino *et al.*, 1994). As already mentioned it is encoded by the *DMD* gene, which causes Duchenne muscular dystrophy if mutated (Koenig *et al.*, 1987; A. P. Monaco *et al.*, 1986).

The dystrophin gene (*DMD*) is the largest human gene spanning 2.4 Mb at the Xp21 locus and comprises 79 primary exons plus 6 alternative first exons (Emery and Muntoni, 2003). However, the coding sequence is only ≈14 kb, less than 1% of its genomic DNA sequence (Hoffman *et al.*, 1987; Koenig *et al.*, 1987; Anthony P. Monaco *et al.*, 1986)

mRNAs for several dystrophin isoforms are transcribed from the *DMD* gene through the use of tissue specific promoters or by alternative splicing. The full-length dystrophin protein has a molecular weight of 427 kDa and the corresponding mRNA is transcribed from 3 different tissue specific promoters: muscle (M), brain (B) and Purkinje cell type (P). The main dystrophin isoform Dp427 is present in the skeletal, cardiac and smooth muscle and is controlled by the muscle specific promoter. It carries a unique N-terminal sequence, which is encoded by exon 1 (Bies *et al.*, 1992). This promoter is also active in glial cells (Chelly *et al.*, 1990). The brain promoter (B) is active in cortical neurons, heart- and cerebellar neurons, while the Purkinje cell specific promoter regulates the cerebellar dystrophin expression (Górecki *et al.*, 1992; Nudel *et al.*, 1989).

Developmentally regulated shorter dystrophin isoforms are transcribed from internal promoters like the retinal dystrophin Dp260 spanning exons 30-79 , the cerebellar and renal isoforms Dp140 spanning exons 45-79 (Lidov *et al.*, 1995), the Schwann cell Dp116 dystrophin

spanning exons 56-79. These three isoforms (Dp260, Dp116 and Dp140) comprise parts of the rod domain and express the cysteine-rich and C-terminal domains, but lack the N-terminal actin binding domain (Byers *et al.*, 1993; D'Souza *et al.*, 1995; Lidov *et al.*, 1995).

A more ubiquitously expressed short isoform is Dp71, which spans exons 63-79 (Figure 3). It has a unique seven residue N-terminus fused to the cysteine-rich and C-terminal domains (Bar *et al.*, 1990; Howard *et al.*, 1995; Lederfein *et al.*, 1992, 1993).

Further dystrophin diversification is provided by alternative splicing throughout the coding sequence of dystrophin (Bies *et al.*, 1992; Sironi *et al.*, 2002). Notably, two alternative splicing sites exist at the 3' end of dystrophin (Feener *et al.*, 1989). Their usage has been well characterized in the Dp71 isoform. In Dp71d (also named Dp71a) splicing of exon 71 does not change the reading frame of the transcript and generates the 13 amino acid long C-terminus common to most dystrophin isoforms. The Dp71f (Dp71b) isoform is generated by alternative splicing of exon 78 which causes a change in the reading frame and produces a C-terminus that contains 31 new amino acids with hydrophobic properties. Another isoform is Dp71c lacking exon 71-74 that encode the 110 amino acid sequence of the syntrophin binding domain. Moreover, exon 78 can be further skipped in the latter isoform creating the Dp71Δ_{110} variant. The expression of these isoforms is differentially regulated during human embryonic development and adulthood (Austin *et al.*, 1995; Bies *et al.*, 1992; Feener *et al.*, 1989). Similar expression patterns have been observed in animal models on the mRNA and protein level (Bies *et al.*, 1992; Daoud *et al.*, 2009).

The various isoforms and splicing variants of dystrophin are highly conserved in mammals and differ in their cellular and subcellular localization as well as in binding partners thus contributing to the pleiotropic functions of dystrophin.
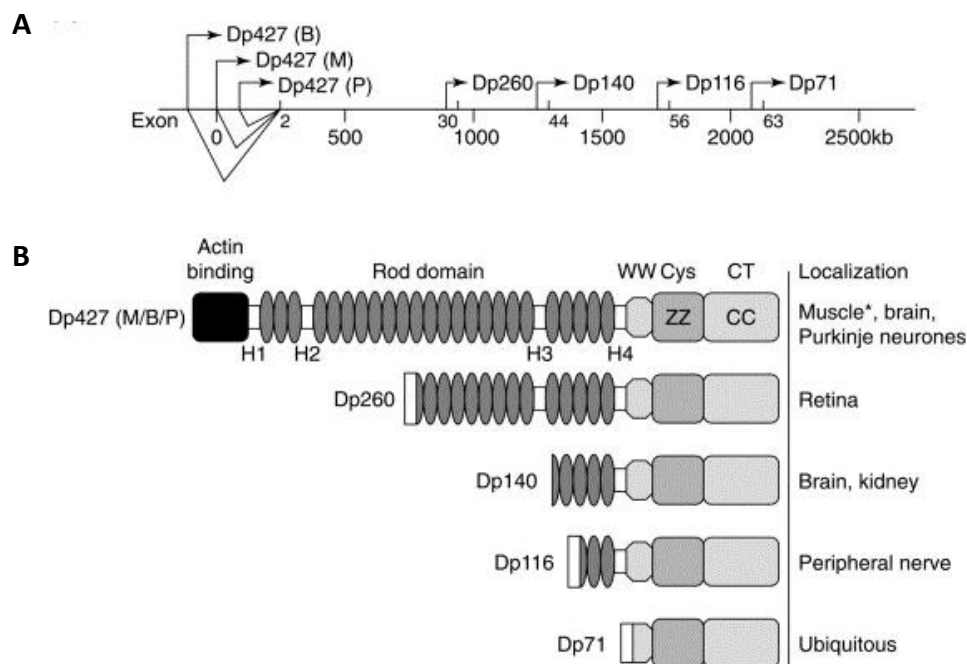
Figure 3: Organization of the DMD gene and its protein products.
(A) The DMD gene is 2.5 Mb long and encodes at 7 different isoforms. The "full-length" dystrophin transcript encodes the 427 kDa isoform which is named Dp427. For this isoform, three different tissue specific promoters exist: brain (B), muscle (M), and cerebellar Purkinje cells (P). Protein products differ in their N-terminal region. Shorter dystrophin isoforms are produced from distally located promoters and expressed in the retina (Dp260); brain and kidney (Dp140); peripheral nerve (Schwann cells) (Dp116) or are expressed ubiquitously (Dp71) **(B)** Schematic representation of the functional domains of different dystrophin isoforms and their localization. H1-H4 hinge regions are proline rich and interrupt the rod, spectrin-like domain. The C-terminal region (CT), which is present in all isoforms, contains binding sites for proteins of the dystrophin associated protein complex (DAPC). The cystein-rich domain includes the WW binding domain, which mediates specific protein-protein interactions with short proline-rich or proline-containing motif, the ZZ-type-zinc finger binding domain and a coiled-coil domain in the C-terminus. Modified from (Blake and Kröger, 2000).

4.4.2. The dystrophin protein in the skeletal muscle

Only full-length dystrophin is expressed in neonatal and adult skeletal muscle where it accounts for 0,002% of the total protein content. In striated muscles, dystrophin is localized at the cytoplasmatic side of the *sarcolemma* (Watkins *et al.*, 1988). In longitudinal sections, dystrophin expression shows a striated pattern and co-localizes with the costamers, when the skeletal muscle fibers are visualized (Ervasti, 2003; Porter *et al.*, 1992; Straub *et al.*, 1992). Furthermore, dystrophin is concentrated around the NMJ (Huard *et al.*, 1991). The full-length dystrophin isoform has a molecular weight (MW) of 427 kDa and is composed of 3,685 amino acids. At the *sarcolemma*, dystrophin assembles several transmembrane and cytoplasmic proteins into the dystrophin associated protein complex (DAPC). *Via* this complex, dystrophin

provides a link between the cytoskeleton and the extracellular matrix (ECM) that assures mechanical stability of the *sarcolemma* and protects the muscle from contraction induced muscle damage.

Dystrophin belongs to the β-spectrin/ α-actinin protein family (Koenig *et al.*, 1988) and can be divided into 4 functional domains: an N-terminal actin binding domain, a central rod-domain, a cysteine-rich, and a C-terminal domain (Figure 3). The N-terminal and part of the dystrophin rod domain interact with cytoskeletal actin (Amann *et al.*, 1998; Norwood *et al.*, 2000). The rod domain folds into α-helical coils composed of 24 spectrin-like repeats interrupted by 4 proline-rich hinges that contribute to the flexible structure of the protein (Blake *et al.*, 2002; Koenig *et al.*, 1988). Behind the hinge region we find a WW protein binding domain, which can also be found in signaling and regulatory molecules (Bork and Sudol, 1994). This WW-domain binds to β-dystroglycan, which in turn connects the DAPC to α-laminin in the ECM, an interaction mediated by α-dystroglycan (Judge, 2006). The WW-domain is followed by the cysteine-rich domain displaying two EF hand motifs that are potential binding sites for calcium ions (Koenig *et al.*, 1988). The ability of dystrophin to bind calcium in a calmodulin dependent manner is facilitated by the ZZ-motif (Anderson *et al.*, 1996), which is enriched with cysteine residues. These are predicted to form the coordination sites for binding divalent metal cations such as zinc ions (Ponting *et al.*, 1996). In the C-terminal domain, another coil-coil region of dystrophin interacts with syntrophin that can bind to nNOS and to dystrobrevin.

A major role of the dystrophin protein is the assembly of the DAPC. Hence, dystrophin provides a link between the cytoskeleton and the extracellular matrix. Absence of this mechanical apparatus is thought to destabilize the *sarcolemma*, making the myofibers more susceptible to damage during contractions (Ehmsen *et al.*, 2002; Lederfein *et al.*, 1993; Pasternak *et al.*, 1995; Petrof *et al.*, 1993; Sacco *et al.*, 1992). Another important role of dystrophin is its scaffolding function for signal transduction through the DAPC and for various ion channels. DAPC members either bind to or are substrates for known signaling molecules like nNOS, caveolin3, growth factor receptor-bound protein 2 (Grb2) and various kinases (Rando, 2001; Sotgia *et al.*, 2000, 2001; Spence *et al.*, 2004; Yang *et al.*, 1995). Dystrophin plays a role in the cytosolic calcium homeostasis, which is impaired in dystrophic muscle due to an alteration of ion channels and pumps (Friedrich *et al.*, 2008). Dystrophin has also a

function at the NMJ. Hence, in dystrophic muscle the post-synaptic membrane shows reduced folding, which disturbs the distribution of AChRs and of other proteins at the post-synaptic membrane. This observation is most likely due to defects in nNOS localization or nitric oxide (NO) production (Shiao *et al.*, 2004).

Most of the studies about functional domains of dystrophin and its binding partners have been conducted using transgenic mice that over-expressed mini- or micro-dystrophins, which contained various functional domains (Cox *et al.*, 1994a; Gaedigk *et al.*, 2006; Harper *et al.*, 2002; Judge, 2006; Lai *et al.*, 2009; Tinsley *et al.*, 1998; Warner *et al.*, 2002).

The mechanical and signaling functions of dystrophin are exerted through the interaction with a complex protein network at the *sarcolemma*, the DAPC, which will be described in more detail in the next section.

4.4.3. Dystrophin associated protein complex (DAPC)

Dystrophin serves as the central player for assembling the DAPC at the *sarcolemma*. The complex provides the mechanical link from actin to the ECM and recruits either directly or indirectly signaling molecules. The importance of dystrophin in assembling the complex is highlighted by the absence of DAPC in dystrophic muscle. The DAPC components can be divided into the following subcomplexes: the dystroglycan complex, the sarcoglycan complex, as well as the cytoplasmic and ECM components including sarcospan, syntrophin, dystrobrevin and nNOS (Figure 4) (Blake and Kröger, 2000; Ehmsen *et al.*, 2002). Beyond that, several components of the DAPC are also found in the CNS generating various DAPC-like complexes.

The **dystroglycan complex** (α- and β-dystroglycan) provides the core of the DAPC. The α-dystroglycan is located in the extracellular matrix where it interacts with laminins 1, 2 and 4, perlecan and agrin and is required for the assembly of the basal laminae. At the NMJ, dystroglycans plays a specialized role where it binds to agrin and laminin 4, two proteins required for NMJ formation. Furthermore α-dystroglycan serves as a cell surface receptor for a number of micro-organisms (Hemler, 1999; Ibraghimov-Beskrovnaya *et al.*, 1992). β-dystroglycan spans the *sarcolemma* and binds with its proline-rich C-terminus to the WW- and EF-domains of dystrophin as well as to the SH3-domain of Grb2. Such and interaction could transmit extracellular signals to the muscle cytoskeleton (Yang *et al.*, 1995). Both

dystroglycans are produced from a single polypeptide and are heavily glycosylated prior to being sorted to their respective location (Winder, 2001). In mice, dystroglycan function is indispensable for survival. Total absence is embryonically lethal due to disruption of extra-embryonic basement membrane formation (Williamson *et al.*, 1997). In the CNS, conditional deletion of dystroglycans leads to impaired synaptic plasticity (Moore *et al.*, 2002). Moreover, genetic loss or defective glycosylation of α-dystroglycan leads to alterations of the basement membrane and abnormal neural migration during development (Perronnet *et al.*, 2010). These findings point out the crucial functions of dystroglycans in non-muscle tissues.

The **sarcoglycan complex** consists of 6 transmembrane proteins (α-, β-, γ-, δ-, ε- ζ-sarcoglycans) and only the γ-sarcoglycan directly interacts with dystrophin. δ-Sarcoglycan is located closer to the dystroglycan complex and forms a tight link with β-sarcoglycan (Chan *et al.*, 1998). Mutations in each of the sarcoglycans lead to a specific form of muscular dystrophy, the so called Limb Girdle Muscular Dystrophy. This disease entity is associated with a reduction or absence of the other DAPC members at the *sarcolemma*. Mutant sarcoglycans are thought to block the formation of the complex and its insertion into the *sarcolemma* thus leading to a dystrophic phenotype (Holt and Campbell, 1998). Further functional roles of the sarcoglycans have been derived from its structure: γ-sarcoglycan has 5 tyrosine residues in its cytoplasmic domain suggesting bidirectional signaling with integrins (Yoshida *et al.*, 1998). Until recently, the expression of sarcoglycans was thought to be restricted to the striated and smooth muscles and to lesser extent to the peripheral nerves. However, recent research has shown that ε-sarcoglycan plays an important role in the brain and that ζ-sarcoglycan is abundantly expressed in the brain as well (Shiga *et al.*, 2006; Zimprich *et al.*, 2001).

Sarcospan is a unique transmembrane protein whose N-and C-termini are both located intracellularly. It forms a sub-complex with the sarcoglycans (Crosbie *et al.*, 1997; Ehmsen *et al.*, 2002).

The C-terminal coiled coil domain of dystrophin represents the binding site for the cytoplasmic components of the DAPC. The **syntrophin** family is composed of five subtypes (α, β_1, β_2, γ_1, and γ_2 syntrophin) that are expressed and differently distributed in the muscle. α -syntrophins are localized at the *sarcolemma* of all fibers, β_1-syntrophins are present in fast-twitch fibers, and β_2-syntrophins can be found at the NMJ. Syntrophins are characterized by two plekstrin homology (PH) domains and a PDZ domain (PSD-95, postsynaptic densitiy

19

protein 95; disc-large and ZO-1, *zonula occludens-1*) domain. They bind directly to dystrophin and to α-dystrobrevin, both of which having two syntrophin binding sites at their C-terminus (Newey *et al.*, 2000). The ErbB4 receptor tyrosine kinase, voltage gated sodium channels, nNOS, stress-activated protein kinases (SAPK), aquaporin-4 (AQP4) and neuroligins, have been proposed as potential binding partners for syntrophins *via* their PDZ domain (Brenman *et al.*, 1995, 1996; Garcia *et al.*, 2000; Gee *et al.*, 1998; Hasegawa *et al.*, 1999; Schultz *et al.*, 1998; Yamakawa *et al.*, 2007). Many of the aforementioned syntrophin interaction partners have important functions in the brain, however, the effects they have on the DAPC-like complexes remains to be elucidated.

Dystrobrevin has five different isoforms, which are generated through alternative splicing and through different tissue specific promoters in a similar manner as already described for dystrophin. Two of the isoforms are highly expressed at the *sarcolemma* where they associate with syntrophin. In skeletal muscle, α-dystrobrevin-2 is the primary isoform associated with the DAPC, and α-dystrobrevin-1 is mainly localized at the NMJ, where it interacts with utrophin (Peters *et al.*, 1998). Moreover, dystrobrevins interacts with syncoilin, which is highly expressed at the *sarcolemma* of skeletal, cardiac and smooth muscles. In addition, syncoilin co-localizes with desmin at the NMJ, Z-lines and *sarcolemma* of skeletal muscle hence providing connection between the DAPC with the intermediate filaments system (Poon *et al.*, 2002). β-dystrobrevin is present in brain, but not in muscle, and can bind directly to dystrophin. It is exclusively expressed in neurons and there expressed at high levels at the postsynaptic densities (PSD) (Blake *et al.*, 1998, 1999; Peters *et al.*, 1997).
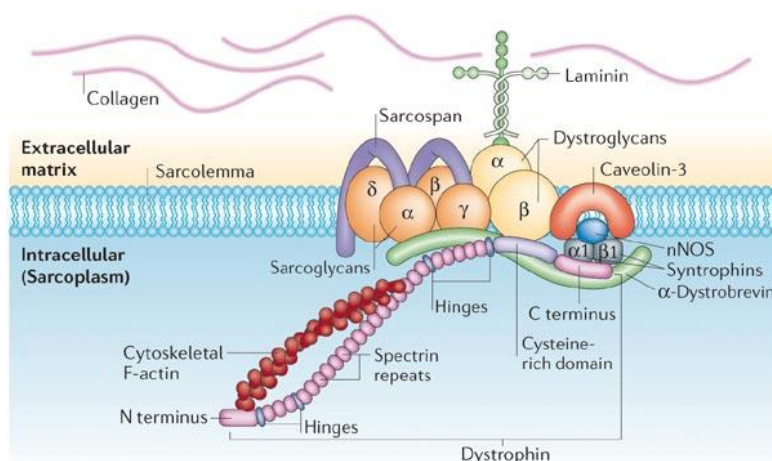
Figure 4: Dystrophin and the dystrophin associated protein complex (DAPC) in muscle tissue.
Dystrophin interacts with actin through its N-terminal domain and part of the rod domain. 24 spectrin repeats compose the rod domain and are followed by a WW protein binding domain, which interacts with β-dystroglycan. The latter connects to laminin at the ECM *via* α-dystroglycan. The dystroglycan complex at the *sarcolemma* interacts with the other big transmembrane complex, which is composed of sarcoglycans. Sarcospan covers the sarcoglycan complex towards the ECM. At the C-terminus dystrophin reacts *via* its cysteine-rich domain with syntrophins that in turn can bind to α-dystrobrevin, nNOS and caveolin-3 (Davies and Nowak, 2006).

4.4.4. Utrophin: a dystrophin homolog

Utrophin is a structural homolog of dystrophin and contains the same protein binding domains, although small differences exist; utrophin lacks the actin binding part, which is located in the rod domain of dystrophin. Utrophin is the autosomally encoded homolog of dystrophin. During embryonic development it is expressed at the *sarcolemma* of the fetal muscle and becomes gradually replaced by dystrophin postnatally (Clerk *et al.*, 1993). It is assumed that dystrophin is better specialized and adapted for the higher workload of skeletal muscle and heart during birth and thereafter (Tinsley *et al.*, 1996). In the adult muscle utrophin is expressed in intramuscular nerves, blood vessels, and in the muscle fibers, where it is localized at the NMJ and at the myotendinous junction (Ohlendieck *et al.*, 1991). Utrophin is thought to be part of the postsynaptic cytoskeleton (Love *et al.*, 1993). Both dystrophin and utrophin, however, are found at different locations of the NMJ, blood vessels, and cardiac muscle (Pons *et al.*, 1994). In myopathies, the expression of utrophin is increased at the *sarcolemma* and it is upregulated in regenerating fibers (Helliwell *et al.*, 1992). The upregulation of utrophin in *mdx* mice could partly compensate for the absence of dystrophin and ameliorate muscle pathology. In muscle dystrophic mice, utrophin overexpression *via* transgene or cDNA delivery and gutted adenovirus improved dystrophic pathology in the animals. Utrophin has been shown to provide sarcolemmal stability and restore the DAPC to

some extent, but the nNOS expression was not restored suggesting that full-length utrophin cannot anchor nNOS at the *sarcolemma* (Gilbert *et al.*, 1999; Li *et al.*, 2010; Tinsley *et al.*, 1998). Therapies aiming at the upregulation of the endogenous utrophin in DMD patients have been subject of many investigations. A small molecule (BMN195) was identified that could modulate the expression of utrophin. In pre-clinical models it showed promise to upregulate utrophin (Tinsley *et al.*, 2011). Nevertheless, a clinical study failed to confirm a clinical benefit due to poor bioavailability (http://www.musculardystrophyuk.org/press-releases/news2568disappointing_results_from_biomarin_s_utrophin_clinical_trial_for_duc henne/). Presently additional candidates that should overcome the limitations of BMN195, but with a similar positive effect on utrophin upregulation are being developed (Tinsley *et al.*, 2014).

4.4.5. Dystrophin in cardiac and smooth muscles

The important role of dystrophin in cardiac and smooth muscles is highlighted by the fact that most of DMD patients die from cardiac and respiratory failure. Patients do not only suffer from skeletal muscle related symptoms but also from cardiac (Emery, 1972; Perloff *et al.*, 1967) and vascular dysfunction (Noordeen *et al.*, 1999) as well as dysfunction of the gastrointestinal tract (Barohn *et al.*, 1988; Chung *et al.*, 1998; Leon *et al.*, 1986).

The muscle (DP427m) and brain specific (Dp427b) dystrophin isoforms are the major ones in heart and smooth muscle. During development, the dystrophin expression at the plasmalemma occurs earlier in cardiac and smooth foetal muscle (8 weeks of gestation) then in skeletal muscle. Of note, in cardiac muscle the brain and muscle isoforms are expressed in parallel (Torelli *et al.*, 1999).

4.4.5.1. Dystrophin in the heart muscle

In cardiac myocytes, dystrophin is localized at the *sarcolemma* and the T-tubules (Klietsch *et al.*, 1993). In contrast to skeletal muscle, where loss of dystrophin dramatically reduces the expression of other DAPC components, their expression in the heart remains unaffected (Townsend *et al.*, 2007). The reason for this striking difference is not yet known. In DMD patients, the primary cellular defect, leading to the demise of cardiac myocytes and subsequent cardiomyopathy, is thought to be the mechanical instability of the cell membrane

(Fanchaouy *et al.*, 2009; Yasuda *et al.*, 2005). These findings confirm the observation from skeletal muscle that the primary role of dystrophin is the mechanical stabilization of the *sarcolemma*. It has been shown that isolated cardiac myocytes from *mdx* mice are more susceptible to membrane damage due to either passive stretch or hypo-osmotic stress. Like in skeletal muscles, this mechanical injury is associated with increased membrane permeability, decreased force production, lateral force transmission, but not with reductions in the force generating capacity of the sarcomere (Fanchaouy *et al.*, 2009; Yasuda *et al.*, 2005).

In addition, abnormalities of dystrophin expression have not only been observed in inherited dystrophinopathies but also in non-inherited conditions such as acute ischemia, enteroviral infection, and isoproterenol-induced cardiomyopathy (Armstrong *et al.*, 2001; Kyoi *et al.*, 2006; Toyo-Oka *et al.*, 2005). It has been shown in mice that dystrophin expression in the heart declines significantly with age (Bodyak *et al.*, 2002). Furthermore, under conditions of isoprotenerol intoxication and ischemia, dystrophin has an enhanced susceptibility to degradation in contrast to integrins and other DAPC proteins (Campos *et al.*, 2008; Rodríguez *et al.*, 2005). Degradation of dystrophin is achieved through calpain proteases, which are calcium-dependent cysteine proteinases. These enzymes can be aberrantly activated in DMD and heart failure (Takahashi *et al.*, 2006; Zatz and Starling, 2005). In transgenic *mdx* mice, overexpression of the calpain inhibitor calpistatin led to reduction in muscle necrosis. Hence, expression of the endogenous calpain inhibitor calpistatin and of other inhibitors might be a therapeutic strategy for DMD and during heart failure (Spencer and Mellgren, 2002). Dystrophin can also be cleaved by the 2A proteases that are expressed by cardiotropic enteroviruses (Badorff *et al.*, 1999). Cleavage disconnects the actin binding and rod domain from the C-terminus, thereby contributing to the destabilization of the DAPC and the *sarcolemma*.

4.4.5.2. Dystrophin in the smooth muscle

DMD patients often suffer from symptoms such as dysphagia, vomiting, gastric dilation, paralytic ileus, severe constipation and bladder paralysis in the later phases of their disease. Most of the information about smooth muscle pathology has been gained by autopsies, where small fiber sizes, atrophy or loss of myofibers, and fibrosis have been noted in

gastrointestinal smooth muscles (Barohn *et al.*, 1988; Chung *et al.*, 1998; Jaffe *et al.*, 1990; Leon *et al.*, 1986; Nowak *et al.*, 1982).

Dystrophin in smooth muscles is found at distinct regions of their plasmamembrane. Dystrophin localizes at the caveolae-rich membrane domains that lie between the ribs of the adherens junctions, together with caveolin, the inositol triphosphate (IP3) receptor and the sodium-calcium-ion exchanger (North *et al.*, 1993).

A study on vascular smooth muscles shows that dystrophin plays an important role in smooth muscle function and differentiation. The dystrophin gene was among the genes whose transcription was induced by actin polymerization and its expression was promoted by the transcription factors myocardin and myocardin-related transcription factor A (Turczyńska *et al.*, 2015). Contractile smooth muscle cells of the vascular system show high degree of plasticity and can undergo reversible phenotypic changes in response to environmental cues and vascular injury. An important function in these processes is attributed to the DAPC by linking the actin filaments to the ECM. A strong correlation between dystrophin expression and the contractile performance of the vascular smooth muscle has been shown *in vivo* and *in vitro*. However, in the presence of serum, dystrophin is not expressed in cultured smooth muscle cells, which causes their dedifferentiation (Lees *et al.*, 1994, 1995).

4.4.6. Dystrophin in non-muscle tissues

The role of dystrophin in muscle has been intensively investigated in DMD patients. The absence of dystrophin from the *sarcolemma* triggers a cascade of events leading to muscle degeneration (Emery and Muntoni, 2003). However, DMD can be considered a multi-systemic disorder and dysfunction of the numerous dystrophin isoforms has pleiotropic effects in non-muscle tissues.

DMD patients do not only suffer from muscle related symptoms, but display CNS dysfunction including cognitive impairment (Dubowitz and Crome, 1969; Mehler, 2000; Yoshioka *et al.*, 1980) as well as impairment of the visual system (Cibis *et al.*, 1993; Costa *et al.*, 2007; D'Souza *et al.*, 1995; Pillers *et al.*, 1993).

In the nervous system all dystrophin isoform have been identified and are expressed in adult life but also throughout neural development. During development, dystrophin is expressed

within the neural tube, selected areas of the embryonic and postnatal neuraxis suggesting a possible regulatory role in neurogenesis, neuronal migration and cellular differentiation (Ceccarini *et al.*, 1997; Cisneros *et al.*, 1996; Sarig *et al.*, 1999; Schofield *et al.*, 1994). During this period, the most prominent isoform is the shortest Dp71. In adulthood, the brain expresses the highest variety of isoforms, whereas Dp260 is restricted to the retina (D'Souza *et al.*, 1995) and the Dp116 isoform is found predominantly in Schwann cells of peripheral nerves (Byers *et al.*, 1993).

The exact role of dystrophin in the CNS as well as its correlation to the CNS phenotype in DMD still remains to be elucidated and is hampered by the complexity and high variety of dystrophin proteins and DAPC-like complexes expressed throughout development and adult life.

4.4.6.1. Dystrophin in the brain

Although dystrophin levels in the brain are only 10% of those in muscles, the highest number of isoforms can be found there. Observations in some DMD patients with impairment of cognition or memory, as well as behavioral problems have focused the research towards the role of dystrophin in the brain. Interestingly, a correlation can be found between the position of a mutation in the *DMD* gene and the presence of cognitive problems. All DMD patients display moderate but specific memory and attention deficits. Since Dp427 isoforms is commonly lost in all DMD patients, a role of full-length dystrophin in brain dysfunction has been suggested. However, the severity and frequency of mental retardation increases with a progressive loss of functional C-terminal isoforms (Bushby, 1992; Lenk *et al.*, 1993). Mutations extending to exon 50 leading to loss of Dp427, Dp260 and Dp140 have been shown to contribute significantly to mental retardation in DMD patients (Bardoni *et al.*, 2000; Emery and Muntoni, 2003; Rapaport *et al.*, 1991). The major features of CNS involvement in DMD have been observed and reported already in the 19th century by Duchenne describing a seven year old boy as dull and with poor language skills (Duchenne, 1868). The mental retardation found in 20-30% of the DMD patients results in lower global IQ performance scores, has been attributed mostly to deficits in the verbal IQ, language and learning ability (Billard *et al.*, 1992, 1998; Ogasawara, 1989). Structural changes have been observed in some DMD patients like cerebral atrophy (Yoshioka *et al.*, 1980), neuronal loss, and gliosis (Jagadha and Becker, 1988).

Most of our understanding of the function of dystrophin in the brain is derived from studies done on *mdx* mice, which express all the small dystrophin isoforms including Dp71, but lack the full-length dystrophin. The behavioral and cognitive changes observed in *mdx* mice include impaired memory retention, spatial memory and procedural learning (Muntoni *et al.*, 1991; Vaillend *et al.*, 1995, 2004). Interestingly, the behavioral abnormalities in *mdx* mice normalize upon restoration of dystrophin suggesting reversal of neuronal function (Goyenvalle *et al.*, 2015).

In the brain, normally, the full-length dystrophin is transcribed from the Brain- and Purkinje cell promoters (Lidov *et al.*, 1990). Dp427 and DAPC-like complexes are expressed at postsynapse of neurons in the hippocampus, cerebellum and cerebral cortex. Altered synaptic plasticity has been observed in hippocampal neurons and in Purkinje cells of *mdx* mice that lack only the Dp427 isoform (Anderson *et al.*, 2004, 2010; Mehler *et al.*, 1992; Vaillend *et al.*, 1998, 1999). Authors have suggested that dystrophin would be involved in the clustering of subpopulations of γ-aminobutyric acid receptors (GABA$_A$-R). γ-Aminobutyric acid is the major inhibitory neurotransmitter in the nervous system suggesting a role of dystrophin at inhibitory synapses. Co-localization between dystrophin and the α2 subunit of GABA$_A$-R was also shown in cultured hippocampal neurons *in vitro* (Brünig *et al.*, 2002). Moreover loss of dystrophin and/or dystrobrevin leads to severe reduction in the number and size of GABA$_A$-R (Grady *et al.*, 1999; Kneussel *et al.*, 1999; Sekiguchi *et al.*, 2009). Although functional molecular data are lacking about the interaction between dystrophin and GABA$_A$-R, electrophysiological studies support this hypothesis (Anderson *et al.*, 2003; Kueh *et al.*, 2008; Vaillend and Billard, 2002). Additional studies are necessary to better characterize and analyze the role of dystrophin at the synapse and its contribution to cerebral network activity. Beyond a direct involvement of dystrophin in neuronal activity, authors suggested a function of full-length dystrophin in the formation and maintenance of blood brain barrier (Nico *et al.*, 2003, 2004).

The Dp140 isoform is manly expressed during development, but expression in the microvasculature of the adult brain was suggested as well. Dp71 is expressed in glia cells, notably in perivascular astrocytes and the Bergmann glia in the cerebellum surrounding the endothelial cells (Blake *et al.*, 1999; Lidov *et al.*, 1995). The distinct expression of Dp71 at the glial-vascular interface observed in humans, as well as in animal models, suggested a role of Dp71 in blood brain barrier function. It has been reported that Dp71 is involved in regulation

of water homeostasis *via* the AQP4 water permeable channel and is involved in potassium (K⁺) buffering mediated by the inward rectifier K⁺ channel (Kir4.1) (Connors *et al.*, 2004; Nicchia *et al.*, 2008). Additionally, Dp71-null mice display cognitive defects that were linked to excitatory synapse organization and function. Hence, another role for Dp71 was proposed at excitatory glutamatergic synapses that was supported by some experimental evidence (Daoud *et al.*, 2009). Further studies need to be done to elucidate the precise functions of Dp71 and its alternative splicing variants.

4.4.6.2. Dystrophin and the retina

In the retina following dystrophin isoforms are expressed: Dp427m, Dp260, Dp140, and Dp71 (Schmitz and Drenckhahn, 1997). In the mouse retina, the full-length and Dp260 dystrophin isoforms are found at the outer plexiform layer (OPL), a region where the highly specialized synapses between the glutamatergic photoreceptor with horizontal and with bipolar cells are located (Dalloz *et al.*, 2003; Pillers *et al.*, 1993; Schmitz and Drenckhahn, 1997). The dystrophin isoforms in this region are associated with the photoreceptor terminals and suggest involvement of dystrophin in synaptic transmission (Ueda *et al.*, 1997), but the precise mechanisms still remain to be elucidated. The short Dp71 dystrophin isoform is present in astrocytes and in the principal glial cells of the retina, the Müller cells, which are located at the inner limiting membrane that is the basal lamina separating the neural retina from the vitreous humour. Like in the brain, Dp71 expression in these cells is limited to the glial-endfeet. Transgenic mice lacking all retinal isoforms as well as Dp71 null mice exhibit a mislocalization of the Kir4.1 potassium channel and the AQP4 channel with reduced AQP4 levels. Thus, like in the brain, a role of Dp71 in the maintenance of potassium and water homeostasis as well as in the regulation of retinal vascular permeability has been proposed (Dalloz, 2003; Sene *et al.*, 2009; Wersinger *et al.*, 2011).

The best characterized non-muscle manifestation of DMD is described in the visual system. In 80% of the patients, there is a reduction in the amplitude of the b-wave response revealed by the dark-adapted (scotopic) electroretinogram (ERG). The ERG measures electric responses of the various cell types in the retina upon light stimulation. Depending on the kind of stimuli and stimuli adaptation different patterns can be recorded reflecting the activity of different cell types in the retina. Usually dark adapted response reflects the activity of the rod

photoreceptors system. The abnormal b-wave in DMD patients and in *mdx* mice, that lack all dystrophin isoforms, reflexts changes of synaptic transmission between the rod photoreceptors and the ON-bipolar cells (Cibis *et al.*, 1993; Pillers *et al.*, 1993). There is a correlation between the type of mutation, the affection of the respective DMD gene product and the presence of an abnormal ERG response. In patients, in whom the mutation does not abolish the expression of the Dp260 isoform have normal ERGs, while most C-terminally located mutations lead to changes in the b-wave. These findings suggest that Dp260 retinal isoform indeed plays a role in the b-wave generation (Dalloz *et al.*, 2003). In dystrophic *mdx³ᶜᵛ* mice that lack all short dystrophin isoforms due to a mutation near the 3' end of *Dmd* show similar abnormalities in b-wave amplitude, further indicting the requirement of specific dystrophin isoforms for normal retinal function (Pillers *et al.*, 1995). It is noteworthy, however, that, unlike in humans, all three isoforms need to be abolished in order to provoke the ERG changes in mice (Pillers *et al.*, 1995). A similar phenotype was observed in dystroglycan deficient mice suggesting a joint role of dystrophin and its DAPC-like complex (Satz *et al.*, 2009). In addition, authors recently reported that some DMD patients, with mutations affecting the Dp260 isoform, exhibites a deficit in red-green discrimination (Costa *et al.*, 2007).

4.4.7. The role of dystrophin in satellite cells

A recent study done by Dumont and colleagues described for the first time a functional role for dystrophin in the muscle stem cells (Dumont *et al.*, 2015). It was generally assumed that dystrophin would not be expressed in satellite cells. However, the study showed expression of full-length dystrophin in activated satellite cells and provided data for the functional role of dystrophin in for the establishment of polarity through interaction with the microtubule-associating protein (MAP)/microtubule affinity–regulating kinase 2 (Mark2). During apico-basal asymmetric division satellite cells give rise to two daughter cells with a distinct cell fate. The one daughter cell differentiates and contributes to the myogenic progenitor cells, which fuse with the myofiber for growth and repair, while the other daughter cell keeps its stem cell potential. During this process the expression of dystrophin was confined to the cell that maintained the satellite cell state. The novel role for dystrophin has a direct impact on the pathophysiological understanding of dystrophin deficient conditions. The authors of the study presented data showing the impaired polarity establishment and loss of asymmetric cell

division in dystrophin deficient *mdx* mice due to dysregulation of mitotic spindle orientation. Subsequently, the animals had reduced numbers myogenic progenitors, which could explain the impaired regeneration observed in dystrophic conditions despite the high number of satellite cells normally observed in *mdx* mice and DMD patients. This novel function of dystrophin opens a new avenue of research of dystrophinopathies. The defects observed in asymmetric stem cell division in dystrophic mice now allow for a re-interpretation of the muscular deficits observed in DMD patients (Dumont *et al.*, 2015).

4.5. Mutations of the *DMD* gene

Thousands of independent mutations have been described in the *DMD* gene that has a high spontaneous mutation rate of 10^{-4} gene/generation (Blake *et al.*, 2002). The "reading frame rule" explains why neither the size nor the position of the *DMD* deletion/mutation shows a good correlation with the phenotype (genotype-phenotype relation). It postulates, in case a deletion disrupts the open *DMD* reading frame, the resulting premature termination of translation prevents the proper expression of dystrophin. The nearly total absence of dystrophin causes the severe Duchenne variant of muscular dystrophy. In cases, where the deletion does not disrupt the reading frame, dystrophin can be produced albeit in a truncated form that consenses only partial function. These mutations tend to cause the milder Becker variant of muscular dystrophy (Monaco *et al.*, 1988).

The mutations found in DMD patients and their corresponding phenotype have vastly contributed to the understanding of the function of specific dystrophin domains and have facilitated the development of mini- or micro-dystrophins that are tested for so-called gene therapeutic interventions (Blake *et al.*, 2002).

Large deletions are the most common mutations in DMD or BMD and are identified in approximately 65% of the patients. Two mutational hotspots spanning exons 45-53 and exons 2-20 have been identified (Koenig *et al.*, 1989; Koenig and Kunkel, 1990). Small deletions and point mutations have been observed in one third of the patients, most commonly leading to premature stop codons (Lenk *et al.*, 1993; Roberts and Bobrow, 1998).

The rod domain has been found to accommodate large in-frame deletions resulting in a mild Becker type dystrophy. The rod domain acts as a bridge or spacer between the functionally important N-terminal actin binding and the cysteine-rich and C-terminal domain. Skipping this

region results in truncated dystrophin protein isoforms that seem to function normally (England *et al.*, 1990).

4.6. Revertant fibers in DMD patients and in *mdx* mice

Mutations in DMD patients and in the *mdx* mouse disrupt the open reading frame and prevent the expression of dystrophin. Nevertheless, the emergence of dystrophin positive fibers, the so-called "revertant fibers" (RFs), in an otherwise dystrophin negative background has been observed (Arechavala-Gomeza *et al.*, 2010; Danko *et al.*, 1992; Hoffman *et al.*, 1990; Nicholson, 1993; Nicholson *et al.*, 1989; S.D. Wilton *et al.*, 1997). RFs express an internally truncated form of dystrophin. This suggests that secondary events must have occurred that resulted in the re-establishment of the reading frame. In the *mdx* mouse, RFs have been studied more intensely, and it has been shown that they emerge around birth in short segments and increase in size and number with age. The revertant event is thought to take place in the muscle precursor cells that are then activated and proliferate during the repetitive cycles of de- and regeneration that are characteristic for the dystrophic muscle. This process leads to the expansion of RFs (Lu *et al.*, 2000; Yokota *et al.*, 2006). RFs form clonal clusters but exhibit *Dmd* splicing pattern, which differs between neighboring independent clusters. The different dystrophin isoforms in the individual clusters have been confirmed on the protein level using exon-specific antibodies (Lu *et al.*, 2000; Thanh *et al.*, 1995), as well as on the mRNA level by RT-PCR (S. D. Wilton *et al.*, 1997). On the mRNA level, such shortened transcripts have also been observed in the normal muscle tissue of the mouse, but whether they are translated into protein has not yet been shown. The size of each cluster can encompass up to 100 fibers and reach 100 mm length at 18 months of age (Lu *et al.*, 2000). Such RFs can also be found in muscles of other breeds of *mdx* mice that bear different mutations (Danko *et al.*, 1992; Echigoya *et al.*, 2013) as well as in the Golden Retriever Dystrophic Dog (GRMD) (Schatzberg *et al.*, 1998). In human DMD patients the percentage of RFs ranges between 0.01 and 7 percent and, in contrast to the *mdx* mice, no RF expansion with age has been observed. A correlation between the emergence of RFs and an improvement of DMD symptoms has not been observed so far (Arechavala-Gomeza *et al.*, 2010). The amount of RFs is not only influenced by the location of the mutation, but also by the genetic background of the mouse (Echigoya *et al.*, 2013). More recent studies, which support the hypothesis of clonal expansion of RFs, suggest the occurrence of *de novo*

reversions throughout the whole lifespan and show that such events could take place in the heart as well (Pigozzo *et al.*, 2013).

The natural emergence of RFs in DMD patients has to be taken into account when assessing the efficacy of (gene) therapeutic approaches. On the other hand, it is important to understand the underlying molecular mechanisms and the origin and expansion of RFs as this phenomenon could be exploited for novel therapies and will contribute to the better understanding of the disease. Furthermore, the natural phenomenon of RFs provides the basis for one of the most promising therapeutic approaches against DMD, the exon skipping which will be explained in the next section.

4.7. Therapies for DMD

Different therapies against DMD exist and are being continuously developed. The aim is to slow the progression of the disease by immune modulation (e.g. *via* steroids and inhibitors of transforming growth factor), by inducing or introducing proteins that may compensate for dystrophin deficiency in the myofiber (e.g. utrophin, biglycan, and laminin), or enhance the regenerative response of the muscle (e.g. myostatin and activin 2B). Alternatively, studies are on the way that aim to introduce a more functional gene into the patient using viral gene transfer (Koppanati *et al.*, 2010; Kornegay *et al.*, 2010) or to repair the DMD gene of the patient. Due to a multitude of technical and biological obstacles, however, the advance of gene therapies and of cell transplantation into the clinic is very slow despite extensive research (Maffioletti *et al.*, 2014; Seto *et al.*, 2012; Tremblay *et al.*, 2009; Wang *et al.*, 2011).

A more promising therapy against DMD has been developed using small molecules, artificial antisense oligonucleotides (AONs) that "repair" the open reading frame of the mutated gene through skipping of exons, which flank the original mutation. If this would be achieved in a highly predictive way, the reading frame could be restored and such transcript translated into a truncated but partially functional dystrophin (Dunckley *et al.*, 1998; Goyenvalle *et al.*, 2011; Matsuo *et al.*, 1991; Yokota *et al.*, 2007). This so-called "exon skipping" approach is similar to the phenomenon of RFs, in which exon skipping occurs "naturally" as described in the previous section. Alternatively, exon skipping can be achieved using specific mRNA splicing molecules (U7 or U1 RNA) which splice out extra exons. A disadvantage of the U7 or U1 RNA

molecules as opposed to AONs is the delivery system which uses viral vectors and could provoke an immune response. (Goyenvalle *et al.*, 2004, 2009; Lorain *et al.*, 2008).

4.7.1. Exon skipping *via* AONs

AONs used in exon skipping recognize a specific exon-intron boundary of the pre-mRNA, result in modulation of the splicing pattern and aim to restore the dystrophin expression. The mutated exon and, if necessary, some of its neighboring exons are thus remioved and the reading frame of the pre-mRNA is reconstituted, albeit shorter. In pre-clinical studies for DMD, the most promising candidate drugs have proven to be the 2'-O-methyl phosphorothioate (2'OMe-PS) and the phosphordiamidate morpholino oligomers (PMO), both targeting exon 51 (Aoki *et al.*, 2012; Heemskerk *et al.*, 2009; Pramono *et al.*, 1996; Yokota *et al.*, 2009). These two compounds entered phase 2/3 clinical trials. However both compounds showed little clinical efficacy likely as the trial duration was too short in order to discriminate a clear clinical improvement (Cirak *et al.*, 2011; Goemans *et al.*, 2011; Mendell *et al.*, 2013; Voit *et al.*, 2014).

A great disadvantage of these two molecules had already been observed during preclinical studies because they were not effective in treating cardiac and the central nervous symptoms. Recently, a novel promising AONs have been developed that overcome these limitations. Peptide-conjugated PMOs offers significantly higher efficiency than PMOs. In animal models, it has been shown that the peptide-conjugated PMOs succefully restored dystrophin expression and improve the function of skeletal and cardiac muscles (Wu *et al.*, 2012). Moreover, an important advance in the treatment of the multi-systemic DMD, Goyenvalle and colleagues used tricycle-DNA oligomers in *mdx* and utrophin/dystrophin double knockout mice and clearly demonstrated dystrophin rescue in skeletal, heart and to some extent in the brain after systemic delivery of the drug (Goyenvalle *et al.*, 2015). Functional tests have confirmed the clinical improvement in the treated animals.

Currently the *mdx* and *mdx52* mice are the most widely used models for testing the efficacy of AONs or other splicing modulators (Aoki *et al.*, 2012; Lu *et al.*, 2003). *Mdx52* bears a deletion of exon 52, which is one of the mutational hotspots in DMD patients. The *mdx52* mouse and can be used to test AONs sequences for skipping exon 51 and 53. (Aoki *et al.*, 2012). The use of animal models to test different AONs and assess their main properties like

stability, efficacy and toxicity (Nakamura and Takeda, 2009) is indispensable. Pre-clinical evidence of the therapeutic potential of AONs have been provided by numerous *in vivo* studies (Aoki *et al.*, 2012; Fletcher *et al.*, 2006, 2007; Gebski *et al.*, 2003; Lu *et al.*, 2003; Yokota *et al.*, 2009).

4.8. Aims of the study

Dystrophin is a protein expressed in all types of muscle as well as in non-muscle tissue (Hoffman *et al.*, 1987, 1988; Uchino *et al.*, 1994). It was discovered almost 30 years ago as the protein missing in Duchenne muscular dystrophy, a severe X-linked disorder known for more than 100 years (Duchenne, 1868; Koenig *et al.*, 1987; Anthony P. Monaco *et al.*, 1986). Dystrophin is a rod-shaped cytoplasmic protein that physically links the cytoskeleton to the extracellular matrix. The identification of dystrophin close to the inner surface of the plasmalemma pushed the research efforts toward understanding the physiological role of dystrophin in the cell membrane. Vast progress has been made in the last two decades in comprehending the role of dystrophin in the muscle. Its protein structure, its binding partners, as well as its coding gene and complex regulatory mechanisms are well characterized.

The advancement of this field was based on studies on DMD patients, and prominent contributions have also been gained through identification and later also generation of animal models. Such models play a tremendously important role in the development of different therapeutic strategies; however, presently DMD cannot be cured. This calls for further investigations into the physiological role of dystrophin, not only in the muscle but also in other organs and tissues where it is expressed. Most of the murine models studying dystrophin are transgenic lines expressing a certain dystrophin isoform or overexpressing mini- or micro-dystrophins in a particular tissue (Cox *et al.*, 1994b; Gaedigk *et al.*, 2006; Greenberg *et al.*, 1994; Hakim and Duan, 2013; Harper *et al.*, 2002; Judge, 2006; Lai *et al.*, 2009; Li *et al.*, 2006; Phelps *et al.*, 1995; Sakamoto *et al.*, 2002; Warner *et al.*, 2002).

However, DMD is a multi-system disorder and dystrophin has a high number of isoforms and splicing variants expressed at different cellular and subcellular localizations. This contributes to the pleiotropic function of dystrophin and different effects of gene mutations depending on their location.

Therefore, it would be beneficial to have a more general model that will facilitate the study of dystrophin expression in various tissues in a non-artificial system. In the work that comprises my dissertation, I strove to generate and characterize a *Dmd^EGFP* reporter mouse, which should express a functional dystrophin-EGFP fusion protein.

Aim 1: To insert an EGFP-tag behind dystrophin exon 79 to create a dystrophin reporter mouse

The fluorescently labeled dystrophin protein should be expressed throughout muscle and non-muscle tissues by the natural endogenous promoters, the aim being to target as many dystrophin isoforms as possible. The C-terminus of dystrophin is an important functional domain, known to be expressed in all functional relevant dystrophin isoforms. The last exon 79 of the dystrophin gene is present in most of these isoforms as well as in revertant dystrophin. We thus aimed to insert the EGFP coding sequence behind the last *Dmd* exon 79, which had to be modified in order for the EGFP sequence to be co-expressed. Thus, we expected to target all full-length dystrophin isoforms (Dp427M, B, P), the retinal specific Dp260 isoform, as well as the shorter Dp140, Dp116, Dp71d and Dp71c isoforms. Only Dp71f and $Dp71_{\Delta110}$ cannot be targeted in our model since alternative splicing of exon 78 excludes also exon 79.

Aim 2: To investigate dystrophin-EGFP expression in different tissues of the mouse

After successful introduction of the EGFP-tag I wanted to investigate the tissue specific expression of the dystrophin-EGFP fusion protein in skeletal, smooth and cardiac tissue as well as in non-muscle tissues like brain and eye. Up to date, no dystrophin reporter mouse model exists and only few models use a fluorescent tag to follow up the expression of dystrophin (Bajanca et al., 2015; Li et al., 2006; Ruf-Zamojski et al., 2015). Through direct visualization of dystrophin, without the necessity of antibody staining the developed *Dmd^EGFP* model will facilitate the studies of dystrophin and dystrophinopathies *ex vivo* as well as *in vivo*.

Aim 3: To exclude the possibility that the C-terminal EGFP-tag causes muscular dystrophy

Adding a C-terminal tag to a protein might hinder its function. Hence, I wanted to analyze the mouse model with respect to possible features of a dystrophinopathy and

to check for mis-localization of other components of the dystrophin associated complex (DAPC) that might have been unintentionally caused by the EGFP-tag.

5. MATERIALS

Chemicals used in the context of this thesis were obtained from AppliChem (Darmstadt, Germany), GE Healthcare (Munich, Germany), Merck AG (Darmstadt, Germany), Roche GmbH (Grenzach-Wyhen, Germany), Carl Roth GmbH (Karlsruhe, Germany) and Sigma Aldrich GmbH (Taufenkirchen, Germany).

Plastic materials were obtained from Becton Dickinson GmbH (Heidelberg, Germany), Biozym Scientific GmbH (Hessisch-Oldendorf, Germany), Braun (Melsungen, Germany), Carl Roth GmbH (Karlsruhe, Germany), Eppendorf AG (Hamburg), Falcon/Corning (BY, USA), GE Healthcare (Munich, Germany), Kisker (Steinfurt, Germany), Sarstedt AG & Co (Nürnbrecht, Germany), Thermo Fischer Scientific Inc. (Langenselbold, Germany), TPP AG (Trasadlingen, Switzerland) and VWR (Darmstadt, Germany).

Media and compounds for cell culture work were obtained from Gibco/ LifeTechnologies (Karlsruhe, Germany), Invitrogen GmbH (Karlsruhe Germany) and VWR (Darmstadt, Germany).

Bacteria and supplies for bacterial culture were obtained from Invitrogen GmbH (Karlsruhe Germany) and Promega (Mannheim, Germany).

5.1. Plastic materials

Table 1: Plastic material for tissue culture and molecular biology

Plastic material	Supplier
Cell culture dishes (Ø 10 cm)	Becton Dickinson, Heidelberg, Germany Sarstedt, Nürnbrecht, Germany TPP, Trasadingen, Switzerland
Cell culture dishes (Ø 35 cm)	TPP, Trasadingen, Switzerland
Cell culture flasks (175 cm^2, 75 cm^2, 25cm^2)	TPP, Trasadingen, Switzerland
Cell culture plates-multiwell (6, 12, 24, 96 well)	TPP, Trasadingen, Switzerland
Conical polysterene tubes (15 ml/ 50 ml)	Falcon/ Corning, NY, USA
Coverslips	Menzel, Braunschweig, Germany
Coverslips, round	R. Langenbrink, Emmendingen, Germany
Cryovials	Thermo Fisher Scientific, Langenselbold, Germany
Cuvettes	Sarstedt, Nürnbrecht, Germany
Disposable hypodermic needle, 22 G x 1$^{1/4}$	Braun, Melsungen, Germany
Film, Fuji Super RX	Röntgen-Bender, Baden-Baden, Germany
Hybond-XL^{TM} – Transfermembran	GE Healthcare, Munich, Germany
Insulin syringes	VWR, Darmstadt, Germany
Pasteur Pipettes	Assistent, Hecht, Sondheim v. d. Rhön, Germany

Pipette tips (10 µl, 200 µl, 1000 µl)	Sarstedt, Nürnbrecht, Germany Kisker, Steinfurt, Germany Biozym, Hessisch-Oldendorf, Germany VWR, Darmstadt, Germany
Pipettes (sterile) (2 ml, 5 ml, 10 ml, 25 ml)	Becton Dickinson, Heidelberg, Germany Falcon/ Corning, NY, USA TPP, Trasadingen, Switzerland
Sephadex-Columns *ProbeQuant G-50 Micro Columns*	GE Healthcare,Munich, Germany
Safe-Lock micro test tubes (1.5 ml, 2 ml)	Eppendorf, Hamburg, Germany
Sequencing plates	ThermoFisher Scientific, Langenselbold, Germany
Scalpel	Braun, Tuttlingen, Germany
Slides Superfrost®	Menzel, Braunschweig, Germany
Stripes, PCR+caps	ThermoFisher Scientific, Langenselbold, Germany
Sterile filter (Ø 0.22 µm / 0.45 µm)	Millipore, Schwalbach, Germany
Syringe 2 ml, 5 ml, 10 ml	Braun, Melsungen, Germany Carl Roth, Karlsruhe, Germany
Whatman Filterpaper	Whatman GmbH, Göttingen, Germany

5.2. Instruments, equipment

Table 2: Instruments and equipment for molecular biological work

Instruments	Supplier
ABI PRiSM Genetic analyzer 3500	Thermofisher Scientific, Berlin, Germany
Analytical balances Kern 770, BP 3100 S	Sartorius Göttingen, Germany
Autoclave Systec V150	Systec GmbH, Wettenberg, Germany
Centrifuge 5415C	Eppendorf, Hamburg, Germany
Centrifuge 5804R	Eppendorf, Hamburg, Germany
DNA-electrophoresis chambers	BioRad, Munich, Germany LifeTechnologies/Gibco, CA, USA
Electroporator	BioRad, Munich, Germany
Electrophoresis unit Ruby SE600	Amersham/Hoeffer, Germany
Magnetic stirrer	Janke & Kunkel GmbH & Co. KG - IKALabortechnik, Staufen, Germany
Molecular Biology Incubator, Heraus	Heraeus, Hanau, Germany
Microwave	Sharp, Germany
NanoDrop ND-1000 Spectrophotometer	Peqlab, Erlangen, Germany
PH-Meter	Greisinger, Regenstauf, Germany
Precision balance	Sartorius, MA, USA
Powersupply	Biometra, Göttingen, Germany BioRad, Munich, Germany
Rotator	MS-L GmbH, Wiesloch
Semidry Blot	Biometra, Göttingen, Germany
Shaker TH25	Edmund Bühler, Tübingen
Shaking incubator	New Brunswick Edmund Bühler GmbH, Hechingen, Germany
Spectrophotometer Helios	Thermo Spectronic, Wuppertal, Germany
Table Centrifuge Ministar	VWR, Darmstadt, Germany

Thermocycler T3000	Biometra, Göttingen, Germany
Thermomixer compact	Eppendorf, Hamburg, Germany
Thermomixer Thermostat plus	Eppendorf, Hamburg, Germany
UV-Transilluminator GelDoc 2000	BioRad, Munich, Germany
Voltage power supply	BioRad, Munich, Germany
Vortexer Janke & Kunkel GmbH & Co. KG	IKA Labortechnik, Staufen, Germany
Water bath shaking	GFL, Burgwedel, Germany

Table 3: Instruments and equipment for tissue culture work

Instruments	Supplier
Biological Safety Cabinet Herasafe	Heraeus, Hanau, Germany
Cell Culture Incubator, Hera cell, Hera cell150	Thermofisher Scientific, Berlin, Germany
Centrifuge 5415R	Eppendorf, Hamburg, Germany
Centrifuge Rotofix32A	Hettich, Tuttlingen, Germany
Freezing chambers Nalgene® Mr Frosty	Thermo Scientific, Dreieich, Germany
Microscope Inverted Leica DMI 3000B	Leica Microsystems, Wetzlar, Germany
Pipetboy acu	Eppendorf, Hamburg, Germany
Pipettes	Eppendorf, Hamburg, Germany Gilson, Bad Camberg, Germany Finnpipette, Dreieich, Germany
Stereomicroscope	Schott, Mainz, Germany
Vortexer Janke & Kunkel GmbH & Co. KG Vortexer	IKA Labortechnik, Staufen, Germany Heidolph, Schwabach, Germany
Water bath	GFL, Burgwedel, Germany

Table 4: Instruments and equipment for histological work

Instruments	Supplier
Cryostat, Leica CM 1900	Leica Microsystems, Wetzlar, Germany
Fluorescence microscope	Leica Microsystems, Wetzlar, Germany
Fluorescence light source	Leica Microsystems, Wetzlar, Germany
Fluorescence light source X-Cite 120	Excelitas Technologies, Wiesbaden, Germany
Rolera MGI camera	Qimaging, BC, Canada
SPOT RT3 camera	Spotimaging, MI, USA
Surgical scissors	neoLab Migge Laborbedarf-Vertriebs, Heidelberg, Germany
Tweezers	GFL, Burgwedel, Germany

5.3. Chemicals

Table 5: Chemicals

Chemicals	Supplier
Acetone	Merck, Darmstadt, Germany
Acrylamide/Bisacrylamide 40%, 29:1	BioRad, Munich, Germany
Agarose MP	Roche, Grenzach-Wyhen, Germany
Albumine bovine fraction V	Serva, Heidelberg, Germany
Ampicillin sodium salt	Carl-Roth, Karlsruhe, Germany
Arabinose	AppliChem, Darmstadt, Germany
Bisodium Hydrogenphosphate-Dihydrate	Carl-Roth, Karlsruhe, Germany
Boric acid	Merck, Darmstadt, Germany

Calciumchloride	Merck, Darmstadt, Germany
Chicken embryo extract	US Biological, VWR International, Karlsruhe, Germany
Chloroquine Diphosphate	Sigma-Aldrich, Taufenkirchen, Germany
Chloramphenicol	AppliChem, Darmstadt, Germany
Collagenase type I (0,2%)	Worthington, MN, USA
p-Coumaric acid	Sigma-Aldrich, Taufenkirchen, Germany
DABCO	Carl-Roth, Karlsruhe, Germany
DAPI	Carl-Roth, Karlsruhe, Germany
DMEM (Dulbecco's Modified Eagles Medium)	Gibco BRL, Karlsruhe, Germany
Dimethyl sulfoxide (DMSO)	AppliChem, Darmstadt, Germany
DirectPCR Lyse Reagenz	Peqlab/VWR, Erlangen, Germany
EDTA Disodium salt dehydrate	Carl-Roth, Karlsruhe, Germany
Ethanol	Merck, Darmstadt, Germany
Ethidium bromide	Carl-Roth, Karlsruhe, Germany
Fetal bovine serum, heat inactivated	Gibco/LifeTechnologies, Karlsruhe, Germany
Formaldehyde solution 37%	Merck, Darmstadt, Germany
Glucose	Sigma-Aldrich, Taufenkirchen, Germany
L-Glutamine	Gibco/Lifetechnologies, Karlsruhe, Germany
Glycerol 87%	Sigma-Aldrich, Taufenkirchen, Germany
Glycine	Sigma-Aldrich, Taufenkirchen, Germany
HEPES	AppliChem, Darmstadt, Germany
Horse serum, heat inactivated	Gibco/LifeTechnologies, Karlsruhe, Germany
Hydrochloric acid 1N	Merck, Darmstadt, Germany
Hydrochloric acid 25%	Merck, Darmstadt, Germany
Isopropanol	Merck, Darmstadt, Germany
Kanamycin	Carl-Roth, Karlsruhe, Germany
LB-Agar-medium	Carl-Roth, Karlsruhe, Germany
LB-medium	Carl-Roth, Karlsruhe, Germany
Luminol	Sigma-Aldrich, Taufenkirchen, Germany
Matrigel	Becton Dickinson, Heidelberg, Germany
Methanol	Merck, Darmstadt, Germany
β-Mercaptoethanol	AppliChem, Darmstadt, Germany
Milkpowder	AppliChem, Darmstadt, Germany
Normal goat serum	Biozol, Eching, Germany
Paraformaldehyde	Merck, Darmstadt, Germany
PBS Dulbecco	Gibco/LifeTechnologies, Karlsruhe, Germany
Penicillin/streptomycin	Gibco/LifeTechnologies, Karlsruhe, Germany
Potassium chloride	Sigma-Aldrich, Taufenkirchen, Germany
Ponceau S	AppliChem, Darmstadt, Germany
Protease Inhibitor cocktail, Complete mini	Roche, Grenzach-Wyhlen, Germany
Protein Assay Dye (Bradford)	BioRad, Munich, Germany
Roti-Free Stripping buffer	Carl-Roth, Karlsruhe, Germany
Roti-Safe	Carl-Roth, Karlsruhe, Germany
SDS	Merck, Darmstadt, Germany
Sephadex G-50 Fine	GE Healthcare, Munich, Germany
SOB medium	Carl-Roth, Karlsruhe, Germany
TEMED	Merck, Darmstadt, Germany
Tris-Base	Calbiochem/ Merck, Darmstadt, Germany
Tris (hydroxymethyl)aminomethane	Merck, Darmstadt, Germany

TritonX-100	Merck, Darmstadt, Germany
Trypan blue, 0,4%	Gibco/LifeTechnologies, Karlsruhe, Germany
Trypsin/EDTA	Gibco/LifeTechnologies, Karlsruhe, Germany

5.4. Kit systems, markers, enzymes and nucleotides

Table 6: Kits

Kit	Supplier
BigDye® Terminator v3.1 Cycle Sequencing Kit	Applied Biosystems, Weiterstadt, Germany
HiSpeed Plasmid Midi Kit	Qiagen, Hilden, Germany
Lipofectamin, LTX	Thermo Fisher Scientific, Wuppertal, Germany
MOM Kit	Vector Laboratories, Enzo, Lörrach, Germany
pGEMT-easy Vector System 1	Promega, Mannheim, Germany
QIAprep® Spin Miniprep Kit	Qiagen, Hilden, Germany
QIAquick® Gel Extraction Kit	Qiagen, Hilden, Germany
QIAquick® PCR Purification Kit	Qiagen, Hilden, Germany
Quickligase Kit	New England Biolabs, Frankfurt, Germany
VenorGEM mycoplasma diagnosis test	Biochrom, Berlin, Germany

Table 7: Standard markers

Markers	Supplier
100 bp Standard marker	New England Biolabs, Frankfurt, Germany
1 kb Standard marker	New England Biolabs, Frankfurt, Germany
Precision Plus Protein ™ All Blue Prestained Protein Standards	BioRad, Munich, Germany
HiMark™ Pre-stained Protein Standard	Thermo Fisher Scientific, Wuppertal, Germany

Table 8: Enzymes

Enzymes	Supplier
Calf intestine Phosphatase	New England Biolabs, Frankfurt, Germany
DNaseI	Invitrogen, Karlsruhe, Germany
GoTaq^{TM} DNA-Polymerase	Promega, Mannheim, Germany
Proteinase K	AppliChem, Darmstadt, Germany
Phusion^{TM} DNA-Polymerase	Finnzymes, Espoo, Finnland
Restriction Enzymes	New England Biolabs, Frankfurt, Germany
Quickligase	Promega, Mannheim, Germany

Table 9: Nucleotides

Markers	Supplier
dNTPs (je 100 mM)	Promega, Mannheim, Germany

5.5. Plasmids

Table 10: Plasmids

Official name	Supplier
pBACe3.6 (Clone bMQ- bMQ389g17)	Source bioscience, Berlin Germany
pCMV-Tag3A	Schuelke lab
pCR-Script-AMP	Stratagene, Amsterdam-Zuidoost, Niederlande
pEGFP-N3-L221K	Schuelke lab
pENTRA1A-Cox8a	Schuelke lab
pGEM-T Easy	Promega, Mannheim, Germany
PL452	National Cancer Institute, Rockville, MD, USA
pTagRFP-Mito	Evrogen, Heidelberg, Germany
pEGFP-N3-L221K	Schuelke lab

5.6. Bacteria

Table 11: Bacteria

Bacteria	Genotype	Supplier
E. coli JM109	endA1 recA gyrA thi hsdR17 (rk-, mk+) relA1 supE44Δ (lac-proAB, [F', traD36, pro AB laqIqZΔM15]	Promega, Mannheim, Germany
E. coli SW106	mcrA Δ(mrr-hsdRMS-mcrBC) ΔlacX74 deoR endA1 araD139 Δ(ara, leu) 7697 rpsL recA1 nupGφ 80dlacZΔM15 galU galK [λc1857 (cro-bioA)<>Tet] galK+gal490 (cro-bioA)<>araC-PBADCre gal+ ΔgalK	National Cancer Institute, Rockville, MD, USA
XL-10 Gold Ultracompetent cells	TetrD(mcrA)183D(mcrCB-hsdSMR-mrr)173 endA1 supE44 thi-1 recA1 gyrA96 relA1 lac Hte [F´ proAB lacIqZDM15 Tn10 (Tetr) Amy Camr]	SINA Science Services GmbH, Berlin, Germany

5.7. Antibodies

Antibodies were purchased from Abcam (Cambridge, UK), Novocastra/Leica (Wetzlar, Germany) Merck/Millipore (Darmstadt, Germany), Roche (Grenzach-Wyhlen, Germany), DSHB (IO, USA), ThermoFisher Scientific (Wuppertal, Germany). All antibodies are listed in Appendix 10.1, Table A2-3.

5.8. Oligonucleotide primers for PCR

All oligonucleotide primers were custom synthesized the the MWG Biotech AG (Ebersberg, Germany) company. A complete list of all used oligonucleotide primers is attached in the Appendix 13.1, Table A1.

5.9. Cell lines

Cell lines were cultured in an incubator at 37°C, 95% humidity and 5% CO_2 atmosphere. All cell culture work was done under sterile conditions in a biological safety cabinet.

Table 12: Cell lines, primary murine cells and media used for culturing

Cell line/Primary cells	Description/medium
293	human embryonic kidney epithelial cells; for transfections →DMEM-standard
COS-1 cells	monkey fibroblasts-like cells derived from kidney, for transfection → DMEM-standard
Primary murine satellite cells/ myoblasts	murine EDL muscle derived; differentiation of satellite cells into myotubes
Single fibers	murine EDL muscle derived, immunofluorescence, satellite cell-derived myoblasts
ES cell line	murine, Sv129 derived

5.10. Animal experiments

5.10.1. Mouse strains and animal husbandry conditions

Animals were bred and kept under specific pathogen-free (SPF)-like conditions in the animal facilities of the Charité Cross Over building, as well as in the central animal facility FEM of the Charité Universitätsmedizin Berlin. Animals for organ preparation were sacrificed by cervical disloction. The experiments were performed in compliance with the local animal experimentation guidelines. Animal experiments were approved by the local authorities (LaGeSo Berlin, T 0222/13).

Table 13: Mouse strains

Name/Reference	Internal name	Supplier
C57BL/10ScSn-Dmd^{mdx}/J	mdx	Jackson Laboratory, Maine, USA
Cre-deleter (Schwenk *et al.*, 1995)	Cre	Birchmeier Lab, MDC-Berlin, Germany
$Dmd^{EGFP-Cre-deleter}$	$Dmd^{EGFPneo}$	
Dmd^{EGFP}	Dmd^{EGFP}	

5.11. Software

Table 14: Software

Program	Supplier	Application
Adobe Photoshop CS5	Adobe GmbH, Munich, Germany	Image editing
DNAStar Lasergene 8	DNA Star Medison, USA	Sequence analysis
Image J	Rasband, WS, USA	Images editing

Image Pro Plus	Media Cybernetics, PA, USA	Camera software
MS Office	Microsoft Corporation WA, USA	Text editing, scheme drawing
Vector NTI	Invitrogen, Karlsruhe, Germany	Cloning

6. METHODS

6.1. Methods for the generation of a transgenic Dystrophin-EGFP reporter mouse

The main aim of this work was to generate a reporter mouse, in which a FLAG-EGFP sequence was inserted behind the last exon of the *Dmd* gene so that a C-terminally tagged dystrophin-EGFP protein would be expressed. This model will facilitate *in vivo* studies on dystrophin and DMD, as there would be no need for antibody staining.

In summary, to generate the *Dmd* reporter allele, I constructed a targeting vector using the method of recombineering so that a 10.943 kb DNA fragment spanning intron 78, exon 79 and part of the 3'UTR of the murine *Dmd* was excised from a genomic X-chromosomal BAC clone and subcloned. Afterwards, the *Dmd* exon 79 was modified by changing the stop codon into a leucine and inserting a FLAG-EGFP sequence in-frame, followed by a neomycin cassette (*neo*) in the 3'UTR that was flanked by two lox*P* sites. The targeting vector was linearized with *Sal*I and electroporated into 129Ola-derived ES cells. Correctly targeted ES clones were selected by Southern blotting *via* restriction enzyme sites (*Bgl*II and *BamH*I) that had been introduced into the vector and injected into C57BL/6 blastocysts. Chimeras were generated and mated to C57Bl/6N mice. Germline transmission of the targeted dystrophin allele was confirmed in the F1 generation of the heterozygous females *via* PCR screening for the neomycin cassette as well as by Southern blot analysis. The ES cell culture and generation of transgenic mice (F1 generation) have been done commercially (Polygene AG, Switzerland). Mice were then bred under normal husbandry conditions. The *neo* cassette was removed by crossing mice from the F1 generation mice with mice that ubiquitously expressed the *Cre* recombinase (Schwenk *et al.*, 1995). Below I describe the single steps in more detail.

6.2. Generation of the targeting vector *via* recombineering

Generation of the targeting vector was done using the method of recombineering *(recombination-mediated genetic engineering)* (Copeland *et al.*, 2001; Liu *et al.*, 2003; Muyrers *et al.*, 2001). Recombineering is a molecular genetic technique based on genetic engineering by *in vivo* DNA manipulation in *Escherichia coli (E. coli) via* homologous recombination. This system allows the construction of DNA molecules with precise junctions and is independent of the location of appropriate restriction sites, which overcomes the

limitations of conventional cloning strategies. It is suitable for modification of murine genomes and for the cloning of long fragments. This method exploits a phage-based recombination system in *E. coli* which forces the introduction of a linear DNA of interest sequence into a plasmid provided there is enough homology at the 5' and 3' end of the DNA of interest. The proteins responsible for homologous recombination are produced by a replication defective λ Phage integrated into the bacterial genome. The red genes *exo*, *bet* and *gam* regulate the homologous recombination allowing insertion of double stranded DNA fragments into plasmids, BACs (*bacterial artificial chromosomes*) or PACs (*P1-derived artificial chromosomes*). The genes are under the control of the PL promoter und a temperature sensitive repressor cI857. At low temperature (30-34°C) the repressor is active, but raising the temperature to 42°C leads to deactivation of the repressor and expression of the red genes. *Exo* encodes a 5'-3' exonuclease that recognizes double strand breaks in linear DNA and digests the 5' end of these DNA strands. The respective 5' overhangs are then bound by the *bet* encoded protein bringing the homologous regions close together (Poteete, 2001; Stahl, 1998). The *gam* encoded protein prevents the degradation of linear DNA *via* inhibition of the bacterial RecBCD-exonuclease activity. This is necessary as the DNA to be integrated *via* recombineering is mostly in the form of short PCR fragments, which would be degraded if RecBCD system was not blocked.

The 10.943 kb genomic fragment spanning intron 78, exon 79 and part of the 3'UTR of the *Dmd* gene was subcloned from a murine Sv129-derived BAC clone (GenomeCube, bMQ389g17) *via* recombineering and gap repair into a pCR-Script vector (Stratagene, Holland) containing homology arms. The HAs enabled the homologous recombination and retrieval of the *Dmd* fragment of interest, thus generating *Dmd* exon 79 retrieval vector. In a second recombineering step, *Dmd* exon 79 was modified so that the stop codon was exchanged for a leucine (TAG>TTG) and a FLAG-EGFP sequence inserted in-frame followed by a sequence in the 3'UTR containing a lox*P* flanked *neo* cassette regulated by PGK and Em7 promoter for expression in prokaryotic and eukaryotic cells, respectively. The so generated targeting vector included also a *Sal*I restriction enzyme site for linearization and subsequent electroporation into ES cells as well as *Bgl*II and *BamH*I restriction sites for Southern blot screening of positive ES clones for homologous recombination. The results of the detailed cloning steps are described in the section 7.1.1.

6.2.1. Plasmid DNA preparation from *Escherichia coli*

Small-scale plasmid DNA preparations for analytical purposes were done using the *QIAprep® Spin Miniprep Kit* (Qiagen, Hilden, Germany). The method is based on the alkaline lysis of bacterial cells, modified after (Birnboim and Doly, 1979). 5 ml of an overnight culture of transformed *E. coli* JM109 or XL-10 Gold bacteria were used according to manufacturer's instructions.

For preparative purposes midi preparations were performed using *HiSpeed Plasmid Midi Kit* from the company Qiagen according to manufacturer's instructions with a total bacterial culture volume of 50-100 ml. The isolation and purification is based on the alkaline lysis of bacterial cells and binding of plasmid DNA to anion-exchange columns under low-salt conditions. DNA was eluted in 150 µl TE buffer and concentration adjusted to 1 µg / µl. All plasmid DNA concentrations were determined using a Nanodrop™ 1000 spectrophotometer.

6.2.2. BAC DNA preparation from *Escherichia coli*

BAC plasmid DNA (clone bMQ389g17, backbone:pBACe3,) encoding a fragment from the *Dmd* gene of the SV129 mouse was prepared from a glycerol stock after plating single colonies and inoculating a 5 ml overnight culture in LB medium supplemented with chloramphenicol. Overnight culture was pelleted for 5 min at 2,000 x *g*, the supernatant removed, the pellet dissolved in 250 µl buffer P1 (from *QIAprep® Spin Miniprep Kit* from Qiagen) and transferred to a microcentrifuge tube. 250 ml P2 buffer were added, followed by mixing and incubation for <5 min at room temperature. Buffer N3 was added, followed by mixing and incubation on ice for 5 min. The supernatant was cleared by two rounds of centrifugation at 13,600 x *g* for 5 min in a tabletop centrifuge. Each time the supernatant was transferred into a new tube. DNA was precipitated by adding 750 µl isopropanol, mixing and centrifugation for 20 min at 13,600 x *g*. The pellet was washed once in 70% ethanol, air-dried and dissolved in 50 µl HPLC-water ('NCI at Frederick: Protocols'). The BAC DNA was analyzed for containing the correct *Dmd* genomic sequence using specific PCR primers that amplified a fragment at around *Dmd* exon 79. BAC DNA was used for recombineering.

6.2.3. Transformation of *Escherichia coli* with plasmid DNA

Chemically competent *E. coli* JM109 and XL10-Gold bacteria were used for transformation with plasmid DNA. The competent bacteria were thawed on ice and aliquots of 50 µl or 100 µl, respectively, were used for each transformation. Plasmid DNA or ligation mixture was added to the cells followed by 30 min incubation on ice. Cells were heat shocked for 2 minutes at 42°C in water bath and put back on ice for 2-3 minutes. The fast change in the temperature leads to stretching of the bacterial membrane, which supports the plasmid uptake. Subsequently, 500 µl pre-warmed SOC – medium (SOB medium plus 20 mM glucose; SOB medium: 0.5% (w/v) yeast extract, 2% (w/v) tryptone, 10 mM NaCl, 2.5 mM KCl, 20 mM $MgSO_4$) were added to the cells and the samples were incubated for at least 45 min in the shaker at 37°C. The bacteria were pelleted at 5,000 x *g* for 2 min and 450 µl medium was discarded. The cells were resuspended in the remaining volume and plated on LB plates supplemented with either ampicillin (100 µg/ml), kanamycin (30 µg/ml), or chloramphenicol (20 µg/ml) for later selection of positive clones transformed with plasmid or BAC DNA, encoding the respective resistance gene. Plates were incubated over night at 37°C.

6.2.4. Culturing conditions and long-term storage of *Escherichia coli*

Single bacterial clones were picked from the plates and used to inoculate a culture with 2-150 ml LB-medium supplemented with the respective antibiotic. Agar plates with transformed bacteria were stored at 4°C for several weeks. For long term storage glycerol stocks were prepared by adding glycerol to the *E. coli* overnight culture to a final concentration of 20%. The mixture was flash frozen in liquid nitrogen and stored at -80°C. Bacteria were recovered by scratching a little amount out of the glycerol stock and plating it on LB agar plates containing appropriate antibiotics. Single positive clones were picked and inoculated into a bacterial culture for small or bigger scale DNA plasmid preparation.

6.2.5. Preparation of electro-competent cells for recombineering and induction of λ-genes

Electro-competent cells for recombineering were prepared by inoculation of 0.5 ml of an overnight culture (*E. coli* SW106) in 35 ml LB medium. The bacterial cells were incubated at 32°C until they reached an OD_{600} of 0.4-0.6. For activation of the recombineering enzymes the bacterial culture was incubated for 15 min at 42°C in a shaking water bath. Half of the culture

was induced; the other half was left at 32°C and used as a control. Both the induced and uninduced cells were rapidly chilled on ice/ -water slurry and incubated for 10 min on ice. Cells were spun down for 5 min at 5,300 x g and washed three times with pyrogen free water. The supernatant was transferred into microcentrifuge tubes and centrifuged at 10,000 x g for 30 sec at 4°C. The supernatant was aspirated carefully and cells suspended in 1 ml of ice-cold H_2O. After repeating this step, the cell pellet was resuspended in 200 µl of sterile cold distilled H_2O and kept on ice until used.

For expression of the *Cre*-gene and subsequent excision of the selectable marker (*neo* cassette), 0.5 ml of overnight *E. coli* SW106 culture were incubated in 35 ml of LB medium at 32°C until reaching OD_{600}=0.4. Subsequently, arabinose was added to a final concentration of 0.1% (w/v) and the cells were incubated for a further 1 h at 32°C. Cells were then used for electroporation.

6.2.6. Electroporation of competent bacterial cells

For the introduction of DNA into electro-competent cells *via* a mixture of bacteria and plasmid-DNA was poured into a pre-cooled electroporation cuvette (width: 0.1 cm) and electroporation was carried out with following parameters: voltage: 1.65 kV, capacity: 25 µF, resistance: 200 Ω. The mixture was then transferred to and resuspended in 1 ml SOC medium, incubated for 1 h at 32°C and streaked onto LB plates without antibiotics (recombineering) or containing appropriate antibiotics (electroporation of retrieval vector or BAC DNA). For the introduction of the *Dmd* fragment from the BAC DNA into pCR-Script and generation of the *Dmd* exon 79 retrieval vector, 100 ng linear plasmid DNA, and 100 ng BAC DNA were added to 50 µl heat-inducted electro-competent cells. For the generation of the targeting vector, electroporation was done using 10 ng retrieval vector and 150 ng linearized PL452 vector containing the modified *Dmd* exon79 with the EGFP-FLAG-lox*P* flanked *neo* cassette. For the excision of the selection cassette, 1 ng plasmid DNA was added to 50 µl arabinose induced electro-competent cells. Correct recombinants and positive clones were then picked and analyzed *via* colony PCR and automatic sequencing.

6.2.7. Polymerase chain reaction (PCR)

The PCR is a method for the exponential amplification of DNA fragments. In the first step (denaturation), the DNA is separated into single strands, followed by the annealing process, at which oligonucleotide primers specific for a particular DNA region bind at the single strands. A heat stable DNA polymerase synthesizes the second DNA strand starting from the matrix complementary double strands (elongation). In this work, Phusion™ DNA-Polymerase (Finnzymes, Espoo, Germany) with a proofreading ability or the GoTaq ™ DNA-Polymerase (Promega, Mannheim, Germany) without proofreading function were used. A standard reaction volume for the Phusion™ polymerase contained the following components: 10 µl of 5 x reaction buffer, 0.2 mM dNTPs, 0.5 µM forward and reverse primers, 3% DMSO, 1 unit DNA-polymerase, and 0.2-150 ng template DNA in a total reaction volume of 50 µl.

Cycling conditions for the PCR reactions were as follows: 95°C, 5 min; 25-35x (95°C, 30-60 sec; 54-65°C, 30-60 sec; 72°C for the duration of 1 min/kb); 72°C, 10 min.

The GoTaq ™ DNA-Polymerase was used for colony PCR to find and verify correctly cloned plasmids in the positive bacterial clones. Clones were picked and diluted in 20 µl water, boiled and 1 µl was used as template for the PCR reaction.

Oligonucleotide primers used for cloning contained 5' of the primer binding sequence overhangs with the characteristic recognition sequence for the restriction endonucleases which allowed the digestion of the linear fragments and their subsequent cloning into a vector. They were specifically HPLC purified to prevent the incorporation of falsely synthesized nucleotides. The modified exon 79 fused with the FLAG sequence was also incorporated into the oligonucleotide *via* primer overhangs.

6.2.8. DNA digestion with restriction enzymes

For restriction analysis plasmid DNA or BAC DNA were digested with restriction endonucleases obtained from New England Biolabs and used in the recommended buffers in a 30 µl reaction volume. For 1 µg DNA 2-10 units restriction enzymes and buffer were used and incubated for 1 to 3 hours at 37°C. Correct digestion was verified by agarose gel electrophoresis (see section 3.1.10). For subcloning of the 10.943 kb fragment from BAC DNA into pCR-Script I used the restriction endonucleases *Sal*I, *Hind*III and *Not*I. For cloning of FLAG-

EGFP-lox*P-neo*-lox*P* into PL452 I used the restriction endonucleases *Kpn*I, *EcoR*I, *BamH*I, *Sac*II. Linearization of the retrieval plasmid and of the targeting vector was done by *Hind*III and *Sal*I digestion, respectively. *BamH*I and *Bgl*II control digestions of the targeting vector were performed as these two enzymes were to be used for Southern blot analysis of successfully transformed ES cell clones after positive selection. For the cloning of the modified *Dmd* exon 79 plus FLAG-mEGFP cassette into pCMV-Cox8 vector *Pst*I and *Hind*III were used.

6.2.9. Agarose gel electrophoresis

Agarose gel electrophoresis separates linear DNA fragments according to their size. 0.7-1.5% (w/v) agarose gels in 0.5 x TBE buffer (5x TBE stock solution: 450 mM Tris Base, 450 mM Boric acid, 10 mM EDTA, add 1 L H_2O) was used. The gels were prepared by dissolving the required amount of agarose in TBE buffer through boiling in a microwave stove. After the solution had cooled down, ethidium bromide was added to the agarose solution to a final concentration [0.3 µg/ml] immediately before casting the gel. Ethidium bromide fluoresces under UV light when intercalating with DNA, hence enabling its detection. Solidified agarose gels were placed into the gel chamber, the DNA samples were mixed with 6 x DNA loading dye (0.25% bromphenol blue; 15% Ficoll 400) and pipetted into the gel pockets. In parallel, a standard molecular size marker was loaded for determination of the fragment lengths. Electrophoresis was performed at 8-12 V/cm in 0.5% TBE buffer. DNA bands were visualized with a transilluminator (λ = 366 nm) and documented with a camera (Gel Doc, Bio-Rad, Munich).

6.2.10. DNA extraction from agarose gels

For the extraction and purification of DNA fragments of interest from an agarose gel, these were visualized on the gel by UV-light (λ = 366 nm) and the gel piece containing the fragment was cut out with a scalpel. The purification was done using the *QIAquick Gel Extraction Kit* (Qiagen, Hilden, Germany) according to manufacturer's instructions. The elution of the DNA fragment was done with 30 µl TE buffer.

6.2.10.1. Purification of the PCR products

PCR products used for cloning were purified after digestion with restriction enzymes in order to remove excessive reaction components and adhering endonucleases. The purification was

performed using the *Qiagen PCR Purification Kit* (Qiagen) according to manufacturer's instructions. Elution volume was 30 µl.

6.2.11. Cloning of DNA Fragments

Digested and purified PCR products and agarose gel fragments were used for cloning into a plasmid that was digested and linearized with the same restriction enzymes as the fragment to be inserted in order to produce compatible ends. The recipient linearized plasmid DNA (backbone) and the DNA fragment to be introduced into the vector (insert) were used in a ligation reaction at a molar ratio of 3:1 (insert:backbone). The molecular mass of each fragment was calculated using the following formula:

insert mass [ng] = 3 x (**insert length** [bp]/ **backbone length** [bp]) x **vector mass** [ng].

In a typical reaction, 20 µl ligation reaction 50 ng backbone vector were used, together with 2x Quickligase® buffer and Quickligase® enzyme (Invitrogen) for 20 min at room temperature. 1-5 µl ligation mix was used for transformation of chemically competent bacterial cells (section 6.2.3).

For the Southern blot analysis, 5' and 3' DNA probes were generated for the identification of positive ES clones that had underwent homologous recombination with the targeted region at the murine *Dmd* locus. The fragments were subcloned into the pGEM-T easy vector (Promega) *via* a process called "TA cloning". The vector contains 5' T-overhangs. Blunt end PCR-Fragments that were generated with the proof-reading Phusion™ DNA-polymerase (Finnzymes, Espoo, Finland) were incubated for 12 min at 72°C with the GoTaq™ DNA-Polymerase (Promega, Mannheim, Germany) and dATPs in order to add 3' A-overhangs to the fragments for subsequent TA cloning. Ligation and transformation were carried out as described above.

Positive clones were identified using colony PCR, DNA was then purified from the bacteria by mini or midi-preparation as described.

6.2.12. DNA sequencing

For each newly cloned DNA fragment, the correct sequence was verified *via* Sanger sequencing (Sanger *et al.*, 1977). The method is based on the use of fluorescently marked di-desoxynucleotides in a reaction that leads to a base specific chain termination during DNA-

synthesis. This leads to generation of DNA fragments of different lengths, which can be separated by various electrophoretic techniques (e.g. capillary electrophoresis) and assigned to the corresponding di-desoxynucleotide. In this way, the nucleotide sequence of a DNA fragment can be determined precisely up to a read length of ≈800-1,000 bp. Automatic sequencing was performed using the BigDye® Terminator v3.1 Cycle Sequencing Kit (Applied Biosystems) according to the manufacturer's instructions and an ABI 3100 Genetic Analyzer (Applied Biosystems). For each sequencing reaction, 150 ng of plasmid were used. The sequence reads were analyzed using the DNAStar software.

6.3. General tissue culture methods

6.3.1. Tissue culture conditions for eukaryotic cell lines

Eukaryotic cell lines and primary, isolated cells were kept in a cell culture incubator at 37°C, 5% CO_2 and 80-90% humidity. The cells were supplemented every 2 to 3 days with fresh medium. The adherent 293 and COS1 cell lines used in this work were cultured in DMEM supplemented with 10% (v/v) fetal calf serum, and 1% penicillin/ streptomycin.

Cells were split at approximately 90% confluence every 3-4 days by trypsination according to the following protocol: Cells were washed once with PBS to remove residual FCS, which would interfere with trypsin activity. After washing, trypsin-EDTA solution (2 ml for 25 cm^2 dishes, 3 ml for 75 cm^2 dishes, and 5 ml for 175 cm^2 dishes) was added. After 1 min, trypsin was removed and residual enzyme was inactivated by addition of an excess DMEM supplemented with FCS. If necessary, the culture flask had to be incubated sometimes for 3-5 min at 37°C until all cells detached. Cells were than resuspended, and eventually split. The isolation and culturing of single fibers with their attached satellite cells is described in section 6.5.3..

All cell cultures were regularly tested for potential mycoplasma contamination using the VenorGEM® Mycoplasma Diagnosis test (Biochrom).

6.3.2. Freezing and thawing of cells

For long-term storage, cells were kept in liquid nitrogen. Adherent cells were trypsinized, diluted in excess of complete culture medium and counted. The cell suspensions were then transferred to a 50 ml Falcon tube and pelleted by centrifugation for 10 min at 200 x *g*. The supernatants were discarded and the cell pellets were resuspended in 90% FCS, 10% DMSO

at a concentration of 10^7 cells/ml. 1 ml aliquots of the cell suspensions were transferred to cryotubes in a pre-cooled (4°C) freezing container and were incubated at -80°C overnight before the cryotubes were stored in liquid nitrogen for permanent storage.

For restauration of cryo-stocks, cells were thawed rapidly in a water bath at 37°C. The cell suspension was diluted in 10 ml pre-warmed medium in a 15 ml Falcon tube and centrifuged for 5 minutes at 200 x g. The DMSO-containing supernatant was discarded and the cell pellet was resuspended using 12 ml of complete medium. Finally, the cell suspension was transferred into a 75 cm^2 cell culture flask and cultured at 37°C.

6.3.3. Cell counting

6.3.3.1. Cell counting by using counting chamber

Cell numbers were determined by using the Neubauer cell counting chamber. 10 µl of well-resuspended cell suspension was mixed with 1x trypan blue solution. Trypan blue stains only dead cell and the viable, unstained cell were counted. ≈10 µl the mixture was filled into the counting chamber and cells were counted. The cell number in two big squares was determined and then divided by 2 to obtain the average count in one big square (one big square corresponds to a volume of 0.1 µl), which gives the value 'counted cells' and can be replaced in the following formula:

$$cells/ml = counted\ cells\ x\ F\ x\ 10^4$$

F is the dilution factor of the cell suspension and can be calculated as follows:

F= (cell suspension 10 µl + trypan blue suspension x µl)/ cell suspension 10 µl

6.3.4. Transient transfection

To test whether the modified exon 79 fragment containing the in-frame FLAG-EGFP cassette was expressed properly, the fragment was subcloned into the mammalian expression vector pCMV-Tag3A and transfected into COS1 cells. The sequence of the *Cox8a* mitochondrial targeting signal was cloned 5' of the start codon of the cassette so that the exon 79*FLAG-EGFP fragment would be targeted into the mitochondria. Therefore, co-transfection with the mammalian expression vector pTag-RFP-mito was performed. This vector fluorescently labels the mitochondria with red fluorescence and co-localization with the EGFP signal would

confirm the correct expression of the EGFP cassette. Transfection was carried out using the Lipofectamine® LTX reagent (LifeTechnologies) according to the manufacturer's instructions. 24 h after transfection cells were imaged for EGFP and RFP fluorescence.

6.4. Animal experiments

6.4.1. Animal husbandry conditions

Mice were kept and bred according to animal welfare guidelines under the registration of the LaGeSo (T 0222/13) in the SPF animal husbandry facility of the Charité (FEM) and of the Charité Cross Over Building. The breeding conditions were constant temperature at 22°C with humidity from 50 to 60%, 12 h light/dark rhythm, light brightness 300 lux, and enriched environment. The animals were fed with a standard pelleted diet and autoclaved drinking water. The general state of health was monitored at regular intervals by the experimenter, by animal care-takers, as well as by a veterinarian. Microbiological and virological tests for common rodent pathogens were performed at regular intervals.

6.4.2. Generation of *Dmd^EGFP* reporter mice

The work comprising homologous recombination in ES cells, screening for correct insertion (using our predesigned Southern blot probes), blastocyst injection, as well as breeding of the F1-generation and screening for germline transmission was done commercially by the Polygene AG, Ruemlang, Switzerland.

6.4.3. ES cell electroporation, generation of chimeric mice and germline transmission

The targeting vector was linearized using *Sal*I and electroporated into SV129Ola-derived ES cells. G418 (0.4 mg/ml) was used to select for stable transfection. After 10 days of selection, a total of 200 clones was picked and analyzed *via* Southern blot analysis. After expansion and freezing of the isolated clones, DNA was prepared and digested with the restriction enzyme *Bgl*II, run by agarose gel electrophoresis and blotted onto a Hybond® membrane. A [^{31}P]-radioactively labeled 5'-external probe was used to detect the proper genomic region on the X-chromosome. The primers used for generation of the probes are listed in Appendix 13.1, Table A1. After hybridization to the *Bgl*II digested genomic DNA, a fragment of 15.8 kb should be detected for the wildtype allele, whereas the targeted allele would result in a fragment of

only 6.2 kb. All positive clones were further analyzed *via* Southern blot analysis on the 3' end for homologous recombination using a 3' external probe. The correct clones were then thawed, expanded, and DNA was prepared. For confirmation, a second Southern blot analysis was performed using the restriction enzyme *BamH*I and the 3' external probe. Correct 129Ola derived ES cells clones were injected into blastocysts of C57Bl/6 mice. Injected blastocysts were transferred into two CD-1 foster mice. The chimeras were mated to C57Bl/6N mice for germline transmission of the modified dystrophin locus at the X chromosome. Germline transmission was confirmed by coat color, as well as *via* Southern blot analysis, PCR genotyping.

6.4.4. Removal of the *neo*-cassette using a ubiquitous Cre-deleter mice

Animals with successful germline transmission of the *Dmd*-FLAG-EGFP-lox*P-neo*-lox*P* construct were then crossed with a ubiquitous *Cre*-expressing (Cre-deleter) mouse in order to remove the lox*P* flanked *neo* cassette. The resulting *Dmd*^{EGFP} mice and their wildtype littermates were subsequently used for analysis and characterization. All animals of the F1 and F2 generation were genotyped *via* PCR on DNA extracted from tail biopsies.

6.4.5. Genotyping of the mice

The DNA was extracted from the tail biopsies using the *GenScript TissueDirect*^{TM} *Multiplex PCR System* (GenScript Corporation, Piscataway, NJ, USA) according to the manufacturer's instructions. Genomic DNA was obtained directly during lysis of the tissue without any further purification steps and used for PCR amplification with gene specific primers (Appendix 13.1, Table A1).

6.4.6. Sacrificing and sectioning of the animals

Donor animals were sacrificed by cervical dislocation. The dead animals were fixed in dorsal position on a cork- tray and disinfected with 70% ethanol. The fur was removed carefully and the following organs were prepared for cryopreservation and subsequent sectioning (section 6.5.1) or used for extraction of single fibers and satellite cells (section 6.5.2): Muscles: *tibialis anterior* (TA), *extensor digitorum longus* (EDL), *quadriceps* (QC), gastrocnemius (GC), *soleus* (SOL) and diaphragm (DIA); as well as heart, stomach, gut, brain, and eyes.

6.5. Methods for analysis of the transgenic mice

6.5.1. Tissue and section preparation

Tibialis anterior (TA), *extensor digitorum longus* (EDL), *quadriceps* (QC), *gastrocnemius* (GC) and *soleus* (SOL) muscles as well as the diaphragm (DIA), heart, *ileum*, *duodenum*, *colon*, stomach, brain, and eye were dissected from 8 to 12-weeks-old (adult) or 6-month-old male Dmd^{EGFP} mice and their age- and sex matched wildtype littermates. The tissue was mounted on Tissue-Tek® O.C.T. (Hartenstein, Germany), frozen in fluid nitrogen cooled isopentane and processed for cryostat sectioning. 8 µm cross sections were collected from the mid-belly of the muscles and either stored at -80°C or directly fixed and stained.

6.5.2. Isolation of EDL-muscle derived myofibers

EDL muscles were dissected from the hind limbs of 8-weeks-old Dmd^{EGFP} mice and their wildtype littermates and digested in 0.2 % collagenase type I (Sigma-Aldrich, Germany) in DMEM as previously described (Pasut *et al.*, 2013). Muscles were transferred to DMEM-filled horse serum-rinsed Petri dishes using a heat-polished glass Pasteur pipette. Muscles were triturated until the fibers became separated, transferred to a fresh dish and incubated at 37°C, 5% CO_2. Intact fibers were transferred under the dissecting stereomicroscope into fresh DMEM-filled horse serum-rinsed dishes using a thinly bored Pasteur pipette to exclude any cell debris. The isolated myofibers were either fixed for immunofluorescence (IF) staining or kept in culture in for satellite cells differentiation.

6.5.3. Culture and differentiation of single fiber-derived satellite cells

The isolated myofibers including their attached satellite cells (SC) were cultured in DMEM supplemented with 20% fetal bovine serum (Sigma-Aldrich), 10% horse serum (HS, Sigma-Aldrich) and 1% chicken embryo extract (CEE, Ultrafiltrate, VWR International, Germany) in dishes that had been coated with 10% Matrigel® (BDBiosciences, Germany) in DMEM (Danoviz and Yablonka-Reuveni, 2012). After 2 days, satellite cells-derived myogenic progenitors started to migrate off the myofibers and formed myogenic colonies composed of proliferating myoblasts that differentiated into myotubes between days 6 and 8. This process was enhanced by changing the growth medium after 5 days to low horse serum (4% HS)

medium. Differentiating myoblasts were observed daily under the microscope and fixed after 8 days for subsequent immunofluorescent staining.

6.5.4. Histological analysis and immunhistochemistry

8 μm cryosections from either adult or aged mice were stained with haematoxylin/eosin (H&E) at the institute of Neuropathology (Charité, Berlin).

8 μm cryosections from adult mice were analyzed *via* immunohistochemistry (IHC) and immunofluorescence (IF). Single fibers and differentiated myoblasts were analyzed *via* immunofluorescence.

Immunohistochemistry on cryosections was performed at the Institute of Neuropathology (Charité, Berlin) with primary antibodies and appropriate biotinylated secondary antibodies and diaminobenzidine visualization of the peroxidase reaction. In order to suppress unspecific background staining, we used the M.O.M.™ kit (Vector Laboratories, Burlingame, CA, USA) for all primary mouse antibodies. All dilutions of the primary antibodies used in this study are described in Appendix 13.5, Table A2-3.

Immunofluorescent staining was performed on single fibers, differentiated myoblasts and 8 μm muscle cryosections. Fibers and myoblasts were fixed in 4% PFA, washed, incubated for 1 h at room temperature in blocking solution (BS) containing 5% normal goat serum, 0.5% BSA and 0.2% Triton X-100), followed by overnight incubation with primary antibodies in BS. The cryosections were fixed in ice cold acetone, washed in PBS, blocked 30 min in 5% normal goat serum with followed by 1 h incubation with primary antibodies in 3% BSA in PBS. For staining with primary mouse antibodies cryosections were blocked additionally for 1 h with an immune globulin blocking reagent from the M.O.M.™ kit. After the primary antibody incubation, fibers, myotubes and cryosections were washed and incubated for 1 h with fluorescent dye coupled secondary antibodies (Alexa488 and 568, LifeTechnologies, CA, USA), washed three times in PBS and counter stained with DAPI.

Primary antibodies in this study were directed against the following proteins or protein-domains: laminin, β-spectrin, dystrophin, Dys2, Dys1, MANDYS19, H4, GFP, FLAG, GFAP, CD31, α-sarcoglycan, β-sarcoglycan, γ-sarcoglycan, α-dystroglycan, nNOS, α-bungarotoxin,

vinculin, α-actinin2 and utrophin. Images were recorded with an inverted fluorescent microscope (Leica DMI4000).

6.5.5. Western blot analysis

In order to analyze the expression of the dystrophin protein and potential isoforms in the muscles of transgenic mice we performed Western blotting. Proteins were extracted from the tissue of interest and separated by SDS-PAGE according to their molecular size. Proteins were then transferred onto a membrane by electro-blotting and incubated with an antibody specific for the protein of interest and visualized using a chemiluminescent reaction. Proteins were extracted from *tibialis anterior* (TA) muscle or brain of 8-weeks-old male *Dmd*^{EGFP} mice and their wildtype littermates after homogenization in liquid nitrogen and sonification in lysis buffer (75 mM Tris, pH 6.8, 1% SDS) containing a proteinase inhibitor cocktail (Complete®, Roche-Diagnostics). The Western blot analysis was done at the Institute of Neuropathology (Charité, Berlin) and at the Université de Versailles St-Quentin (Montigny-le-Bretonneux, France). Briefly, 50 µg protein were loaded on a 3-8% tris-acetate gradient gel (Novex, LifeTechnologies), electrophoresed and wet-blotted onto a nitrocellulose membrane. The blots were probed with mouse antibodies against the dystrophin rod domain (Dys1) and the dystrophin C-terminus (Dys2) in 5% milk powder for 2 days at 4°C followed by incubation with the secondary goat-anti-mouse IgG peroxidase conjugated antibody. Bands were visualized by chemiluminescence. Subsequently, the blot was stripped and re-probed with a second mouse monoclonal anti-GFP antibody and rabbit polyclonal anti-α-actinin 2 antibody. For Western blots on brain tissue, protein extraction was done using a combination of following two buffers containing proteinase inhibitor cocktail: (i) 250 mM sucrose, 10mM Tris-HCl, pH 8.2 and (ii) 20% SDS, 20% glycerol, 10% beta-marcaptoethanol, 12,5% western blot running buffer in water. NuPage LDS sample buffer (Invitrogen) was used for the gel electrophoresis. The blots were probed using the iBind Flex Western System (Invitrogen, LifeTechnologies) with a mouse antibody against the dystrophin rod domain (Dys1,) and a rabbit polyclonal antibody against the dystrophin C-terminus (clone H4, gift from Cyrille Vaillend) together with secondary fluorescent antibodies (Alexa Fluor 700 and 800 respectively). A second blot was probed with monoclonal anti-GFP antibody together with a secondary fluorescent antibody (Alexa Fluor 700). As loading control, a mouse monoclonal anti-vinculin antibody was used.

Bands were visualized using the Odyssey CLx system (Li-Cor). All antibodies are listed in the Appendix 13.5, Table A2-3.

7. RESULTS

7.1. Generation of *Dmd*^{EGFP} reporter mice

The first part of my study was focused on the generation of a novel *Dmd*^{EGFP} reporter mouse. For this model, the gene encoding the Enhanced Green Fluorescent Protein (EGFP) had to be integrated into the *Dmd* locus after the last exon 79. This way, *Dmd* splice isoforms containing exon 79 would be automatically tagged with EGFP at their C-terminus. The dystrophin-EGFP fusion protein will facilitate the study of dystrophin expression in different tissues *in vivo* and *ex vivo* without the need for antibody staining.

The single steps leading to the generation of the *Dmd*^{EGFP} reporter mice are summarized in Figure 5. In order to modify the murine dystrophin locus on the X-chromosome, a targeting vector was designed. The vector encodes a modified sequence of the last dystrophin exon (removal of the natural termination codon), an in-frame insertion of a FLAG-EGFP sequence, followed by a lox*P* flanked *neomycin (neo)* cassette in the 3'UTR. Flanking the targeting cassette, homologous *Dmd* stretches were inserted into the vector that will enable homologous recombination in embryonic stem cells (ES cells). Successfully targeted ES cells were used for blastocyst injection, generation of chimeric mice and germline transmission of the modified allele. The part of this work including the ES cell culture and generation of transgenic mice in the F1 generation was done by a commercial company (Polygene AG, Switzerland). Transgenic mice expressing the dystrophin-EGFP fusion protein were then crossed with ubiquitous Cre-deleter mice to remove the *neo* selection cassette. The targeting strategy for modification of the *Dmd* locus using the targeting vector is depicted in Figure 6. All plasmid maps and primers used for cloning of the targeting vector and for genotyping the mice are attached in the Appendix 13.1 and 13.2. The cloning software Vector NTI® (Invitrogen, Germany) was used to visualize and *in silico* test the design strategy.

Subcloning of a genomic *Dmd* fragment spanning exon 79
(*Dmd* exon 79-retrieval vector)
↓
Cloning of a mini targeting cassette with a modified Exon79-FLAG-EGFP
and a lox*P* flanked *neo* selection cassette
(Vector PL452-mini targeting cassette)
↓
Introduction of a mini targeting cassette that contains
the modified exon 79-FLAG-EGFP and a lox*P* flanked *neo* sequence
into the retrieval vector, thereby modifying the *Dmd* gene fragment
(Targeting vector)
↓
In vitro expression tests of the targeting construct
↓
Linearization of the targeting vector
↓
Electroporation of the targeting vector into ES cells
↓
Selection of positive ES cell clones with G418 resistance
↓
Southern blot analysis for confirmations of successful
homologous recombination in ES cells
↓
Blastocyst injection of recombined ES cell clones
(Generation of chimeric mice)
↓
Confirmation of germline transmission, genotyping
of the F1 generation and Southern blot analysis
↓
Removal of the neomycin selection cassette by crossing
F1-generation mice with ubiquitous Cre-deleter mice
↓
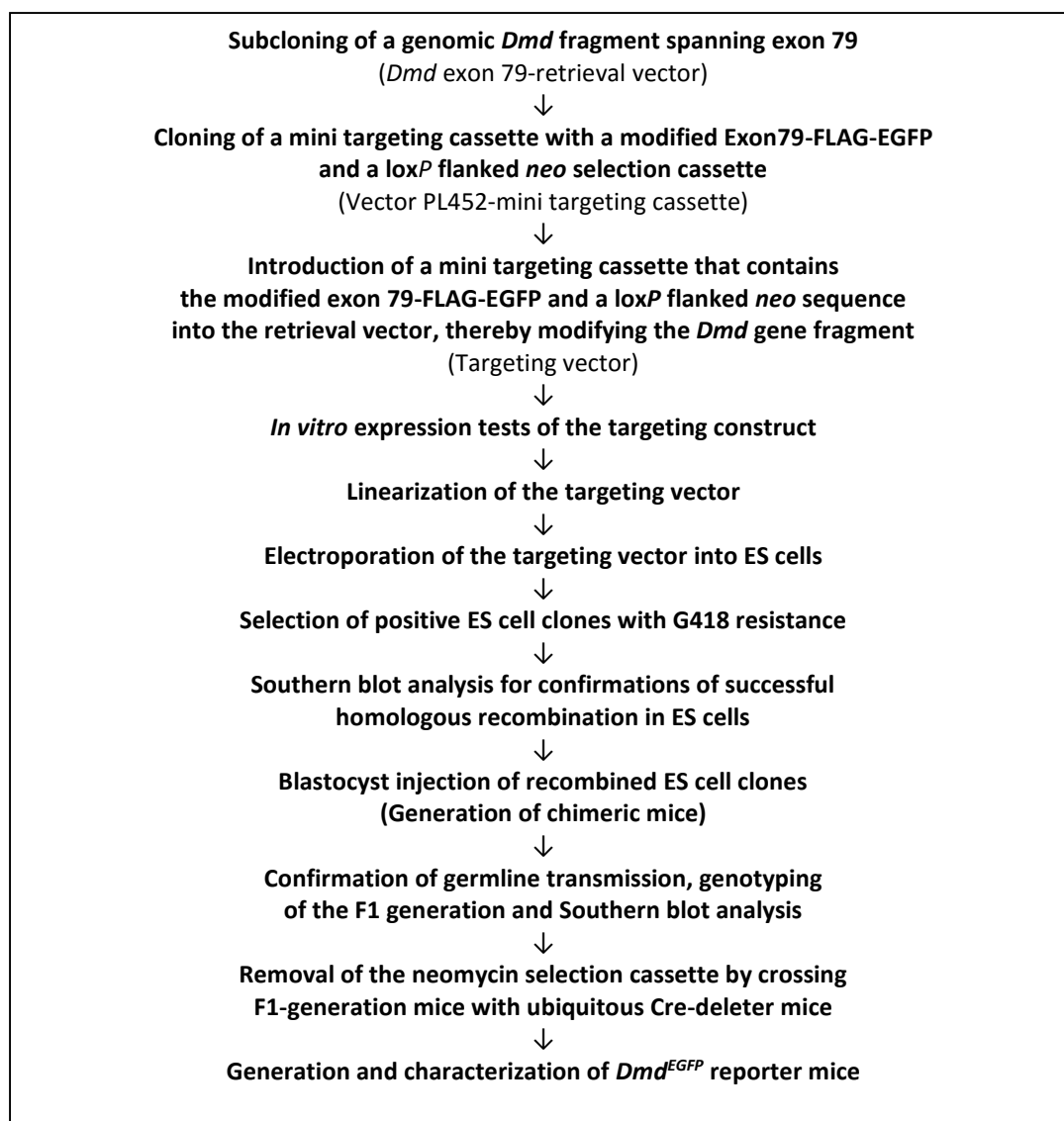Generation and characterization of *Dmd*^{EGFP} reporter mice

Figure 5: Flowchart for the generation of *Dmd*^{EGFP} reporter mice.
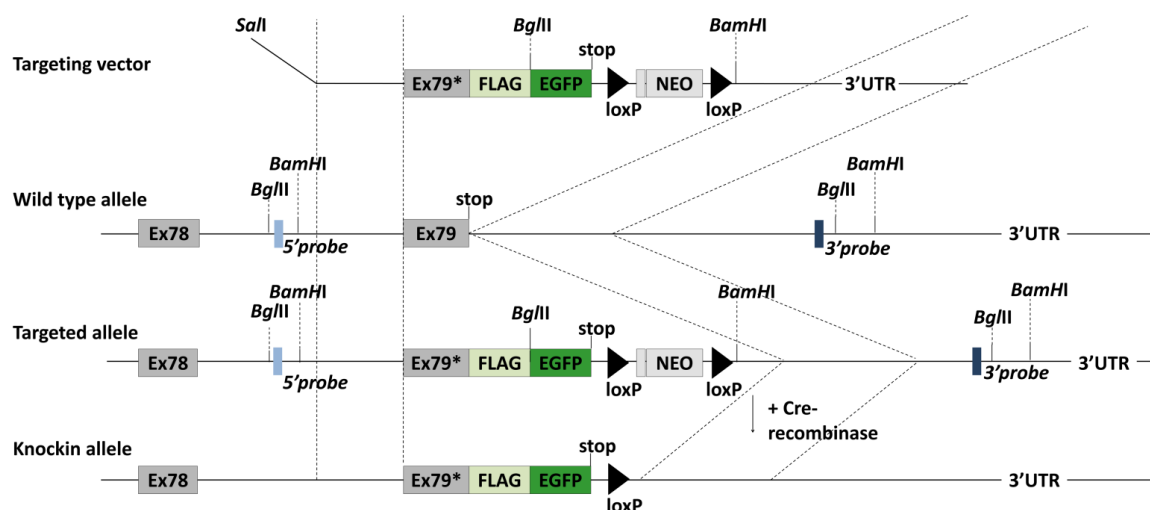
Figure 6: Strategy for genomic modification of the murine *Dmd* locus.
A targeting vector was constructed for insertion of a FLAG-EGFP coding sequence into the 3'UTR of the *Dmd* gene so that a dystrophin-EGFP fusion protein would be expressed. The last exon 79 was modified by exchanging the stop codon to a leucine (an asterisk indicates the modified exon 79, and a FLAG-EGFP sequence with a lox*P*-sites flanked *neo* cassette was inserted. The *Dmd* wildtype allele was targeted in ES cells after electroporation of the *Sal*I linearized targeting vector and subsequent homologous recombination. Dashed lines represent homologous regions. *Bgl*II and *Bam*HI restriction sites were artificially inserted into the transgene to facilitate identification of targeted ES cells by Southern blot analysis using either 5' and 3' hybridization probes (blue squares) located outside of the targeting vector. Positive ES cells were used for generation of transgenic mice. The *neo* cassette was removed by crossing the F1 generation mice with ubiquitous Cre-deleter mice (constructs are not drawn to scale). Ex: exon.

7.1.1. Generation of the targeting vector

The results of the process of making the targeting vector are described in more detail in the next sections. The targeting cassette consists of three regions: (i) the region encoding the modified exon 79 together with the FLAG-EGFP tag, (ii) a *neo* resistance gene flanked by lox*P* sites and (ii) two homology arms enabling homologous recombination in ES cells.

7.1.1.1. Subcloning of a genomic *Dmd* fragment containing the coding sequence of *Dmd* exon 79

In order to modify the *Dmd* locus we used a bacterial artificial chromosome plasmid (BAC) DNA (Sv129 derived, bMQ389g17, Source Bioscience, Germany) covering the dystrophin genomic region comprising intron 78, exon 79, and part of the 3'UTR. We selected a 10.943 kb *Dmd* fragment around exon 79 for modification and subcloned it from the BAC into the pCR-Script-AMP vector to facilitate subsequent cloning steps. The subcloning was done by gap repair *via* recombineering (see section 6.2.5), a cloning method that uses homologous

recombination in bacteria without the need of restriction enzymes. Figure 7 shows the cloning strategy. Homology arms, no longer than 238 bp, flanking the selected *Dmd* region were amplified from the BAC clone (5' and 3' Homology Arms; HAs). We used 5'-tailed oligonucleotide primers for amplification that contained restriction enzyme recognition sequences enabling cloning of the arms into the pCR-Script-AMP vector. Thereafter, the pCR-Script+HAs vector was linearized using *Hind*III, a restriction enzyme cutting exactly between the two homology arms, leaving a gap. The linearized DNA was electroporated into recombination competent *E. coli* SW106 cells that carried already the BAC. Recombination between the HAs on the BAC and on the linearized pCR-Script+HAs vector led to gap repair of the plasmid and retrieval of the 10.943 kb *Dmd* fragment of interest. The ensuing vector was named *Dmd* exon 79-retrieval vector. The retrieval vector was then further modified in order to generate the targeting vector for homologous recombination in ES cells.
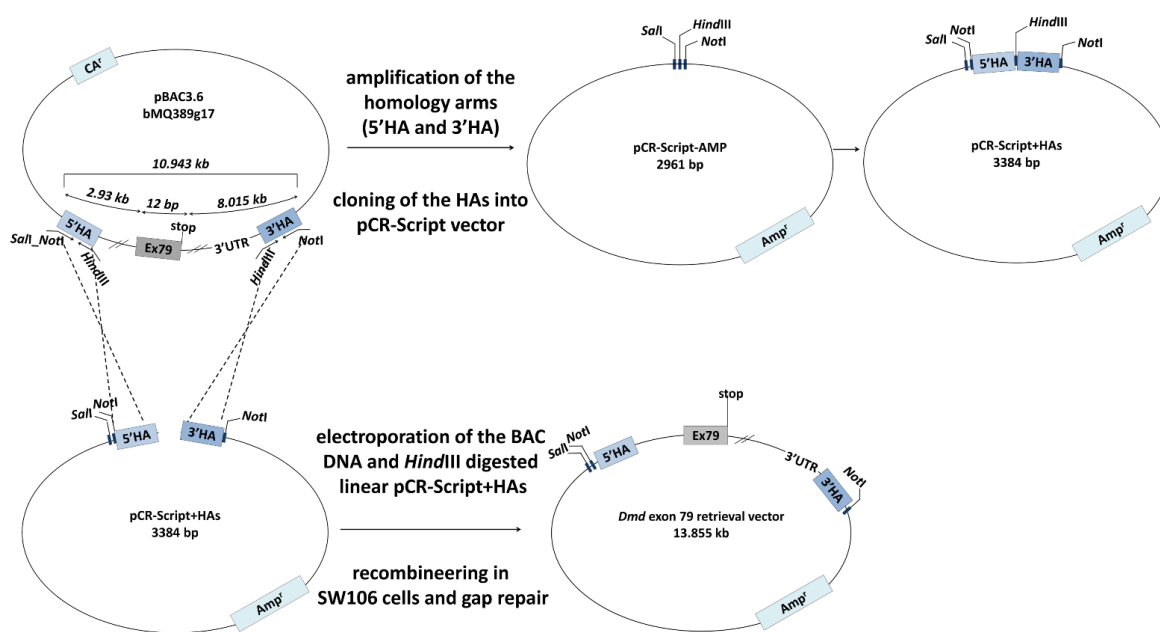
Figure 7: Subcloning of the 10.943 kb *Dmd* exon 79 genomic fragment by gap repair.
Homology arms (HAs) were amplified from BAC DNA using primer pairs with the following restriction enzyme sites: *Sal*I, *Not*I, and *Hind*III (5'HA) as well as *Hind*III and *Not*I (3'HA). HAs were cloned into the pCR-Script-AMP vector. In a second step BAC DNA was electroporated into *E. coli* SW106 cells. Subsequently, recombineering genes were induced and the *Hind*III linearized pCR-Script+HAs DNA was transformed into these cells. After successful recombination *via* gap-repair the 10.943 kb *Dmd* exon 79 fragment was cloned into the pCR-Script+HAs vector generating the *Dmd* exon 79-retrieval vector. Positive clones were selected by their ampicillin (*Amp^r*) resistance. Ex: exon, HA: homology arms.

7.1.2. Generation of a mini targeting cassette

For the modification of the retrieval vector by inserting the FLAG-EGFP coding sequence and the loxP flanked *neo* cassette and thus generating the targeting vector, a mini targeting cassette was cloned. As a recipient of the mini targeting cassette, we used the PL452 vector that already contained a loxP flanked *neo* resistance gene, which is transcriptionally controlled by a hybrid PGK/Em7 promoter. PGK drives *neo* expression in mammalian cells and Em7 permits the expression of *neo* in bacterial cells. A modified *Dmd* exon 79-FLAG-EGFP sequence was inserted upstream of the loxP-*neo*-loxP cassette. Furthermore, mini homology arms were designed and cloned into the vector to enable recombination. A mini targeting cassette was designed in such a way that the two homology arms (5' and 3' mini homology arms, 200 bp each) span DNA regions next to each other on the genomic *Dmd* exon 79 fragment, and the 5' mini arm includes exon 79. The 3' mini arm starts downstream of the stop codon sequence in exon 79.

Both homology arms were amplified from the BAC DNA and cloned into the PL452 vector using 5'tailed oligonucleotide primers as already described and shown in Figure 7. During the amplification of the 5' mini arm modifications were introduced *via* the reverse 3' primer: (i) the primer binds to the exon 79 sequence, however, introduces a single nucleotide mismatch changing the natural stop codon of exon 79 into a leucine coding sequence ($TAG_{Stop} > TTG_{Leu}$), (ii) this long primer further contained the FLAG sequence fused to the exon 79 sequence and (iii) a unique *Bgl*II site for later Southern blot analysis as well. The 5' mini homology arm thus still contains the *Dmd* homology region of 200 bp but with a slight modification of the exon 79 stop coding sequence and a FLAG coding sequence. The arm was inserted upstream of the *neo* cassette in into PL452 vector. The 3' mini homology arm, which contains a region from the 3'UTR was cloned downstream of the loxP flanked cassette. The vector PL452+mini HAs was generated (Figure 8).

In the next step, an EGFP sequence was cloned into the vector downstream of the FLAG sequence. EGFP was amplified from the plasmid pEGFP-N3-L221K again using 5'-tailed oligonucleotide primers. This vector encodes a monomeric version of EGFP in which a hydrophobic residue is exchanged for a positively charged residue (L221K). EGFP was digested with *EcoR*I and cloned into the PL45+mini HAs (Figure 8). The new vector contained the mini targeting cassette consisting of the modified *Dmd* exon 79-FLAG-EGFP sequence (inserted in-

64

frame) and the loxP flanked *neo* cassette. The homology arms flank this cassette and can be used for recombineering (Figure 8).
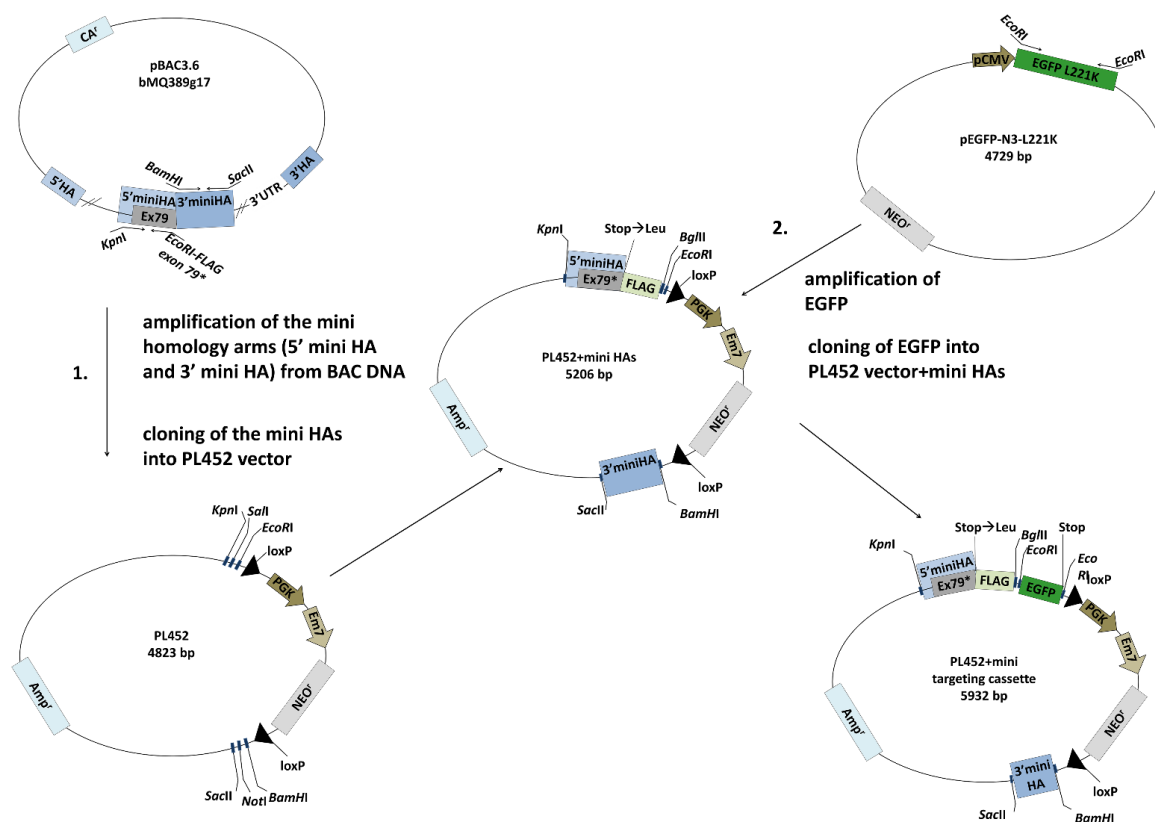

Figure 8: Generation of the PL452+mini targeting cassette.
In the first step **(1.)** 5' and 3' mini homology arms were amplified from BAC DNA using 5'-tailed oligonucleotide primers: for the 5' mini arm spanning exon 79, *Kpn*I and *EcoR*I-*Bgl*II-FLAG-modified exon 79* containing primers were designed. The 3' mini arm contained the *BamH*I and *Sac*II recognition sequences. After amplification, the 200 bp mini arms together with the PL452 vector were digested and the fragments were inserted: the 5' mini arm with exon 79*-FLAG upstream of the loxP-neo cassette, and the 3' mini arm downstream of the loxP flanked *neo* cassette. In a second step **(2.)** an EGFP sequence was amplified with *EcoR*I flanked primers from pEGFP-N3-L221K and cloned into PL452+mini HAs downstream of the FLAG sequence generating the PL452+mini targeting cassette. A unique *Bgl*II site was included for later Southern blot analysis. Asterisk (*) indicates the modified exon 79. Ex: exon, HAs homology arms, Amp[r]: ampiciline resistance, NEO[r]: neomycine resistance.

7.1.3. Generation of the targeting vector

In order to generate the final targeting vector, the mini targeting cassette was digested from the PL452 vector and electroporated together with the *Dmd* exon 79-retrieval vector into recombineering competent *E. coli* SW106 cells. Successful recombination of mini homology arms resulted in the modification of the *Dmd* exon 79 retrieval vector by inserting the modified exon 79 sequence followed by FLAG-EGFP-loxP-*neo*-loxP cassette between the two mini homology arms (Figure 9). Thus, the targeting vector was generated and could be used

for electroporation into embryonic stem cells and modification of the murine dystrophin locus. The plasmid maps of all vectors used in the cloning strategy are depicted in Appendix 13.2, Figure A1.
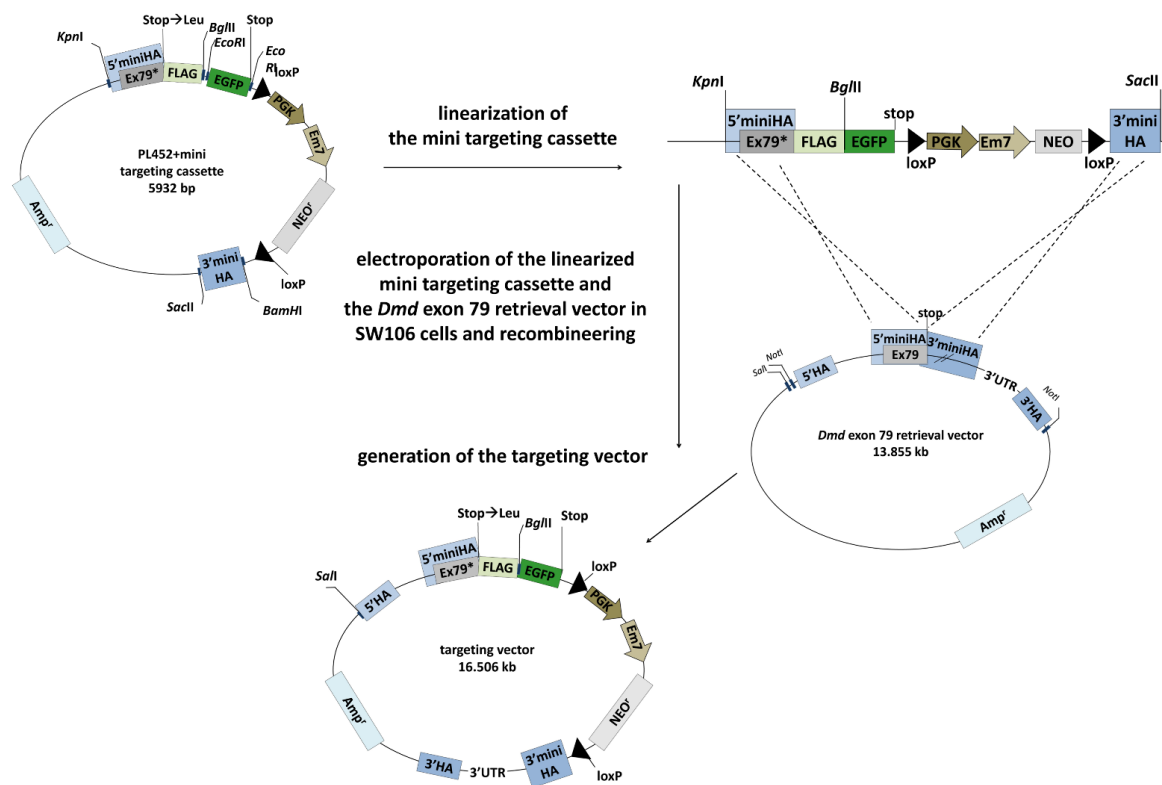

Figure 9: Generation of the targeting vector.
The mini targeting cassette was digested from the PL452 vector using *Kpn*I and *Sac*II restriction enzymes and electroporated together with the *Dmd* exon 79-retrieval vector into *E. coli* SW106 cells, in which the recombineering genes had been induced. Homologous recombination resulted in the insertion of the mini targeting cassette into the retrieval plasmid, thereby modifying the *Dmd* fragment. The targeting vector can be linearized with *Sal*I. Ex: exon, HAs homology arms, Amp[r]: ampiciline resistance, NEO[r]: neomycine resistance.

7.1.4. *In vitro* testing of the targeting vector

To confirm proper function of the targeting vector I performed two *in vitro* functional tests.

7.1.4.1. Modified *Dmd* exon79-FLAG-EGFP cassette

The modified exon 79-FLAG-EGFP coding sequence was tested for in-frame insertion and proper EGFP-expression in mammalian cells. For that, the cassette was amplified from the mini targeting vector using specific tailed primers and was subcloned into a mammalian expression vector (pCMV-Tag3A). A *Cox8a* mitochondrial targeting signal sequence was inserted upstream of the *Dmd* cassette so that the EGFP fluorescence signal should be

66

localized only in the mitochondria after transfection of COS cells. A plasmid expressing red fluorescent protein (RFP) only in the mitochondria (Mito-RFP, Evrogen) was co-transfected and was used as localization control. Figure 10 shows the expression of the two plasmids and their co-localization in the mitochondria confirming proper expression of the targeting cassette.
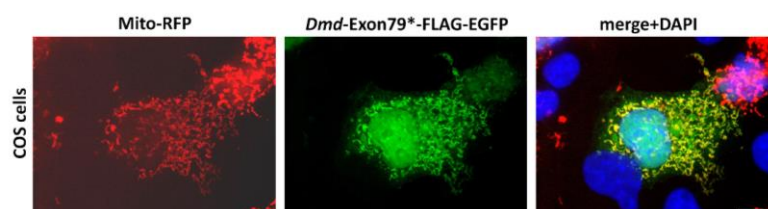

Figure 10: Functionality test #1: Expression of the *Dmd* exon 79*-FLAG-EGFP cassette in mammalian cells. COS cells were transfected with the control plasmid Mito-RFP and the pCMV-Tag3A-Cox8a vector expressing the subcloned modified *Dmd* exon 79*-FLAG-EGFP cassette. One RFP positive (red) cell shows also EGFP expression (green) and both signals co-localize (merge + DAPI, yellow). The asterisk depicts the modified exon 79 with absence of the stop-codon. Scale bar = 20 μm.

7.1.4.2. Excision of the *neo* cassette

The lox*P* flanked *neo* cassette in the targeting vector allows kanamycin selection after transfection into ES cells. However, after successful targeting of the genomic allele, it has to be excised in order to prevent unpredicted interference at the *Dmd* locus. This has to be done by breeding the F1-mice with ubiquitously expressing Cre-deleter mice. This leads to the excision of the lox*P* site-flanked *neo* cassette in the germ-cells of the succeeding F2-generation. Hence, the recognition sequence and its functionality had to be confirmed *in vitro* as well. The modified *Dmd* exon 79 targeting vector was electroporated into *E. coli* SW106 bacteria. In these cells, the expression of the *Cre*-recombinase was induced by growing them on arabinose containing medium. Clones were analyzed for the excision of the *neo* cassette using colony PCR (Figure 11A) with specific primers. The amplified fragments were visualized on agarose gel. Figure 11B (lanes 7-9) shows three positive clones in which a 500 bp fragment was amplified only if recombination had taken place. A second PCR using a primer that binds in the *neo* cassette shows no bands in these three clones, thus confirming the excision.
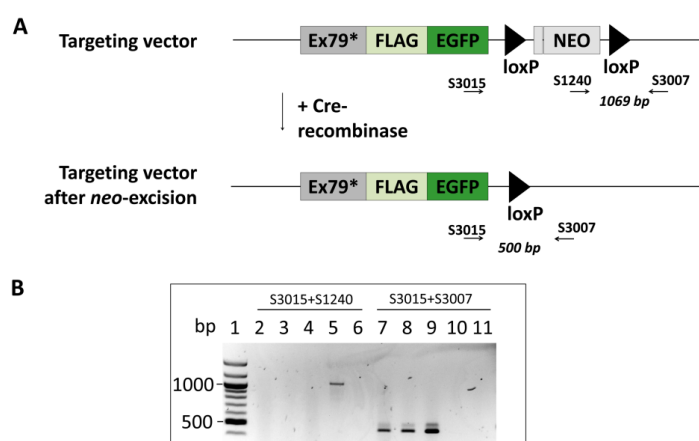
Figure 11: Functionality test #2: Excision of *neo* cassette.
(A) In the presence of the *neo* cassette in the targeting vector primer pair#1 (S1240 and S3007) amplified a 1069 bp fragment, which would be absent after excision of the *neo* cassette. Primer pair#2 (S3015 and S3007) amplified a 500 bp fragment only after removal of the *neo* cassette. **(B)** Colony PCR of three clones after transformation of *Cre*-recombinase induced *E. coli* SW106 bacteria with the targeting vector using primer pair#1 (lanes 2-6) and primer pair#2 (lanes 7-11). **Lane 1**: 5 µl 100 bp marker; **lanes 2, 3, 4** and **7, 8, 9**: DNA from three positive bacterial clones after *neo* excision, **lanes 5** and **10**: PCR products from the DNA of the control targeting vector containing the intact *neo* cassette; **lanes 6** and **11**: negative water control. The three positive clones show the 500 bp band (lanes 7-9) and no band (lanes 2-4), thus confirming the excision of the *neo* cassette. Only from the DNA of the control targeting vector the 1069 bp fragment could be amplified verifying the presence of the *neo* cassette. bp: base pairs, Ex: exon.

7.1.5. Electroporation of ES cells and selection of positive ES cell clones

The targeting vector was linearized using *Sal*I and electroporated into 129-derived ES cells. After G418 selection, positive clones were picked and analyzed *via* Southern blot analysis. The screening strategy and the probes for the Southern blot were provided to the company by me.

7.1.5.1. Screening for positive ES cell clones *via* southern blot analysis

For the Southern blot analysis, I generated 5' and 3' oligonucleotide probes that were located outside of the 10.943 kb homologous regions (Figure 12A, for plasmid maps of the subcloned probes, see Appendix 13.2, Figure A1). For the analysis, unique restriction enzymes recognition sites were used that had previously been artificially inserted into the targeting vector. A 5' DNA probe detects a 15.9 kb fragment in *Bgl*II digested genomic DNA if the wildtype allele is present, whereas in the targeted allele the probe binds to a 6.2 kb fragment (Figure 12B). Ten positive ES clones with a correctly targeted allele were identified *via* Southern blot with 5' probe. DNA from 6 of these clones was further tested using the 3' probe

after digestion with *Bgl*II or with *BamH*I in order to confirm the successful recombination at the 3' side of the construct. The ES cells used for homologous recombination were from male donors and since *Dmd* is located on the X-chromosome, we expected to see only one band. Nevertheless, the presence of a second wildtype band was visible in some of the positive ES clones suggesting either incomplete digestion by the restriction endonucleases or a contamination with wildtype DNA, possibly due to microheterogeneity.
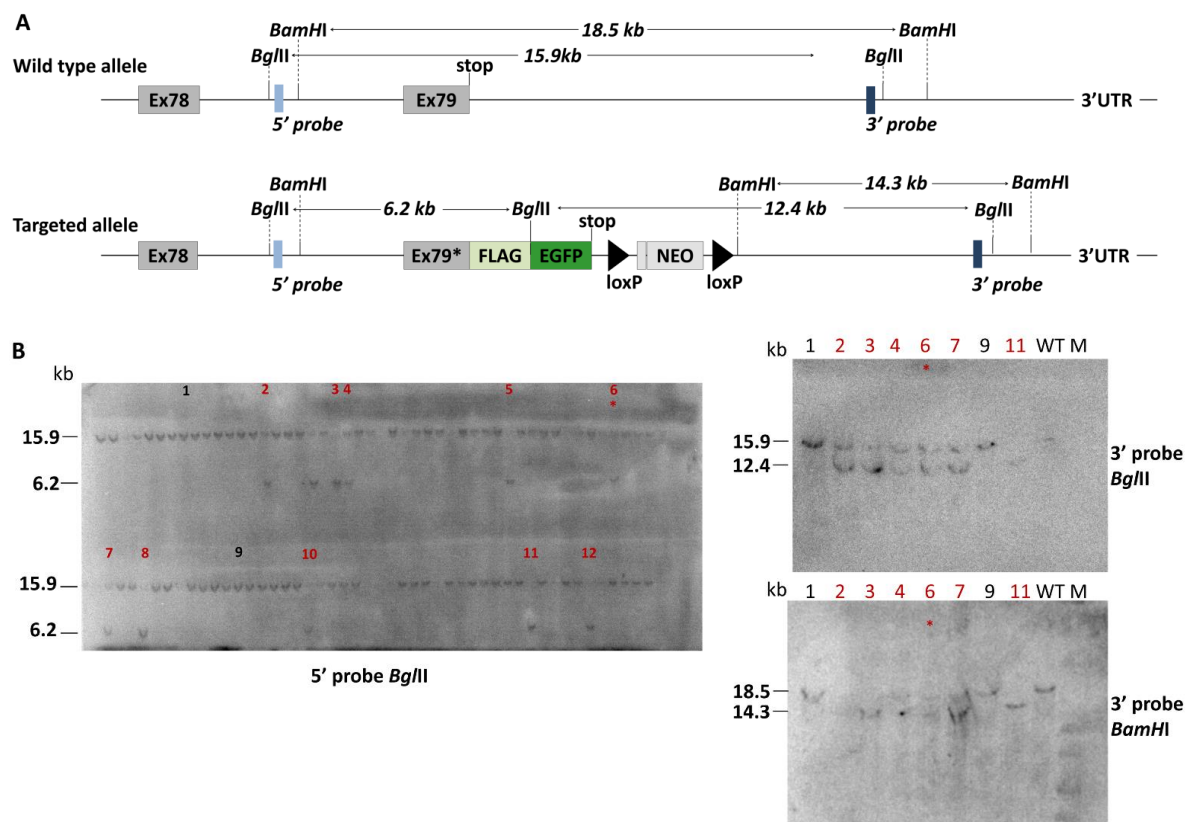

Figure 12: Detection of homologous recombination in ES cells *via* Southern blot analysis.
(A) 5' and 3' DNA probes (blue squares) complementary to a genomic region outside of the targeting cassette were generated. In the wildtype allele the 5' and 3' probes detects a 15.9 kb band after digestion with *Bgl*II, whereas in the targeted allele a 6.2 or 12.4 kb band can be detected, respectively. Using *BamH*I for DNA digestion the 3' probe hybridized to an 18.5 kb fragment in the wildtype and to a 14.3 kb fragment in the targeted cells. **(B)** DNA from ES cell clones was digested with *Bgl*II and hybridized with the 5' probe. Ten positive clones with the recombinant allele are numbered and marked with red (left blot) and two wildtype clones were numbered and marked in black. The DNA from positive clone **2**, **3**, **4**, **6**, **7** and **11** was further hybridized with the 3' probe after *Bgl*II and *BamH*I digestion (right blots). As control, wildtype clone **1** and **9** (black) were tested. **Clone 6** marked in red with an asterisk was the one that later led to the successful generation of chimeric mice and germ line transmission. Wildtype DNA was used as control. WT: wildtype, M: marker, kb: kilobase-pair, Ex: exon.

7.1.6. Generation of chimeric mice *via* blastocyst injection of positive ES cell clones

Positive ES cell clones were injected into C57BL/6N blastocysts. Surviving blastocysts were transferred into CD1 foster mice, which gave birth to mice with different percentages of coat color chimerism. Good chimeras (>80%) were picked and mated to C57Bl/6N mice. After several rounds using different positive ES cell clones for blastocyst injection, clone 6 gave rise to good chimeras that were mated to C57Bl/6N mice and germline transmission of the targeted allele was achieved (Figure 13).
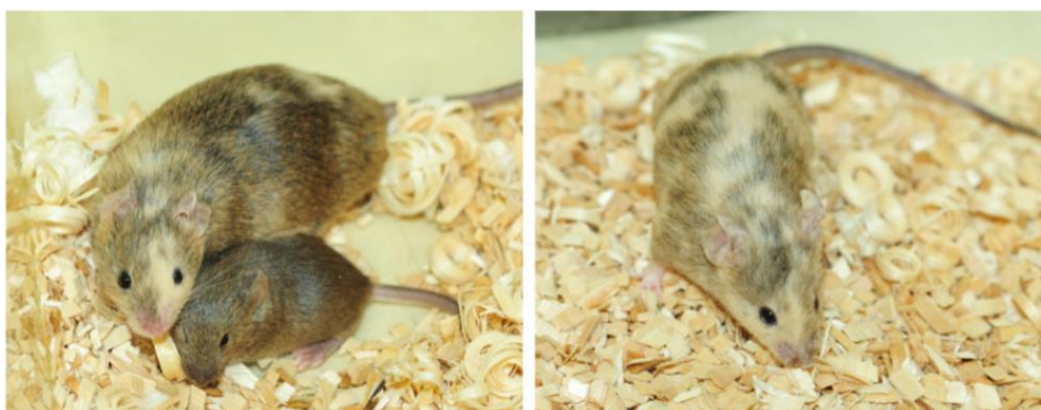

Figure 13: Chimeric mice generated from ES cell clone 6.
Germline transmission was achieved from chimera number 14 (left picture).

7.1.7. Confirmation of germline transmission *via* genotyping and Southern blot analysis

Agouti offspring from the mating of chimeric with C57BL/6N mice was screened for the presence of the *neo* cassette. Specific primers (Appendix 13.1, Table A1) were used for the screening PCR. A positive PCR reaction obtaining a 542 bp band was taken as evidence for germline transmission of the targeted dystrophin allele. Three animals of the F1 generation and offspring of chimera 14 were analyzed. Agarose gel electrophoresis of the PCR amplified fragments is shown in Figure 14A. In animals 1018 and 1019 the *neo* fragment was amplified, suggesting germline transmission, whereas animal 1020 did not show any band corresponding to the wildtype allele. To further confirm the PCR results, DNA was prepared from tail biopsies, digested with the enzyme *Bgl*II, Southern blotted, and labeled with the 5' probe as in section 7.1.5.1. In confirmation of the PCR screening, the targeted fragment of 6.2 kb could only be detected in the animals 1018 and 1019, whereas animal 1020 showed the

wildtype 15.9 kb band (Figure 14B). As expected all positive mice were females as the targeted allele is located on the X-chromosome.
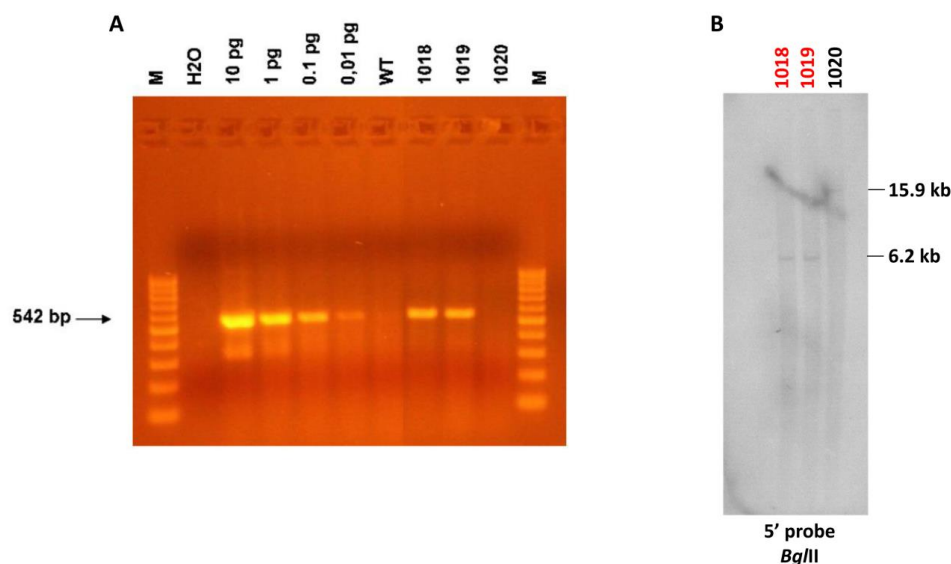

Figure 14: Genotyping PCR and Southern blot analysis for the targeted allele.
(A) PCR screening of mice from the F1 generation for the presence of the *neo* cassette using *neo*-specific primers for amplification of a 542 bp fragment. Different concentrations of the targeting vector were used as positive controls. The animals carrying numbers 1018 and 1019 were positive for the *neo* cassette, whereas in animal 1020 no band was detectable. **(B)** Southern blot analysis confirms the PCR results. DNA from tail biopsies was digested with I*Bgl*I and probed with the 5' probe. The 6.2 kb band for the targeted allele can be observed in animals 1018 and 1019. Mouse 1020 showed the wildtype band running at 15.9 kb. M: Marker, WT: wildtype, pg: picogram, kb: kilo bases, bp: base pairs.

7.1.8. Excision of the *neo* cassette by crossing the *Dmd*^EGFP-neo^ mice with Cre-deleter mice and genotyping of the F2 generation

After confirmation of the presence of the targeted allele in the F1 generation, the mice were sanitized and entered into a breeding program at the SPF facility at the Forschungseinrichtungen für Experimentelle Medizin (FEM) of the Charité *via* embryo transfer.

In order to remove the *neo*-cassette, animals from the F2 generation were mated with Cre-deleter mice, which ubiquitously expressed the *Cre*-recombinase. This enzyme excises the *neo*-sequence between the two lox*P* sites in the whole body, including the germ cells. Mice from the F3 generation were genotyped *via* tail biopsy PCR (Figure 15). The genotype of the transgenic *Dmd*^EGFP^ mice was verified by a three primer PCR that allows the distinction between wildtype, female heterozygous and homozygous as well as male hemizygous animals. Figure 15B shows an agarose gel electrophoresis of PCR products from different

animals (1-8). Amplification of the wildtype allele yields a 202 bp band (lane 1-3) while amplification of the Dmd^{EGFP} allele resulted in a 304 bp band (lane 4, 5, 6 and 8). In lane 6 both fragments were detected suggesting that the animal is a heterozygous female.
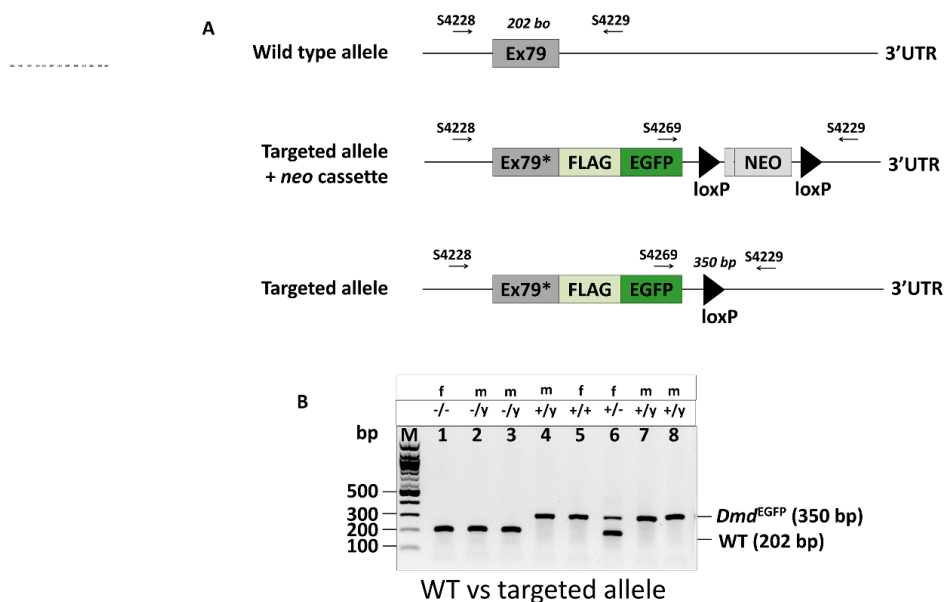

Figure 15: Genotyping PCR for the targeted dystrophin allele and *neo* cassette excision in transgenic mice. **(A)** A three primer PCR was used for genotyping. Primer S4228 binds to intron 78, primer S4269 binds to the EGFP sequence and primer S4229 to the 3'UTR. A 202 bp band is only detectable in samples from wildtype animals (S4228 and S4229), amplification using primer S4269 and S4229 will generate a 350 bp band only from the recombinant allele, after removal of the *neo* cassette. **(B)** Agarose gel electrophoresis of the genotyping PCR. Animals 1-3 had the wildtype allele and were either male (-/y) or female (-/-). In Dmd^{EGFP} homozygous male (+/y) and female (+/+) mice the 350 bp band is detected (lanes 4, 5, 7, 8). In heterozygous females (+/-) both amplicons were detected (lane 6). Ex: exon, bp: base pair, M: Marker, WT: wildtype.

7.2.   Characterization of Dmd^{EGFP} reporter mice

After verification of the successful targeting and modification of the dystrophin locus the Dmd^{EGFP} reporter mice were characterized. Transgenic mice were viable and did not show any obvious phenotypic defects. We investigated the expression and localization of the dystrophin-EGFP fusion protein throughout different tissues exploiting the natural EGFP fluorescence. The C-terminus of dystrophin is an important functional domain and it is expressed in the most dystrophin isoforms as well as in revertant dystrophin. Introducing a FLAG-EGFP tag of 27.9 kDa at its C-terminus might have an impact on the muscle physiology and potential dystrophic changes had to be ruled out. Therefore, I analyzed muscle histology as well as the location and expression of dystrophin interaction partners from the DAPC. Furthermore, I investigated the EGFP expression in isolated myofibers and in differentiating

satellite cells. For the experiments we used 8-12 weeks old male *Dmd^EGFP* reporter mice and their wildtype littermates. Histological changes that would only come with age were screened in animals that were 6 months or older.

7.2.1. Expression of the tagged dystrophin-EGFP protein

The expression of native EGFP was observed in all skeletal muscles of the *Dmd^EGFP* reporter mice at sarcolemmal level. Figure 16 shows a strong native EGFP fluorescent signal on cross and longitudinal sections from the *tibialis anterior* (TA) muscle. Moreover, staining of TA muscle sections with an anti-FLAG-tag antibody showed exact superposition of the immune signal with the natural EGFP fluorescence (Figure 17).
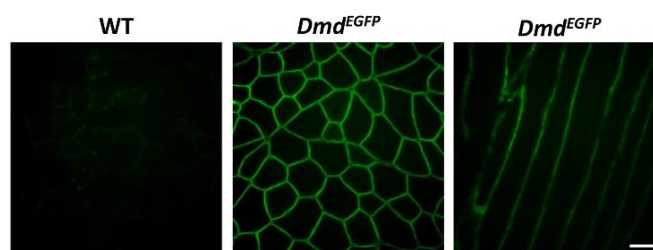

Figure 16: Native EGFP expression in *tibialis anterior* (TA) muscle sections.
TA cross and longitudinal sections show natural EGFP fluorescence in *Dmd^EGFP* mice that can be detected at the *sarcolemma* without amplification of the signal. No fluorescent signal was observed in the wildtype (WT) cross section with the same illumination parameters. Scale bar = 50 µm.
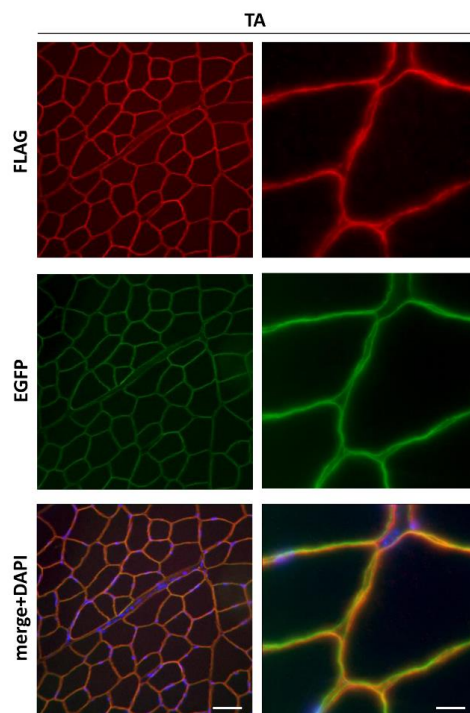
Figure 17: Co-localization of EGFP- and FLAG-tag in *tibialis anterior* (TA) muscle sections.
TA cross sections from *Dmd^EGFP* mice were stained with anti-FLAG (red) antibody and showed co-localization with the natural EGFP fluorescence. Sections were counterstained with DAPI (blue). Scale bar = 50 μm (left column). Higher magnification of the stained TA section is depicted in the right column. Scale bar = 10 μm.

We confirmed the correct expression of the EGFP-tagged dystrophin by Western blot analysis using dystrophin antibodies against the rod- and C-terminal domains (Dys1 and Dys2 respectively) (Figure 18). The bands from wildtype dystrophin and from dystrophin-EGFP had the same expression intensities detected by the rod-domain specific antibody, and the band intensity of the *Dmd^EGFP* samples was a bit lower when we used the Dys2 antibody. The molecular sizes of the proteins detected in both samples were comparable, since differences in molecular weight of 27.9 kDa between full-length dystrophin and dystrophin-EGFP would not be detectable on the Western blot at molecular weights (MW) above 400 kDa. An EGFP band in the dystrophin molecular size range was only detected in the *Dmd^EGFP* muscle sample.
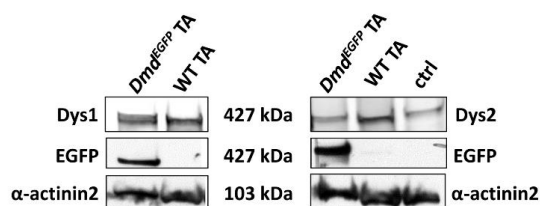
Figure 18: Western blot analysis of dystrophin-EGFP expression in *tibialis anterior* (TA) muscles.
Western blot analysis of whole TA muscle extract using dystrophin antibodies specific to the rod domain (Dys1) and to the C-terminal domain (Dys2) reveals normal expression of the full-length protein in the *Dmd*[EGFP] mice. The anti-GFP antibody detects the tagged dystrophin protein in the transgenic animals. For control a human muscle sample was tested with the Dys2 antibody. α-Actinin2 served as loading control. WT: wildtype, ctrl: control.

7.2.2. Expression and localization of dystrophin-EGFP in different tissues

In the next experiments we analyzed the expression and localization of dystrophin-EGFP in different tissues to confirm the tagging of different dystrophin isoforms.

7.2.2.1. Dystrophin-EGFP in skeletal muscle

We confirmed the correct localization of native EGFP fluorescence at the *sarcolemma* in TA, *gastrocnemius* (GAS) and *soleus* (SOL) muscles. Co-immunostaining with the dystrophin antibodies MANDYS19 (against the rod domain) and Dys2 (against the C-terminal domain) as well as with the cytoskeletal anti-β-spectrin antibody, showed an exact overlay of the fluorescent signals (Figure 19A-C). Importantly, the comparison between signals for EGFP and laminin, which is an extracellular matrix protein, reveals – as expected – a distinct staining pattern with the EGFP signal being present more towards the interior of the fiber (Figure 19D). The anti-β-spectrin and anti-laminin antibodies stained also the capillaries that did not show any EGFP signal. Other skeletal muscles showed a similar EGFP expression pattern (data not shown).
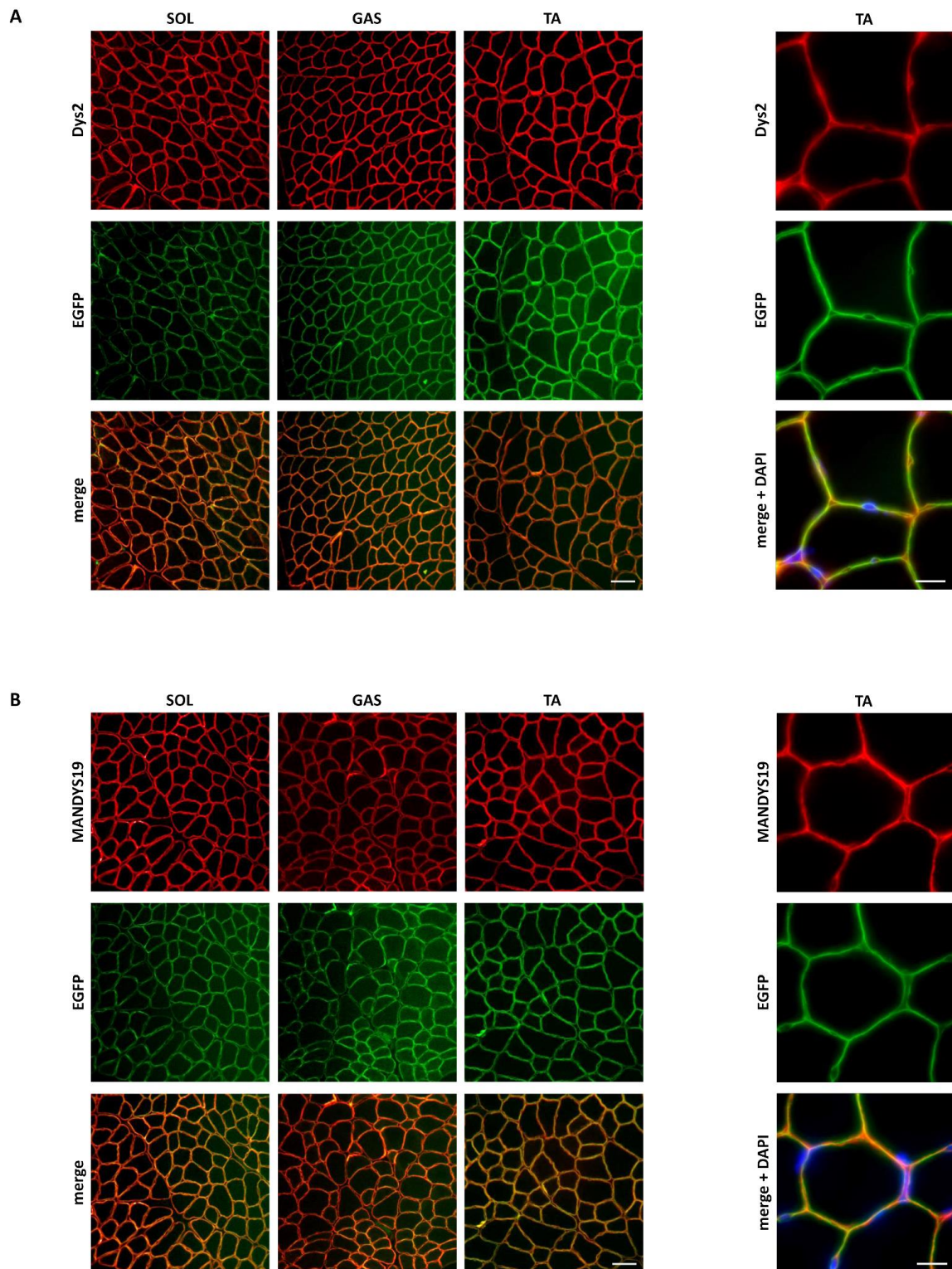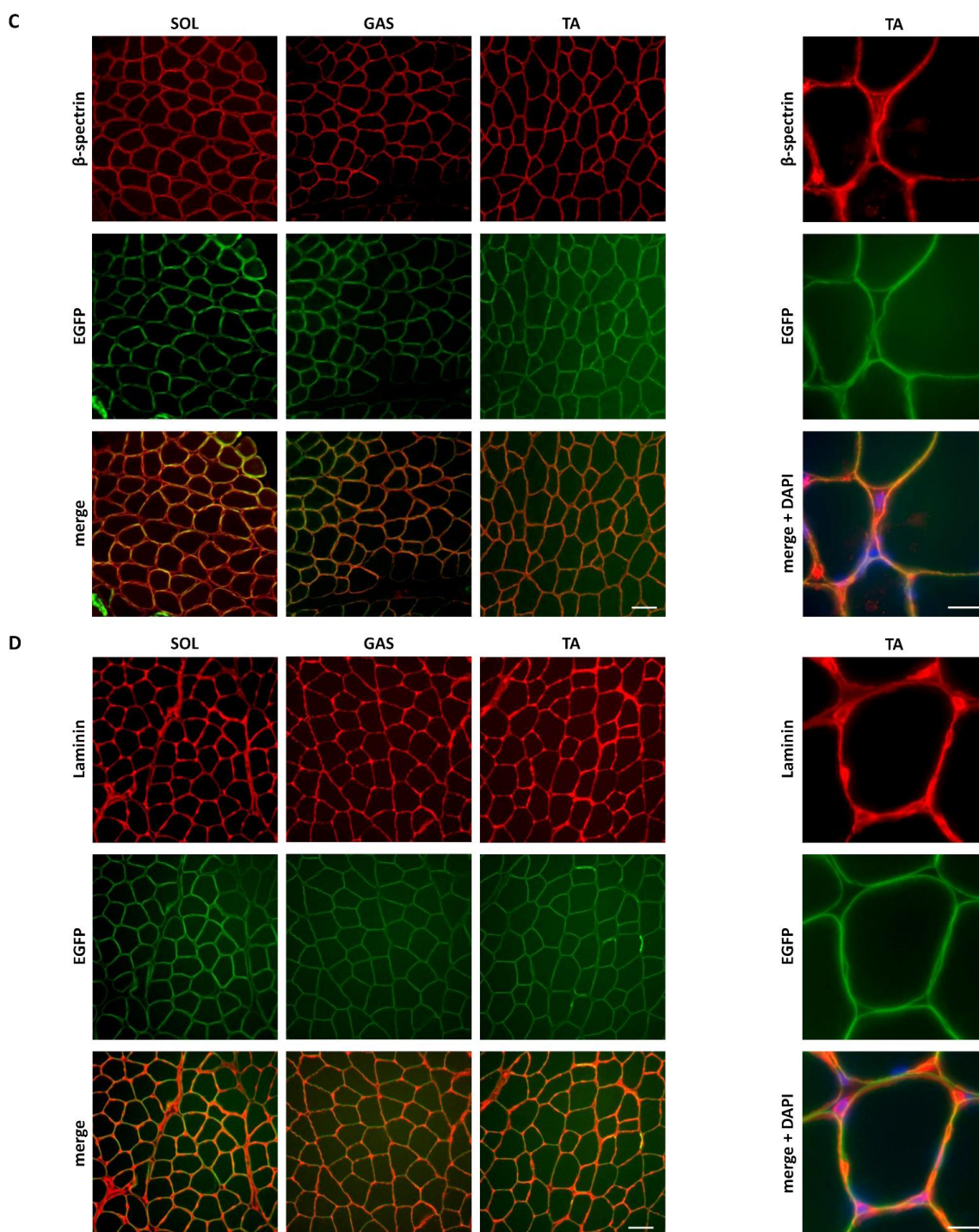
Figure 19: Correct localization of the EGFP-tagged dystrophin at the sarcolemma.
Immunofluorescent staining of cross sections from *soleus* (SOL), *gastrocnemius* (GAS) and *tibialis anterior* (TA) muscles of transgenic mice with dystrophin antibodies specific to the C-terminal domain (Dys2) **(A)**, the rod-domain (MANDYS19) **(B)**, and antibodies specific to the cytoskeletal β-spectrin **(C)** and the basement membrane protein laminin **(D)** all colored in red. Exact co-localization was observed between the natural EGFP fluorescence (green) and the signals deriving from the two anti-dystrophin antibodies. Scale bar = 50 μm. The columns on the right side depict a higher magnification of the stained TA sections counterstained with DAPI (blue). Scale bar = 10 μm.

7.2.2.2. Dystrophin-EGFP in cardiac tissue

We confirmed the correct dystrophin-EGFP expression and localization in the heart by verifying co-localization of the EGFP-signal with the signals generated by anti-dystrophin immunofluorescent staining (Figure 20A). Furthermore, EGFP expression was detected in blood vessels (arteries or veins) of the cardiac muscle that stained positive with anti-CD31 antibody directed against platelet endothelial cell adhesion molecule (Figure 20B). This staining pattern suggests the expression of dystrophin-EGFP in the smooth muscles of the vessel walls.
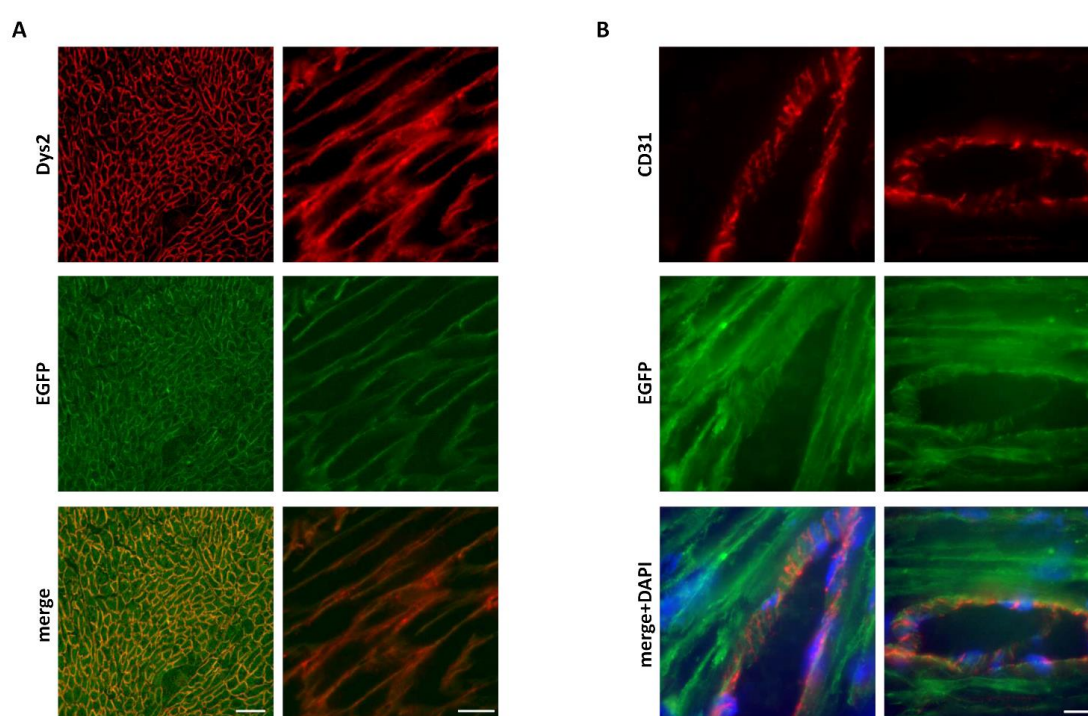
Figure 20: EGFP expression in the heart.
(A) Immunofluorescence staining of heart sections with the Dys2 antibody (red) showed co-localization of the natural EGFP signal with dystrophin in the cardiac myocytes. Scale bar = 50 μm. A higher magnification is depicted on a second column, which showed the localization of dystrophin-EGFP at the sarcolemma more clearly. Scale bar = 20 μm **(B)** Blood vessels in the heart were stained with anti-CD31 (red) and also showed co-localization with EGFP signal; counter stain with DAPI. Scale bar = 10 μm.

7.2.2.3. Dystrophin-EGFP expression in smooth muscle

We also analyzed the EGFP expression of dystrophin in the smooth muscles of reporter mice. Cross sections of *ileum*, *duodenum*, stomach and *colon* revealed a positive fluorescent signal in the circular and longitudinal smooth muscle cell layers (Figure 21A). Additionally, *colon* and

78

ileum sections were stained with a C-terminal dystrophin antibody revealing co-localization of dystrophin and EGFP signal, further confirming the proper tagging and expression of the fusion protein in this tissue (Figure 21B).
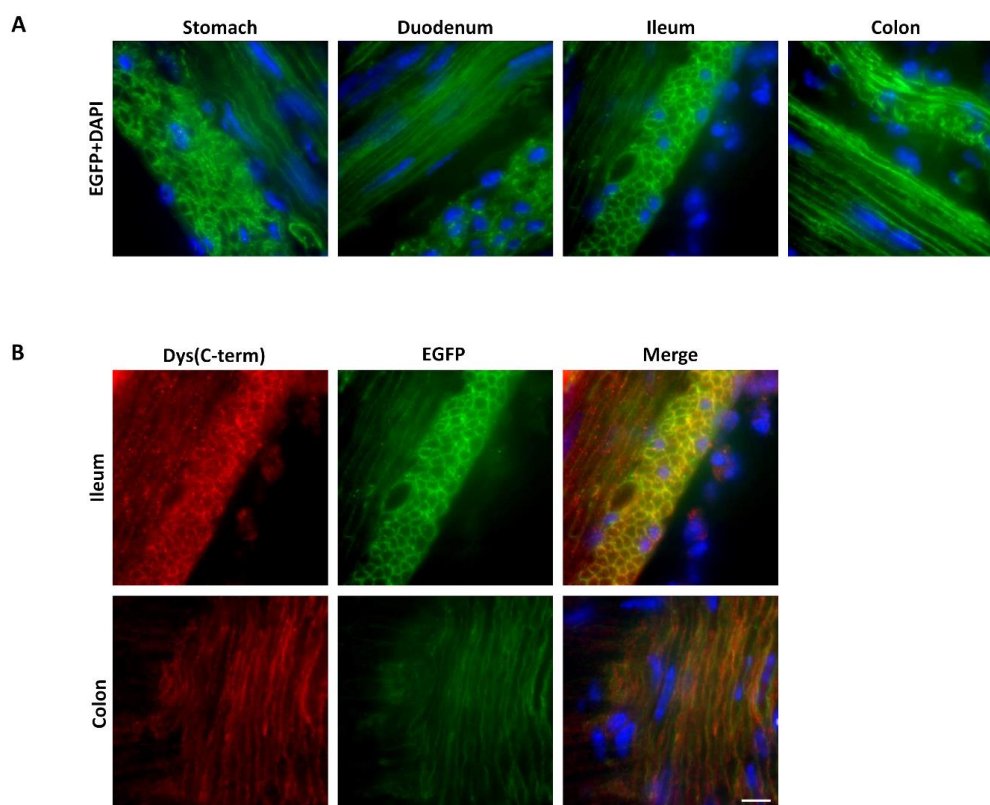
Figure 21: EGFP expression in smooth muscle.
(A) Sections from the stomach, *duodenum*, *ileum* and *colon* of *Dmd*^{EGFP} mice were fixed and stained with DAPI (blue). Strong natural EGFP expression was detectable in these organs. Scale bar = 10 μm. **(B)** Immunofluorescence staining with an anti-dystrophin antibody (C-terminal, rabbit) (red) of *ileum* and *colon* sections verifies co-localization with natural EGFP fluorescence. Sections were counterstained with DAPI (blue). Scale bar=10 μm.

7.2.2.4. Dystrophin-EGFP expression in non-muscle tissue

In order to investigate whether the different dystrophin isoforms were tagged in non-muscle tissues as well, we analyzed the EGFP expression in brain and retina of *Dmd*^{EGFP} mice. We performed a Western blot analysis on whole brain lysates from reporter mice and wildtype littermates (Figure 22). The full-length Dp427 isoform was detected at a very low level in wildtype samples using the C-terminal anti-dystrophin antibody H4. In the same sample a strong band corresponding to Dp71 was detected by the H4 antibody. In the brain lysates of reporter mice the Dp427 isoform was not detected using either H4 or anti-GFP antibodies.

Incubation of the blots with anti-GFP antibody revealed a strong band running at approximately 100 kDa in the transgenic samples which would correspond to an EGFP-tagged Dp71 isoform. No bands were detected in either of the samples using the rod-domain specific anti-Dys1 antibody.

Furthermore, we analyzed brain sections for dystrophin-EGFP expression. In Figure 23 natural EGFP expression in the cerebellum of *Dmd^{EGFP}* mice is depicted. The EGFP signal showed co-localization with the anti-dystrophin signal. Moreover, brain blood vessels expressed EGFP as demonstrated by co-labeling the vessels with anti-CD31 and partial co-localization of the respective fluorescence signals (Figure 23A). In addition, we detected expression of dystrophin in glial cells localized at the glial-vascular interface in the cerebellum as well as in the hippocampus, shown by a partial co-localization of the EGFP signal with the immune signal from an antibody against the glial fibrillary acidic protein (GFAP).

In the retina of *Dmd^{EGFP}* reporter mice, EGFP expression was observed at the outer plexiform layer (OPL), the inner limiting membrane (ILM) and sporadically at the inner nuclear layer (INL) (Figure 24A). A strong punctate EGFP signal co-localized with dystrophin immunofluorescence and was detectable in the OPL of the retina (Figure 24B). An exact co-localization of the EGFP signal was detected when using a C-terminal specific anti-dystrophin antibody (Dys2). Using the rod domain specific MANDYS19 antibody, not all EGFP positive structures were stained confirming that we have obviously targeted different isoforms. EGFP expression was also observed in at the inner nuclear layer. In addition, in retinal blood vessels of reporter mice the EGFP signal also co-localized with anti-CD31 signals. Dystrophin-EGFP at the blood vessels was not identified with the MANDYS19 antibody. At the ILM the principal glial cells of the retina – the Müller cells – were stained with the anti-GFAP antibody. Co-localization of the GFAP immunosignal in this region with EGFP expression was observed only at certain regions of the glial cells, most probably the glial endfeet (Figure 24C).

The EGFP expression patterns in brain and retina thus verify the successful tagging of different dystrophin isoforms in the *Dmd^{EGFP}* reporter mice.
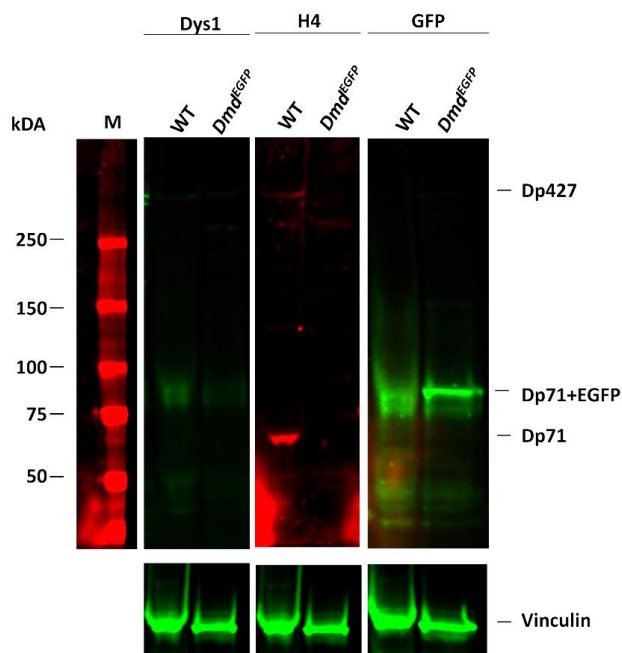
Figure 22: Western blot analysis of dystrophin-EGFP expression in the brain.
Western blot analysis of **whole brain lysates** using dystrophin antibodies specific against the rod domain (Dys1) and C-terminal domain (H4) revealed normal expression of Dp427 and Dp71 in wildtype mice, but no signal was detected in the *Dmd^EGFP* mice. The anti-GFP antibody detected the tagged Dp71-EGFP protein in the transgenic animals with an estimated size of 100 kDa. No bands were detected using anti-Dys1 rod specific antibody. Vinculin served as loading control. WT: wildtype, kDa: Kilodalton, M: marker.
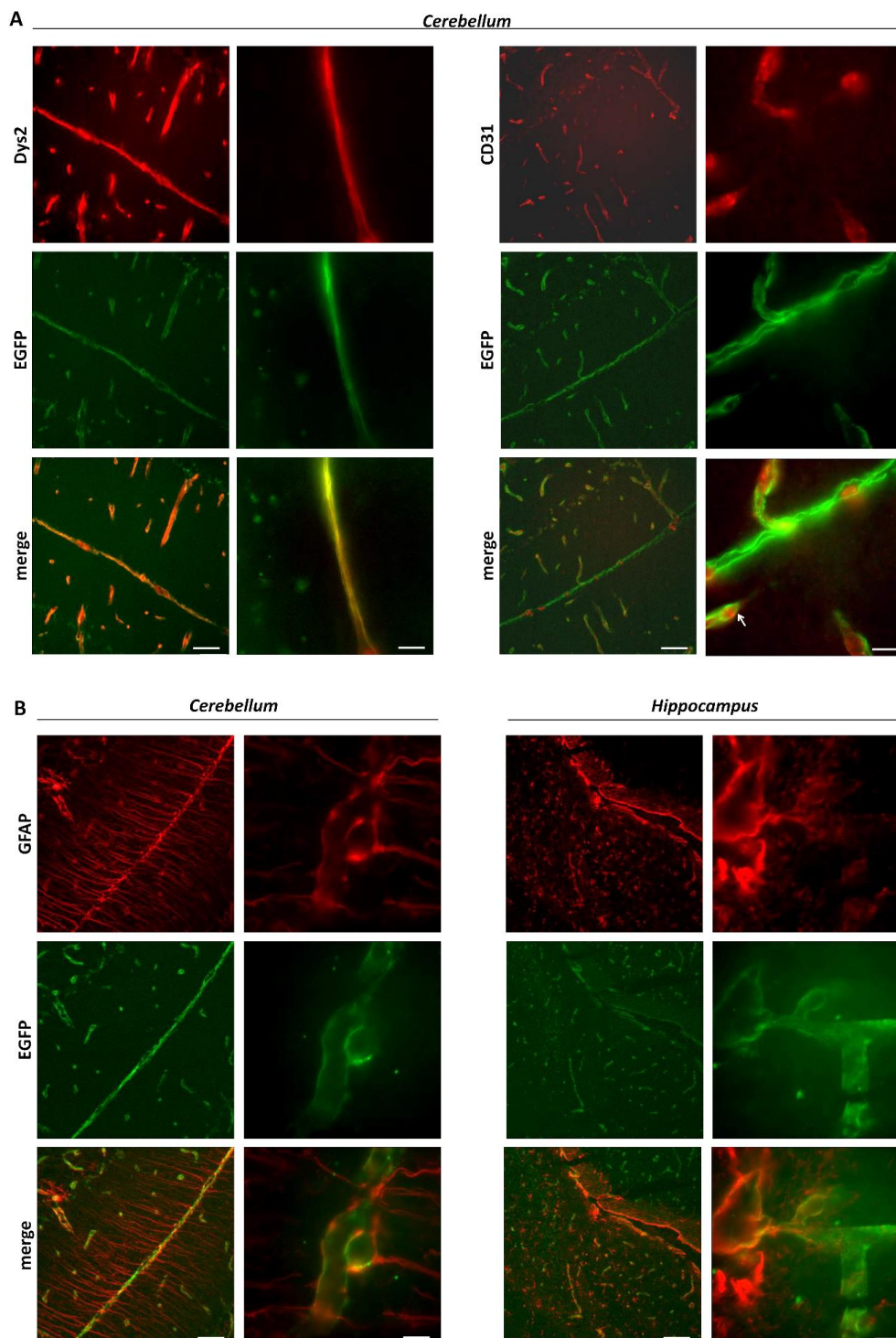
Figure 23: EGFP expression in brain.
(A) Immunofluorescence staining of brain sections with the Dys2 antibody shows co-localization of the natural EGFP signal with the anti-dystrophin signal in the *cerebellum* of the mouse. The partial co-localization of the EGFP signal with the anti-CD31 signal confirmed dystrophin expression also in the blood vessels in the brain. Scale bar = 50 µm (left column of each stain). Scale bar = 10 µm. **(B)** Immunofluorescence staining with anti-glial fibrillary acidic protein (GFAP) shows co-localization with the EGFP signal at the glial endfeet in the cerebellum and hippocampus. Scale bar = 50 µm in the left column of each region stained with anti-GFAP. A higher magnification is shown in the right columns. Scale bar = 10 µm.
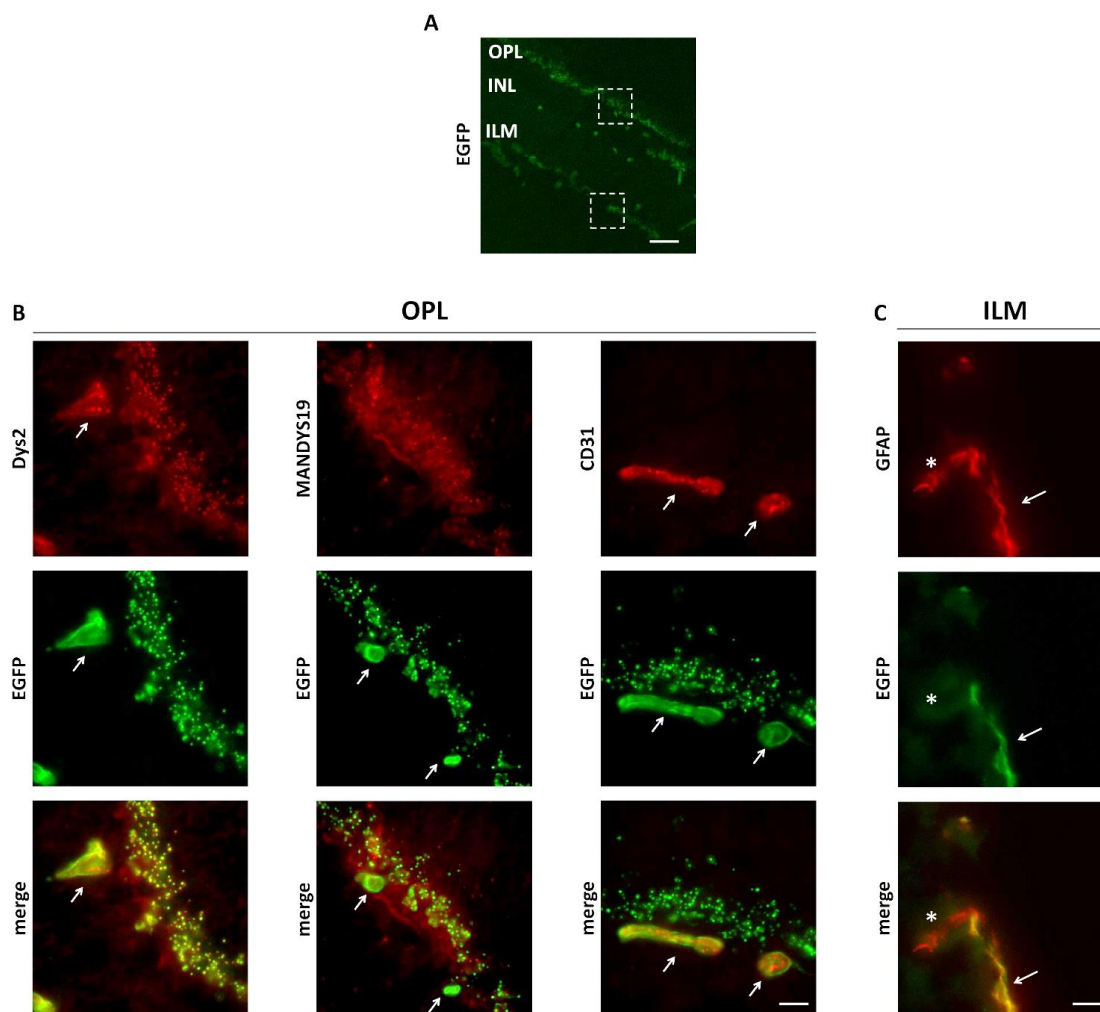
Figure 24: EGFP expression in the retina.
(A) Presence of the natural EGFP signal in the different regions of the retina. A higher magnification of the regions highlighted by the squares is presented in **B** and **C**. Scale bar = 50 μm. **(B)** Immunofluorescence staining with antibodies against dystrophin (Dys2, MANDYS19, red) and CD31 (red) showed differential co-localization of natural EGFP signal in the retinal OPL of *Dmd^EGFP* mice. Arrows indicate EGFP positive retinal blood vessels that were detected with Dys2 and anti-CD31 antibody, but not with the rod-specific antibody. Strong punctuated expression of the natural EGFP was observed in the OPL region corresponding to the photoreceptor terminals. In this region, exact superposition with the Dys2 signal and some overlay with the MANDYS19 signal were observed, whereas no anti-CD31 signal was detected. Scale bar = 10 μm. **(C)** Immunofluorescence staining with antibodies against the glial fibrillary protein (GFAP, red) showed partial co-localization with the natural EGFP signal at the ILM. Arrows indicate co-localization between GFAP and EGFP at the glial endfeet. The asterisk marks the GFAP positive region which did not express EGFP, corresponding to the glial cell body. Scale bar = 10 μm. OPL: outer plexiform layer, INL: inner nuclear layer, ILM: inner limiting membrane.

7.2.3. Histological analysis of the *Dmd^EGFP* reporter mice

The C-terminal domain of dystrophin plays an important role in the binding and assembly of the DAPC, which has a crucial role for muscle function and sarcolemmal stability. Addition of a 27.9 kDa EGFP-tag to the C-terminus of dystrophin might interfere with proper protein

83

folding, its subcellular localization, and protein function, thereby possibly provoking a muscular dystrophy similar to that seen in the *mdx* mouse model of Duchenne muscular dystrophy.

7.2.3.1. Muscle morphology

We performed H&E staining in adult and aged transgenic mice and their wildtype littermates. This investigation revealed normal skeletal muscle morphology in adult and aged *Dmd*EGFP mice and the entire absence of dystrophic changes such as increased myofiber size variability, fibrosis and centrally located nuclei (Figure 25, Appendix 13.3, Figure A2). Thus, histological analyses confirmed that EGFP tagging of the dystrophin did not cause any overt muscle pathology, neither in young mice nor with advancing age.
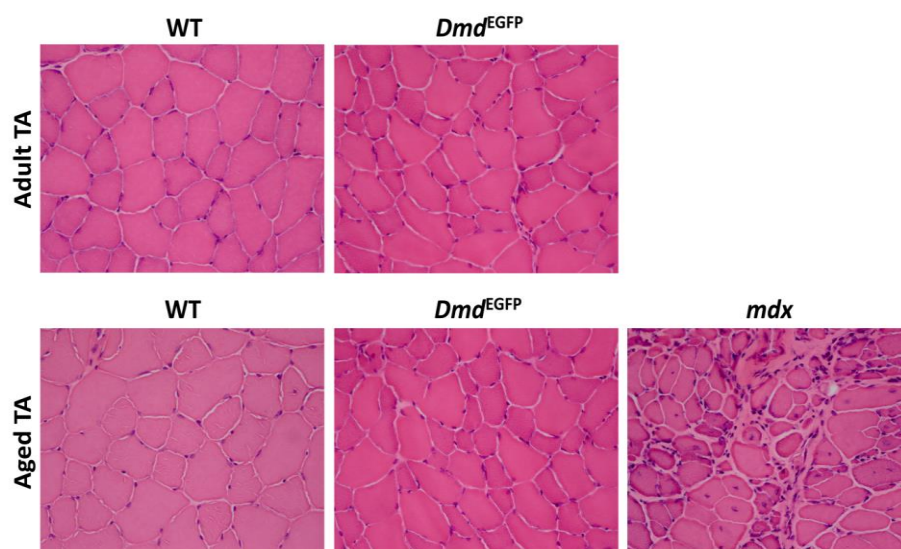
Figure 25: *Dmd*EGFP reporter mice show normal histopathology.
(A) Haematoxylin and Eosin (H&E) stained *tibialis anterior* (*TA)* sections from adult and aged wildtype (WT) and *Dmd*EGFP mice showed normal morphology. H&E staining of an aged-matched *mdx* TA muscle section demonstrated the morphological characteristics of muscle dystrophy comprising a large variation in fiber size, mononuclear cell infiltrates, fibrosis, and abundant centrally located myonuclei. Scale bar = 20 μm.

7.2.3.2. Expression of DAPC members

In a next step, we investigated whether the introduction of the C-terminal EGFP tag would influence the correct assembly of the DAPC. We hence investigated the expression of the following DAPC members in different skeletal muscles: dystrophin, α-dystroglycan, α-, β-, γ-sarcoglycan, nNOS, as well as utrophin (Figure 26, Appendix 13.4, Figure A3). Figure 26 depicts normal sarcolemmal expression of γ-sarcoglycan, α-dystroglycan and nNOS in TA muscle

sections. However, expression levels differed between individual sections because we used DAB-mediated antibody labeling to circumvent autofluorescence. Utrophin upregulation can be observed in DMD patients as well as in *mdx* mice, and it is used as an unspecific marker for muscle dystrophy. However, we did not find any upregulation of utrophin in the *Dmd*[EGFP] TA muscle, further confirming that the dystrophin-EGFP fusion protein did have a negative impact on muscle integrity (Figure 26). The same expression pattern was observed in the GAS, QUAD, SOL and EDL muscles (Appendix 13.4, Figure A3).
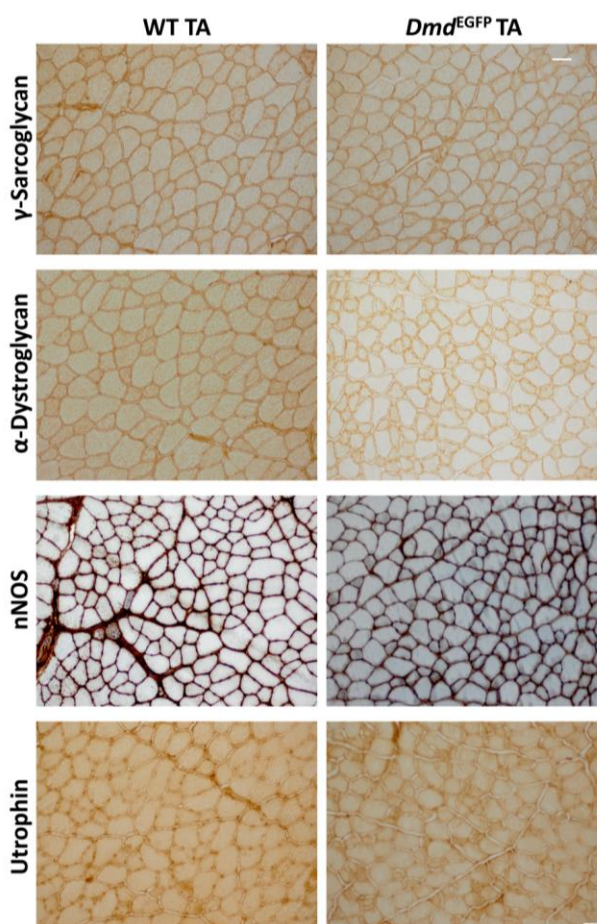
Figure 26: *Dmd*[EGFP] reporter mice showed normal histopathology.
Wildtype and transgenic mice showed normal localization and expression of the DAPC components α dystroglycan, γ-sarcoglycan and nNOS in tibialis anterior (TA) cross sections. Utrophin was not up-regulated in the TA muscles of transgenic animals. Scale bar = 50 μm.

7.2.4. *Ex vivo* and *in vitro* expression of dystrophin-EGFP in single fibers and differentiating satellite cell-derived myoblasts

Another interesting question would be whether the presence of dystrophin-EGFP would allow the live-imaging of dystrophin expression in cultures of isolated myofibers. Indeed, isolated

myofibers from *Dmd^{EGFP}* were strongly EGFP fluorescent standing in contrast to the entire absence of an EGFP signal from wildtype fibers (Figure 27A). In addition, strong dystrophin-EGFP expression was detected at the neuromuscular junction of single fibers that have been co-stained with fluorescently labeled α-bungarotoxin (BTX) that marks acetylcholine receptors (AChR). Interestingly, the EGFP expression at the NMJ of fixed fibers was stronger then the signal observed at this structure after BTX staining procedure (Figure 27B-C).

Further, we tested whether dystrophin-EGFP would be increasingly expressed in cultures of differentiating satellite cell-derived myoblasts. For this, we cultured isolated myofibers together with their attached satellite cells. As previously reported (Pasut *et al.*, 2013), satellite cells detached from their fiber, proliferated and formed myotubes after 8 days in differentiation medium. However, native EGFP-fluorescence was too weak to be detected in single myotubes. Remarkably, co-immunocytochemistry using both anti-GFP and anti-dystrophin antibodies demonstrated an extremely intense GFP signal, which co-localized with dystrophin (Figure 28). Of note, the anti-dystrophin signal in the myotubes was very weak, a known disadvantage of studying dystrophin *in vitro*. Thus, *Dmd^{EGFP}* derived myogenic precursor cells are capable to produce the dystrophin-EGFP *in vitro* and the signal is superior to the classic anti-dystrophin antibody-mediated dystrophin signal.
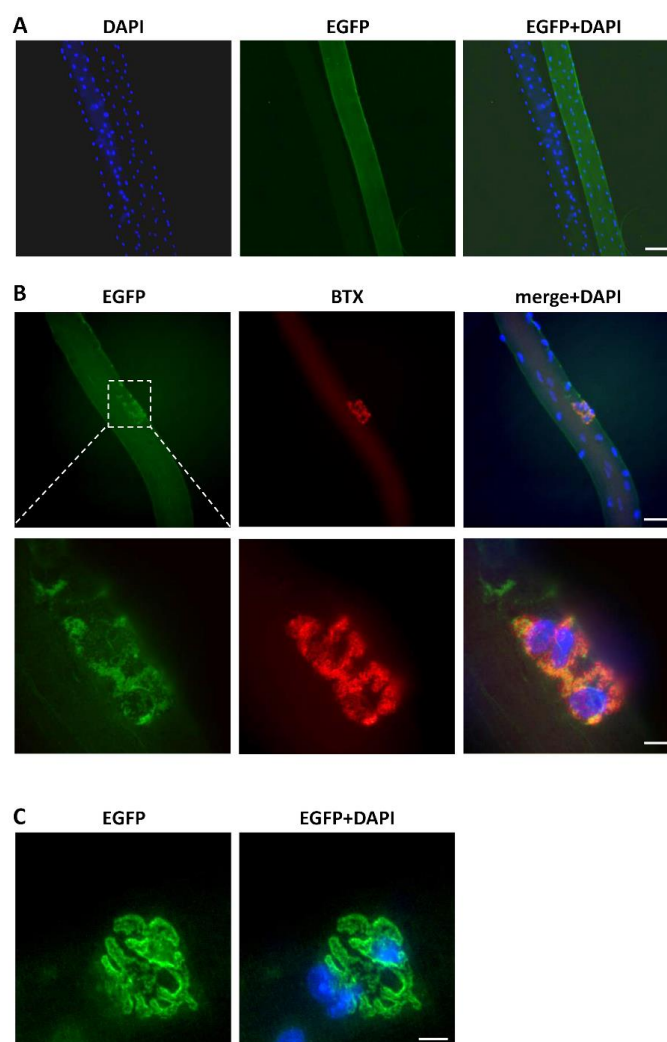
Figure 27: EGFP expression of single fibers.
(A) Individual fixed single fibers from EDL muscles were easily distinguished between *Dmd*^{EGFP} mice and wildtype littermates based on the natural EGFP fluorescence without further amplification of the signal. Fibers were fixed and stained with DAPI. Scale bar = 50 μm. **(B)** Natural EGFP expression at the neuromuscular junction of single fibers stained with an acetylcholine receptor binding neurotoxin (α-Bungarotoxin, BTX, red), Scale bar = 50 μm. In the second row, higher magnification shows the co-localization of dystrophin-EGFP with the acetylcholine receptor. Scale bar = 10 μm. Fibers counterstained with DAPI. **(C)** Natural EGFP expression at the neuromuscular junction of single fibers, fixed and conterstained with DAPI. The NMJ without an immunofluorescent staining shows stronger EGFP signal then in the BTX stained one. Scale bar = 10 μm
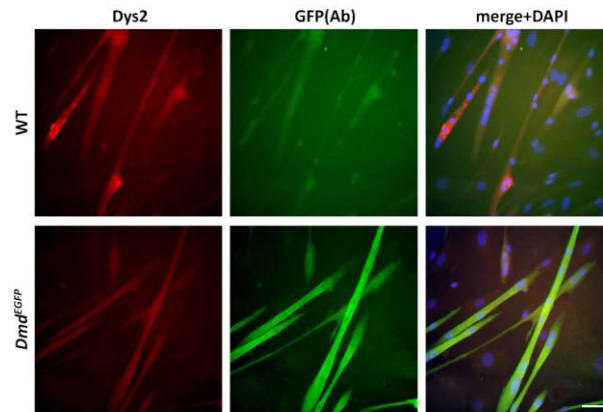
Figure 28: EGFP expression in satellite cell derived myotubes.
EGFP expression of *in vitro* differentiated satellite cells. Single fibers with their attached satellite cells from wildtype and *Dmd*^{EGFP} mice were cultured for 4 days and differentiated for further 8 days. Myotubes were fixed and stained with anti-GFP and Dys2 antibodies and counterstained with DAPI. Scale bar = 50 µm. WT: wildtype.

8. DISCUSSION

The aim of the present work was to generate and characterize a *Dmd^EGFP* reporter mouse that expresses a fluorescent EGFP protein fused to the endogenous dystrophin protein. This model should facilitate the study of dystrophin expression in different tissues and serve as a useful model for future applications investigating the function of dystrophin, understanding DMD pathology and improving current therapeutic approaches like exon skipping aimed to restore the open reading frame of dystrophin.

8.1. Generation of *Dmd^EGFP* reporter mice

The development of genetically modified animal models has contributed vastly to the advancement of biomedical and human disease research. Genetic and physiological similarities between humans and mice have placed the mouse as an important mammalian model for numerous studies in health and disease. These models have extended our understanding of basic biological processes, disease states and have led to the development of therapeutic strategies.

In the late 70ies and beginning of the 80ies, different groups developed strategies for the introduction of exogenous DNA into the murine genome conferring Mendelian inheritable traits (Costantini and Lacy, 1981; Gordon and Ruddle, 1981; Harbers *et al.*, 1981; Palmiter *et al.*, 1982; Stewart and Mintz, 1981; Tremblay *et al.*, 2009; Wagner *et al.*, 1981). The method used to achieve this result was the introduction of specific cloned sequences into the pronuclei of zygote stage embryos *via* microinjection. The manipulated embryos were then transferred into pseudo-pregnant recipient females, went through normal embryonic development and were born as viable offspring. The huge potential of this novel technology led to the rapid development in this research field, improving and optimizing the method. Transgenic lines have been developed expressing specific genes both in spatially and temporally defined manner. Abrogation and overexpression of disease causing genes have been investigated extensively in mouse models with engineered gene specific mutations.

Further progress was achieved with the identification and development of embryonic stem (ES) cell cultures that were established in parallel by independent researchers (Evans and Kaufman, 1981; Smithies *et al.*, 1985; Thomas *et al.*, 1986). With the help of molecular genetic manipulation of ES cells, endogenous genes can be deleted and/or modified, a strategy called

"gene targeting" that enables the generation of knockin/knockout mice. Injection of these ES cells into blastocysts and subsequent re-implantation into the murine uterus may then lead to offspring with germline transmission of the transgene to subsequent generations of the transgenic animals. We used this strategy to modify the murine dystrophin gene through in-frame insertion of a fluorescent tag behind its C-terminal coding sequence to trace and visualize dystrophin *in vivo* without the need for immunohistological staining.

A large majority of the studies on DMD as well as most of our understanding about the function of dystrophin in normal and diseased state have been gained through mouse models. The first and still most widely used mouse model for DMD is the natural mutant *mdx* mouse. Additionally, various other dystrophic models have been developed on different genetic backgrounds (Krivov *et al.*, 2009; Schmidt *et al.*, 2011; Wasala *et al.*, 2015) and bearing different *Dmd* mutations (Araki *et al.*, 1997; Chapman *et al.*, 1989). Most of the studies on the structure and function of dystrophin have been conducted on transgenic reporter mice using cDNA expression vectors. These models offer many advantages and have provided important information for gene therapeutic approaches, however, they have limitations and disadvantages. Usually tissue specific promoters are used to restrain the expression of the transgene. Despite this precaution, the transgene expression might still not exactly mirror the expression from the natural locus. Therefore, the protein expression patterns might considerably deviate from the natural situation. Moreover, these methods usually bypass endogenous control mechanisms of gene expression such as cell cycle regulation of transcription, microRNA regulation of translation, position effect or alternative splicing (Ciotta *et al.*, 2011). To circumvent these limitations and the toxic effects by transfection and overexpression, we generated a model by which the fluorescent labeled protein is expressed throughout muscle and non-muscle tissue by the natural endogenous promoters. Up to date, no dystrophin reporter mouse model exists, in which the endogenous natural protein was tagged and could be traced and analyzed. For other animal models, only one study that has been published this year described a zebrafish gene trap line, in which a fluorescent citrine gene sequence is spliced in-frame into the rod-domain of zebrafish *dmd* (Ruf-Zamojski *et al.*, 2015). Furthermore, only few models exist in which transgenic dystrophin expression can be followed by means of a fluorescent tag that would greatly facilitate such investigations (Bajanca *et al.*, 2015; Li *et al.*, 2006). The huge size of the dystrophin gene spanning 2.4 Mbp

and encoding 79 exons constitutes a challenge and may explain why up to date so few reporter models for *in vivo* real time monitoring of dystrophin expression exist. Here we describe the generation and characterization of a *Dmd^EGFP* reporter mouse, in which the fluorescent EGFP protein was fused to the C-terminus of endogenous dystrophin, hence targeting all major dystrophin isoforms that are expressed in different muscle and non-muscle tissues.

8.1.1. C-terminal tagging of the murine endogenous dystrophin with a fluorescent protein

For the generation of the *Dmd^EGFP* reporter mouse, we used the method of gene targeting *via* homologous recombination. For the targeting strategy, we had to consider what kind of fluorescent tag to use and at what position to insert it into the *Dmd* gene.

The *Dmd* gene is a huge gene with a high degree of complexity in its regulation. At least 8 different promoters regulate the expression of tissue specific isoforms, which are beyond that also developmentally regulated. Furthermore, alternative splicing from each promoter contributes to diversity of dystrophin expression. The last *Dmd* exon 79 is present in all major dystrophin isoforms. In order to create a more "general" reporter model, the best position for insertion of the fluorescent tag sequence was deemed 3' of the *Dmd* gene in its 3'UTR. Expression of the fluorescent tag at the C-terminus of the protein will enable the labeling of most of the dystrophin isoforms. Furthermore, in revertant dystrophin exon 79 is rarely spliced out. Further issues have to be addressed and concern the location of such a fluorescent tag with respect to the functional domains of the tagged protein. In dystrophin, the C-terminal domain harbors the most important functional domains of the protein and the insertion of the tag might influence protein structure and function. However, *in vitro* experiments using reverse transfection microarrays showed that protein tagging with GFP at its C-terminus in general is superior to tagging of the N-terminus (Palmer and Freeman, 2004) with respect to correct protein localization, suggesting that the main functional characteristics might be maintained.

The second important question in the development of the targeting strategy was the choice of the fluorescence tag. In the ideal case, the signal from the tag will replicate the signal from a high affinity antibody or would be even more accurate with regard to its subcellular location because unspecific staining could be ruled out. A further advantage of such a fluorescent tag

would be its detectability without the need for immunohistological staining that would open the possibility for live-cell imaging and investigation of dynamic processes.

A milestone in the transgenetic research was achieved by the cloning of the gene that encodes the green fluorescent protein (GFP) (Prasher *et al.*, 1992) 30 years after its discovery in the luminous hydromedusan, the jellyfish *Aequorea victoria* (Shimomura *et al.*, 1962). Since then, GFP was used as a fluorescent *in vivo* marker in bacteria, *C. elegans*, mice and in other living organisms to study and visualize cells and their behavior (Chalfie *et al.*, 1994; Okabe *et al.*, 1997). Many modifications and optimizations have led to the development of modified versions of the *Aequorea*-based GFP with different emission spectra or chemical properties. The enhanced GFP (EGFP) is among the brightest and most photostable fluorescent proteins. For the tagging of the murine dystrophin gene, we hence opted for EGFP. The only drawbacks of EGFP as a fusion tag are its slight sensitivity to pH and a weak tendency to dimerize, the latter being a characteristic common to all GFPs.

Skeletal muscle dystrophin is a cytoplasmic protein located in the vicinity of the sarcolemma where it is part of a huge multimeric complex. Dystrophin interacts with its C-terminus with integral membrane proteins of the sarcolemma as well as with cytoplasmic proteins thus lending mechanical stability and serving as a scaffold for signaling molecules. Dimerization of EGFP at the C-terminus of dystrophin could thus be a major confounding factor and might have a negative impact on the function of the fusion protein. Furthermore, dimerization could lead to incorrect assumptions and measurements when applying advanced quantitative fluorescence techniques such as fluorescence resonance energy transfer (FRET). Therefore, we used a modified EGFP version in which dimerization was prevented. It has been shown that all *Aequorea* derived GFPs and mutants of any color contain a hydrophobic patch of Ala206, Leu221, and Phe223 responsible for dimerization of the beta-barrel. To circumvent an unwanted dimerization, we used a mutated EGFP (mEGFP) version in which the hydrophobic Leu221 was exchanges by the positively charged residue lysine. No significant alteration of the spectral properties have been reported for the monomeric mGFPs(Zacharias *et al.*, 2002).

In order to use a fluorescent tag that will be useful for tracing a protein of interest, the concentrations of the fluorescent protein that are required for visualization over background fluorescence in cells have to be considered. In order to achieve a twofold increase in

fluorescence over background, fluorescence EGFP must be expressed at minimum at 200 nM (Patterson *et al.*, 1997; Snapp, 2005) which is the case for skeletal and heart muscles.

8.1.2. Recombineering: a rapid method for the generation of a targeting vector

To generate *Dmd*^EGFP^ reporter mice, we tagged the murine *Dmd* gene with FLAG-EGFP sequence exactly adjacent to the C-terminal *Dmd* coding sequence behind exon 79. The process of generating the *Dmd*^EGFP^ reporter mice involved different successive steps that are summarized in Figure 5. In the first part, a targeting vector was designed. We also inserted a FLAG sequence before the fluorescent tag sequence so that a broader range of experiments could be conducted with the reporter mice. FLAG is a short sequence of an antigenic peptide for which good antibodies exist and that can be used for protein tagging. This facilitates localization studies by immunohistochemistry and their purification as well as identification of binding partners (Hopp *et al.*, 1988).

Applying the method of gene targeting, we used a cassette containing a modified sequence of *Dmd* exon 79 (with the stop codon removed) and FLAG-EGFP sequence followed by lox*P* flanked *neo* cassette for targeting the wildtype dystrophin allele in murine ES cells *via* homologous recombination. The targeted allele was then transferred to mice progeny and through crossing them with ubiquitous Cre-deleter mice the lox*P* flanked *neo* cassette is excised creating the desired "pure" knock-in allele (Figure 6).

For the introduction of the modified sequence into the genome, the natural process of homologous recombination was exploited. It is a type of genetic recombination, a universal biological mechanism, present in all domains of life. Nucleotides are exchanged between identical or similar DNA molecules. Such mechanism is used to repair double strand breaks, to create newly arranged DNA sequences during meiosis thereby contributing to genetic variation in the offspring and in horizontal gene transfer in bacteria and viruses (Alberts *et al.*, 2002). For successful recombination and identification of positive clones as well as for confirmation of the modified allele's presence in ES cells and mice, different elements have to be constructed and engineered into the targeting cassette by cloning. Cloning is a time consuming process and different methods exist to speed up this process. We applied the method of "*recombineering*", which greatly facilitates the cloning procedure since it is independent of the presence of natural restriction endonuclease recognition sites. Knock-in

vectors can thus be rapidly constructed from BAC clones *via* recombineering followed by gap-repair (Murphy, 1998; Zhang *et al.*, 1998). We used a commercial BAC clone spanning the genomic DNA sequence of the murine *Dmd* containing exon 79. BAC clones are large (>100 kb) and thus not very suitable for modification and cloning steps. Hence we subcloned a smaller fragment of 10.943 kb DNA surrounding exon 79 into a pCR-Script vector *via* recombineering (Liu *et al.*, 2003). Modification of *Dmd* exon 79 was facilitated on this retrieval vector, which contains long enough stretches of homology upstream and downstream of exon 79 to ensure recombination in ES cells and targeting of the dystrophin allele. The homology arms on the targeting construct were around 3 kb for the 5' arm and 8 kb for the 3' arm. Arms of this size have proven to be sufficient to achieve good recombination with a high frequency (Hasty *et al.*, 1991). In order to fuse the FLAG-EGFP tag to the C-terminus of dystrophin, the sequence of the tag was inserted directly behind the last *Dmd* exon 79. The nucleotide sequence of the stop codon was modified so that the exogenous DNA could be read through and co-expressed as a fusion protein. For both recombineering steps **(i)** the generation of the retrieval vector and **(ii)** the modification of the retrieval vector, short homology arms had to be used to enable recombination. Although homologies of 50 flanking base pairs are more than sufficient for recombination, we used longer homology arms of 150–200 base pairs to further improve the targeting efficiency, which substantially decreased the effort required for subsequent screening of correct recombinants (Murphy, 1998; Sharan *et al.*, 2009). To obtain these homology arms, we amplified each homology stretch by PCR and directionally cloned it into the plasmid by "classic" cloning using restriction endonucleases and DNA-ligase. The targeting vector now contained, besides the long arms of homology, the modified exon 79 followed by the FLAG-EGFP sequence and further downstream a lox*P* flanked *neo* sequence controlled by two promoters, which drive the expression of the selectable marker in prokaryotic as well as in eukaryotic cells. This *neo* cassette would later be used for screening of recombinant ES clones using G418. The selectable marker would be no longer necessary after ES cell selection and was excised in the F1 generation of the transgenic mice *via* a cross with Cre-deleter animals. This was done to make sure that the *neo* cassette would not exert any unwanted positional effect on the *Dmd* gene or on any other downstream genes. In the targeting vector the lox*P* flanked *neo* cassette was tested for its functionality shown in Figure 11. Furthermore, we engineered unique restriction enzyme sites into the transgene. The *Sal*I

restriction enzyme site was not present in the targeting cassette and would be located outside of the targeting region of the vector so that the vector could be linearized and electroporated in ES cells. In the targeting cassette a *BglII* and *BamHI* site were introduced that would assure the distinction between wildtype and modified allele in genotyping of the ES-cells *via* Southern blot. Those endonuclease restriction sites had to present only once in the targeting vector but also in the genome close to but outside of the recombination cassette (Figure 12). Another important issue that we had to keep in mind while constructing the recombination cassette, was to prevent too harsh an alteration of the *Dmd* 3'UTR through insertion of the FLAG-EGFP-lox*P*-neo-lox*P* sequence. Important regulatory sequences are located in this 3'UTR region, which are highly conserved in the dystrophin gene (Greener *et al.*, 2002; Larsen and Howard, 2014; Lemaire *et al.*, 1988).

8.1.3. Modifying the endogenous dystrophin gene in ES cells and generation of transgenic mice

We used the constructed targeting vector to modify the dystrophin locus in murine 129Sv ES cells. ES cell lines for genetic manipulations are derived from the inner cell mass of 3.5-day-old mouse embryo and the first line successfully grown *in vitro* was established in the early 80ies (Evans and Kaufman, 1981). The most successful ES cell lines were generated from the 129/Sv mouse strain, which is still the most widely used one (Schoonjans *et al.*, 2003). ES cells are pluripotent and characterized by their capacity to self-renew. An additional characteristic of the ES cells is their ability to integrate into a developing mouse embryo when injected into a blastocyst (Bradley *et al.*, 1984). They contribute to the developing embryo and produce the chimerism in the so generated mice. The contribution of the ES cells to the germline cells of the chimeric mice is dependent on the truly totipotent state of the ES cells in the culture, an important condition in the process of generating transgenic animal models. Different culture methods for ES cell exist and are constantly optimized in order to keep the cells in totipotent, undifferentiated state for gene modification and keep their germline potency. For this purpose cells were grown the on a feeder cell layer, usually mitotically inactivated murine embryonic fibroblasts (Heuer *et al.*, 1993). The discovery of the cytokine myeloid leukemia inhibition factor (LIF) contributed to a big advancement of ES cell culturing techniques (Schöler *et al.*, 1989; Williams *et al.*, 1988). LIF-mediated signaling *via* activation of STAT3 blocks cellular differentiation (Burdon *et al.*, 1999) . Using LIF containing, feeder free systems

for culturing ES cells that use a support matrix like gelatin or Matrigel® have been widely established. In order to maintain a homogenous and undifferentiated population, we used 0.1% gelatin and LIF in serum-containing medium. We supplemented the ES cell culture media with β-mercaptoethanol and nonessential amino acids that were reported to provide further refinement to maintain the viability and totipotency of the cultured stem cells (Limaye *et al.*, 2009). The introduction of the targeting vector was done by electroporation, which is the most preferred method for introducing exogenous DNA into ES cells, although not the most efficient one. In order to select for successful recombinants, cells were grown on geneticin (G418), a toxin which only allowed the growth of cells expressing the *neo*-gene from the targeting cassette, an enzyme that inactivates neomycin and its structural relatives such as G418. Once the positive clones are identified and verified the *neo* cassette was no longer necessary and was excised. This could be done directly in the ES cells by using the recombinant *Cre*-recombinase, but this method requires another round of transfection, which often greatly diminishes the germline potential of the ES cells. Alternatively, the *neo* cassette can be removed in the mouse after successful germline transmission. We applied the latter method for the generation of *Dmd^{EGFP}* reporter mice by crossing the F1 generation with ubiquitous Cre-deleter mice.

The event of homologous recombination in ES cells is infrequent rare event and usually large numbers of clones have to be screened for correct recombination. The screening of positive ES cells was done by Southern blot analysis, which is the more precise method to distinguish between the wildtype and the modified allele. One can also use PCR-based screening of positive clones, which is a more rapid process but has a larger degree of false positive and false negative results. If the recombination frequency is low, it is possible that the PCR analysis will not detect the clones. If applying Southern blot analysis, the recombination has to be verified for both homology arms *via* a 5' and 3' specific probes that bind to regions outside of the targeting cassette. The strategy we used is represented in Figure 12. Since we were targeting the dystrophin gene located on the X-chromosome, male ES cells were used for homologous recombination ideally resulting in only one band being visible on the Southern blot. In Figure 12B on the first blot *Bgl*II digestion and 5'-probe hybridization yielded 10 positive clones. 7 of them were further tested using the same enzyme and 3' probe or *BamH*I digestion and the 3'-probe. All clones displayed the targeted allele but showed an additional

96

signal of the wildtype band. Most likely a contamination or a mixture with DNA from wildtype cells (micro-heterogeneity) would explain the presence of the wildtype band in the samples with positive recombinant cells. An incomplete digestion by the enzyme would also yield the same result, which could have happened due to adhering DNA-binding proteins that could have obscured the respective endonuclease restriction site. Nevertheless, the positive signal verified the presence of ES cells carrying the modified allele on the X-chromosome and therefore the ES cells were used for blastocyst injection. After several rounds of injecting different positive clones, chimeric mice were generated that transmitted the knock-in allele to the F1 generation. The ES cell clone that in the end successfully achieved germline transmission of the modified *Dmd* allele originally had yielded two bands on the Southern blot analysis.

The generation of transgenic mice took more than 2 years. The huge delay was due to problems in the ES culture of the commercial company. The process of electroporation of ES cells was repeated twice since the first round had not yielded chimeras. The ES culture methods could be the reason for the failure of germline transmission in the first round, where other factors than the supplements used to keep the cells in undifferentiated state may play an important role as well. The cell morphology and confluency are additional factors that influence the chimerism and later germline transmission, especially if the cultures are overgrown or at plateau. The concentration of the DNA construct as well as the electroporation parameters could also affect the viability of the cells. Furthermore, chromosomal abnormalities often observed in murine ES cells, may also contribute to low chimerism. This can be excluded by karyotyping of the positive ES clones and would save time on the long run.

Finally, the successfully generated F1-generation of $Dmd^{EGFP-neo}$ mice still bearing the selection cassette were analyzed *via* PCR and Southern blot and crossed with ubiquitous Cre-deleter mice to generate the Dmd^{EGFP} reporter mice. The reporter mice were born at Mendelian ratios and their genotypes were determined from tail biopsies using a triple primer PCR that enabled us to distinguish between wildtype, hetero-/homozygous female and hemizygous male mice.

8.2. Characterization of the *Dmd^EGFP* reporter mice

The reporter mice were analyzed and characterized to ensure proper expression of the dystrophin-EGFP fusion protein throughout different tissues. We were able to image dystrophin *in situ* based on its fluorescence signal in tissue sections as well as in single fibers. Furthermore, we wanted to find out, whether an EGFP signal could be detected *in vitro* in myotubes generated from differentiated satellite cells.

8.2.1. Dystrophin-EGFP is expressed at the sarcolemma of skeletal muscle

As already mentioned above, a C-terminal tag appended to the endogenous dystrophin might influence its folding and localization at the sarcolemma or might disturb the function of the protein. We therefore set out to investigate the muscle for correct localization of the dystrophin and is binding partners as well as to search for dystrophic features. In muscular dystrophy research the *tibialis anterior* (TA) muscle of the *mdx* mouse was frequently used as a representative muscle for investigation. Hence we decided to preferably use this particular muscle in our experiments as well **(i)** to make sure that our experiments are comparable to previous findings and **(ii)** to be able to investigate a mixed muscle with oxidative and glycolytic portions.

The expression of dystrophin-EGFP was confirmed by Western blot analysis of proteins extracted from TA muscles that displayed the correct molecular size (Figure 18). We used C-terminal (Dys2) and rod domain specific (Dys1) anti-dystrophin antibodies, which detected the fusion protein on Western blot at the same molecular size as the wildtype 427 kDa full-length dystrophin. The addition of the FLAG-EGFP tag would generate a 454 kDa fusion protein, but on a Western blot such small a difference could not be detected in the high MW range.

The expression levels we observed in the *Dmd^EGFP* samples appeared to be somewhat lower when using the C-terminal Dys2 antibody. A possible explanation could be the reduction of binding affinity of the Dys2 antibody through competition with the FLAG-EGFP-tag. A similar observation was made in the Western blot analysis of brain samples, where we used another C-terminal anti-dystrophin antibody (H4), the results of which will be discussed in more detail in section 8.2.4. The equal staining intensities when using the rod-domain specific antibody

(MANDYS19) let us conclude the differences seen with antibodies against the C-terminus are most likely the effect of steric hindrance.

Our goal was to generate a fusion protein that would be traceable using fluorescence microscopy without the need for *ex vivo* antibody staining. In skeletal muscle we verified that the native EGFP fluorescence was strong enough to identify the dystrophin at the sarcolemma. Signals from immunofluorescent staining with C-terminal and rod-domain specific dystrophin antibodies nicely co-localized with the proper EGFP fluorescent signal. The anti-dystrophin rod domain specific antibody (MANDYS19) recognizes and binds to the dystrophin amino acid sequences encoded by exons 20 and 21 (Man *et al.*, 1990). The Dys2 antibody recognizes the last 17 amino acids of human full-length dystrophin, which differs in two amino acid positions from the murine one. The cross sections of *soleus*, *tibialis anterior* and *gastrocnemius* muscles showed an exact superposition of the EGFP fluorescence with the MANDYS19 immune signal suggesting the correct expression of the skeletal muscle full-length dystrophin isoform. All the alternative dystrophin promoters that control the expression of shorter dystrophin isoforms are located downstream of intron 29 and would not be picked up by the MANDYS19 antibody. Hence, the signal from the MANDYS19 antibody, which was similar to the signal of the Dys2 C-terminal antibody, confirmed tagging of the skeletal muscle Dp427 isoform and its correct localization. Furthermore, we additionally verified the sarcolemmal expression of dystrophin using the Dys2 and Dys1 antibodies *via* immunohistochemistry in cryosections of the *gastrocnemius*, *soleus*, *tibialis anterior*, *quadriceps* and *extensor digitorum longus* muscles (Appendix, 13.4, Figure A3).

Dystrophin, as part of the DAPC at the sarcolemma, provides a link between the actin cytoskeleton in the cytosol and the extracellular matrix (ECM). Therefore, we also investigated the expression of two major players, laminin in the ECM and the cytoplasmic β-spectrin. Laminins are heterotrimeric extracellular matrix glycoproteins. In the muscle different laminin isoforms are expressed during myogenesis, as well as at the myotendinous and the neuromuscular junction (NMJ). Moreover, they play a role in synaptogenesis (Patton *et al.*, 1997). In adult skeletal muscle the most abundant isoform is laminin-211 (α2/β1/γ1, previously called merosin) (Ehrig *et al.*, 1990; Sasaki *et al.*, 2002). Laminin-211 interacts with two integral sarcolemmal proteins, with (i) integrin α7β1 and with (ii) dystroglycan, which is the core-component of the DAPC. α-Dystroglycan is heavy glycosylated, which is essential for

the binding of its extracellular domains to laminin-211 and to other ECM proteins (Yoshida-Moriguchi *et al.*, 2010). Hence, a link between extracellular laminin to intracellular actin is ensured by a non-covalent binding of α-dystroglycan to β-dystroglycan, which interacts with the C-terminus of dystrophin. In turn dystrophin completes the linking chain through its interaction with the cytoskeletal actin (Ervasti and Campbell, 1993). An immunofluorescent staining for laminin of the skeletal muscles is represented in Figure 19D. The distinct locations of dystrophin and laminin expression can be clearly seen with the dystrophin-EGFP signal located towards the interior of the fiber. In addition, laminin stained the blood vessels in the interstitial region between the fibers where no EGFP was detected.

Spectrin, like dystrophin, belongs to the spectrin protein superfamily of actin binding, membrane-anchoring proteins that are responsible for the maintenance of membrane integrity and cytoskeletal structure. Multiple spectrin isoforms exist, which are regulated in a complex, tissue- and time-specific manner in a variety of cells (Winkelmann *et al.*, 1990). In skeletal muscle, spectrin is a component of the membrane associated cytoskeleton, and the predominant isoform is β-spectrin. It has been localized to the "costameres", which are rib-like structures that lie on the cytoplasmic surface over the Z and M lines of adjacent sarcomeres (Craig and Pardo, 1983; Pardo *et al.*, 1983; Porter *et al.*, 1992, 1997). At the costameres β-spectrin co-localizes with dystrophin (Porter *et al.*, 1992, 1997). In the *Dmd*^{EGFP} reporter mice this co-localization was maintained thus further confirming the correct expression and co-localization of the membrane associated cytoskeleton in the reporter mice (Figure 19C). Interestingly, the endothelial cells of the endomysial capillaries were also stained by the anti-β-spectrin antibody, whereas dystrophin-EGFP expression was absent. This shows that the expression of dystrophin in the vascular system is confined to those larger vessels that possess a *tunica media* (e.g. arteries and larger veins) (Rivier *et al.*, 1997).

8.2.2. Tagging of the endogenous dystrophin does not induce a dystrophic phenotype and does not disturb DAPC assembly in skeletal muscle of *Dmd*^{EGFP} reporter mice

Although we were able to demonstrate that the dystrophin-EGFP protein was correctly localized at the sarcolemma, it remained to be shown that the DAPC complex was correctly expressed and localized as well. Furthermore, we wanted to make sure that no changes in muscle morphology could be observed and hence no dystrophic phenotype was induced.

Dystrophin exerts its most important function through assembly of the DAPC complex, which is responsible for its mechanical as well as its signaling functions. The addition of a 27.9 kDa fluorescent protein might change the 3D-folding of dystrophin or mask its binding sites thereby disrupting important interactions. Loss of expression of DAPC components generally destabilizes the sarcolemma and triggers dystrophic changes (Kanagawa and Toda, 2006).

The protein structure of GFP comprises 11 β-sheets with an internal α-helix and short helical segments on the ends of the cylinder, which constitute a protein folding structure named β-can. The fluorophores are protected inside the cylinders. Residues on the outside are predominantly polar. In the case of standard GFP, the dimerization domain consists of a small hydrophobic patch and numerous hydrophilic contacts (Yang *et al.*, 1996). In the mutant EGFP-p.L221K used by us, this hydrophobic interaction is disrupted. For the C-terminus of dystrophin, which is expressed from exons 78-79, the predicted folding pattern is a β-sheet with few hydrophobic residues (≈16%) at the surface and a global positive charge.

For the splice variant that encodes the embryonic Dp71 (Dp71f) isoform, an alternative splicing event excludes exon 78 and generates a modified C-terminus (Austin *et al.*, 1995). The new ORF has a stop codon, which is located downstream in the 3'UTR and produces a dystrophin with a 31 amino acid tail instead of the shorter 13 amino acid tail if exon 78 would be included. With the alternative C-terminus, the newly created amphipathic α-helix contains a higher percentage of hydrophobic residues and a global negative charge, which has been suggested to confer different biophysical and functional properties (Rau *et al.*, 2015). In order to exclude steric incompatibilities of the EGFP tag, which constitutes a significant addition to an important functional domain of the protein and may thus have unwanted effects on protein folding, function, or targeting we analyzed the morphology of the muscle.

H&E staining of cross sections from different skeletal as well as from heart muscle did not show any differences between the adult reporter mice and their wildtype littermates (Figure 25, Appendix 13.3, Figure A2). Moreover, no dystrophic changes were detected in aged *Dmd*^{EGFP} (10 months old) mice, which were well beyond the age, when dystrophic changes are commonly seen in *mdx* mice. For comparison, we analyzed aged-matched dystrophic *mdx* mice, which showed strong muscle degeneration, fibrosis, immune cell infiltration, and central nucleation – all hallmarks of an advanced dystrophic process.

In addition, we screened different skeletal muscles for the expression of representative members of the DAPC sub-complexes, the sarcoglycan-complex, the dystroglycan-complex as well as the cytoplasmic nNOS. (Figure 26, Appendix 13.4, Figure A2). Normal sarcolemmal expression patterns for α-, β-, γ-sarcoglycan, α-dystroglycan, and nNOS were confirmed suggesting proper function of the fusion protein and no obvious changes in the protein structure that might have disturbed those interactions.

In some of the cryo-cross sections of the TA the fiber in *Dmd*[EGFP] reporter mice appeared smaller than in the corresponding wildtype animals (Figure 26). This might be due to the fact that images taken were from different regions of the TA. The deep part, which is closer to the bone, contains generally fibers with smaller cross sectional areas, which increase towards the superficial region of the muscle (Chiyoko *et al.*, 2001). However, to rule out a systematic difference in fiber diameters, a morphometric analysis of complete TA cross sections at different levels of the muscle has to be done.

Although we have verified the correct localization of the DAPC members, it remains to be shown whether the dystrophin-EGFP expression influences the amount of the other proteins in the complex expressed. Reduced levels of DAPC members have been observed in dystrophic muscles in *mdx* mice and DMD patients. However, quantification of protein expression or localization is challenging. Such investigations could be done by semi-quantitative Western blot, which would, however, only pick up large differences. The limitations of Western blot could be overcome by mass spectrometry, especially by the SILAC method (Ong *et al.*, 2002), which would however require a specific breeding program. As an alternative, we could exploit the presence of the FLAG or the EGFP tag in our dystrophin of *Dmd*[EGFP] reporter mice to perform an immunoprecipitation. The group of Montanaro has optimized a simple and rapid protocol for antibody-based purification of dystroglycan and interacting proteins directly from skeletal muscle tissues followed by direct protein identification by tandem mass spectrometry. This method could thus be applied to precipitate the Dystrophin-EGFP and subsequently identify and quantify the co-precipitated binding partners (Yoon *et al.*, 2012).

8.2.3. Dystrophin-EGFP fusion protein is expressed in the heart and the smooth muscles

An important consideration for our targeting strategy was the site of EGFP insertion into the endogenous dystrophin. The aim was to target the major dystrophin isoforms expressed in different tissues and to find out whether the endogenous fluorescent signal would be strong enough for detection.

The absence of dystrophin in the heart leads to dilated cardiomyopathy, the most common cause of death in DMD patients. This underlines the importance to understand the function of dystrophin in the heart. Up to date, very few animal models exist that aim to address this question (Bostick *et al.*, 2009). In the *Dmd*EGFP mouse we observed clear dystrophin-EGFP expression in the heart and co-localization with the dystrophin immune signal, which suggests the proper expression of the Dp427 isoform (Figure 20). The dystrophin expression in the heart is controlled by the muscle- and brain-specific promoters. Moreover, intramuscular blood vessels in the heart sections showed an EGFP-signal as well, which partially co-localized with the anti-CD31 signal (Figure 20). Dystrophin is known to be expressed in the walls of large arteries, large veins and small arteries (Rivier *et al.*, 1997). This expression pattern hints towards a mechanical role of dystrophin in the membrane of smooth muscle cells since these arterioles have contractile properties and actively participate in the regulation of vascular tone and diameter as well as of blood pressure, while dystrophin is absent from small veins, whose diameter is only passively regulated by the blood volume and elastic fibers (Rivier *et al.*, 1997).

We confirmed that the smooth muscle isoform in the walls of the blood vessels was successfully targeted in the cardiac tissue as well. The successful tagging and the strong EGFP-signal observed in the heart will facilitate further studies on dystrophin expression in the heart as well as in the vascular smooth muscles. In future experiments we now have to address the question, whether *in vitro* cultured and differentiated cardiomyocytes from *Dmd*EGFP reporter mice would express the fusion protein as well.

The localization of dystrophin near the plasma membrane of smooth muscle cells *via* its EGFP-fluorescence could be readily observed also in the cryosections of intestinal organs. In cross-sections of the stomach, *ileum*, and *colon* of *Dmd*EGFP mice we observed bundles of longitudinal and circular layers of smooth muscle cells with dystrophin located at their

periphery. The distribution of the signal was punctuate and this is in line with previous studies using dystrophin antibodies to depict dystrophin in the duodenal wall (Byers *et al.*, 1991). This distribution is due to the exclusion of dystrophin from the *adherens* junctions between smooth muscles. This was demonstrated in smooth muscle of guinea pigs, where dystrophin and vinculin, a protein expressed in adherens junctions, had a mutually exclusive location (North *et al.*, 1993; Porter *et al.*, 1992).

In the *colon* of *Dmd^EGFP* reporter mice, we were also able to demonstrate co-localization between the anti-dystrophin immune signal and EGFP fluorescence (Figure 21B). For the labeling dystrophin in the *colon* we used a rabbit polyclonal C-terminal anti-dystrophin antibody in order to evade unspecific staining by the secondary anti-mouse IgG antibody since we expected a higher presence of immune cells and of immune globulin deposits in the gut of the mouse.

8.2.4. Non-muscle dystrophin isoforms are successfully tagged in the brain and retina of *Dmd^EGFP* reporter mice

The highest variety of dystrophin isoforms can be found in the brain and the short Dp71 is the predominant one. Brain isoforms commonly include the domains involved in β-dystroglycan and syntrophin binding, but lack the actin binding domains (Culligan and Ohlendieck, 2002).

Full-length dystrophin in the brain is expressed almost exclusively in neurons of the *cerebellum*, *cortex* and *hippocampus* (Lidov *et al.*, 1990). Different studies have reported that dystrophin and DAPC-like complexes are involved in modulating synapse function at a subset of GABAergic synapses in the *hippocampus* and *cerebellum* of mice. An association with clusters of inhibitory GABA$_A$ receptors has been reported (Brünig *et al.*, 2002; Kneussel *et al.*, 1999). As already mentioned in the introduction, a functional proof of the interaction between dystrophin and the GABA$_A$ receptor has not yet been presented. However, it is important to understand the role of dystrophin and its DAPC at the inhibitory synapses as it might explain some of the behavioral and electrophysiological findings in dystrophin deficient *mdx* mice (Anderson *et al.*, 2003; Graciotti *et al.*, 2008; Kueh *et al.*, 2008).

Other authors have proposed the expression of dystrophin at the postsynaptic density which mainly contains excitatory neurotransmitter receptors (Kim *et al.*, 1992). These contradictory

findings underline the importance to develop models that will improve the capability to study of the subcellular localization of dystrophin in neurons.

Unfortunately, we were unable to detect any EGFP fluorescent signals in the Purkinje cells of the *cerebellum* and in the neurons of the *hippocampus* using natural fluorescence of the *Dmd*[EGFP] mice. It is possible that the fluorescence signal was too weak to be detected by conventional fluorescence microscopy. We used 8 µm cryosections and standard methods for tissue preparation with no prior perfusion of the mice paraformaldehyde. Perfusion has been shown to improve antibody staining in the brain, while the effect on the natural EGFP fluorescence could be diminished (Moore *et al.*, 2002; Nguyen *et al.*, 2013; Sekiguchi *et al.*, 2009). Using confocal imaging or two photon microscopy on thicker brain sections/slices might also help to improve the visualization and confirm the expression of full-length dystrophin in these brain regions.

In Western blot analysis of brain lysates from *Dmd*[EGFP] mice, we used antibodies against GFP as well as against the rod- and C-terminal domain of dystrophin (Dys1 and H4, respectively). With this method we were unable to detect any bands (Figure 22). In wildtype brain, incubation with the H4 antibody revealed a very weak band and the Dys1 antibody did not bind at all. The H4 antibody is a C-terminal rabbit polyclonal antibody that recognizes the last 11 amino acids of dystrophin. In skeletal muscle we observed a weaker signal for dystrophin in the *Dmd*[EGFP] samples when using the C-terminal Dys2 antibody as compared to wildtype samples, while staining with the rod-domain Dys1 antibody revealed similar band intensities. Obviously, also in brain the EGFP tag causes steric hindrance against binding of the H4 and Dys2 C-terminal antibodies. This would also explain why we were unable to detect the Dp427 band in the brain of *Dmd*[EGFP] mice, where the dystrophin expression is only 10% of that in skeletal muscle. In order to show that we have tagged also the full-length isoform of brain dystrophin, we will test further antibodies and plan to perform a Western blot with protein extracts from isolated *hippocampus* and *cerebellum*, brain regions with a relatively higher neuronal dystrophin expression.

The Dp140 isoform of dystrophin is highly expressed in the fetal brain where it might have a role during early brain development. In the adult brain its expression was reported to be in the microvasculature (Lidov *et al.*, 1995; Morris *et al.*, 1995). The shortest Dp71 isoform of dystrophin is abundant in the adult brain and its important function was investigated using

105

animal models like the Dp71-null mice (Sarig *et al.*, 1999). Dp71 is expressed around blood vessels of the brain and is detected in different marcoglia cells throughout the brain and retina like astrocytes in the *cortex*, Bergman glial cells in the *cerebellum*, radial glial cells in the *hippocampus* and Müller glial cell in the retina (Blake *et al.*, 1999; Dalloz, 2003; Enger *et al.*, 2012; Haenggi *et al.*, 2004). The expression of Dp71 is confined to the glial-vascular endfeet, suggesting a role in blood-brain as well as the blood-retina barrier.

In the brain and retina of *Dmd^EGFP* mice we observed natural dystrophin-EGFP expression around blood vessels that were stained with the anti-CD31 endothelial cell marker (Figure 23, Figure 24). Moreover, staining with an antibody against the glial fibrillary acidic protein (GFAP) reveled partial co-localization of the dystrophin-EGFP with the Bergmann glia in the *cerebellum*, the glial cells of the *hippocampus*, and the Müller cells at the inner limiting membrane of the retina (Figure 23B, Figure 24C). In these regions the EGFP signal again only co-localized with the glial endfeet, which confirms a characteristic expression pattern of the Dp71 isoform (Enger *et al.*, 2012). On the other hand, dystrophin is expressed also in the blood vessels, mainly in the wall surrounding the endothelial cells. The EGFP signal was at some locations exactly surrounding the CD31 immunosignal, suggesting expression of the dystrophin in the outer walls of the vessels but not in the vascular endothelium. However, from our immunofluorescent images it did not become entirely clear, whether the green fluorescence really derived from the vessel wall or from the glial endfeet that constitute part of the blood-brain barrier. Additional stainings as well as improved high-resolution light imaging techniques (e.g. STED or STORM microscopy) will help to solve this question.

Furthermore, Western blot analysis of brain lysates from transgenic mice using the anti-GFP antibody showed a strong band migrating at approximately 100 kDa. This band corresponds to the Dp71 isoform with an appended EGFP tag of 27.9 kDa. The anti-dystrophin C-terminal H4 antibody, which was binding to the Dp71 isoform in wildtype samples did not detect any band in the transgenic brain lysates. This observation further verifies our assumption that H4 binding is impeded by the EGFP tag and could explain why we did not detect the Dp427 band in the brain of the reporter mice. Using the *Dmd^EGFP* reporter mice the complex role of dystrophin isoforms at the glial-vascular interface and their role in brain vascularization and blood brain barrier modulation could be further studied and better characterized. It is yet not clear how alterations in blood brain barrier observed in Dp71 null mice emerged. A direct link

to the function of Dp71 in water homeostasis and potassium buffering has not been made) (Nicchia *et al.*, 2008; Vajda *et al.*, 2002). Alternations of the blood brain barrier in *mdx* mice are better characterized. Loss of Dp427 leads to changes in vascular permeability, injury of endothelial cells, and disturbances of tight junctions and AQP4 assembly in glial cells (Nico *et al.*, 2003). These observations were explained by activation of the hypoxia inducible factor-1α together with upregulation of vascular growth factors and rearrangement of ZO-1 and claudin-1 proteins of the tight junctions (Nico *et al.*, 2007). Still a more detailed analysis need to be performed in order to understand these complex processes in the brain.

Dystrophin plays also an important role in the retina. The photoreceptors (rods and cones) of the retina are located at the outermost region called outer nuclear layer. At the outer plexiform layer (OPL) the terminals of the rods and cones interact with the postsynaptic bipolar and horizontal cells. In this region expression of dystrophin Dp427 and Dp260 have been associated with the photoreceptor terminals (Dalloz, 2003; Howard *et al.*, 1998). In our *Dmd^{EGFP}* mice the natural EGFP fluorescence could be detected in the OPL with a punctuate distribution as previously described. The signal co-localized with the immunosignal from the Dys2 antibody. Using the rod domain MANDYS19 antibody, dystrophin superposition with the EGFP signal was detected only in some regions. This finding confirms the targeting of the full-length dystrophin as well as of the Dp260 isoform, which is not recognized by MANDYS19 (Figure 24B). In this region blood vessels stained with the anti-CD31 antibody and associated with the natural EGFP signal and with Dys2 staining, but **not** with MANDYS19 staining, reflect the expression of Dp71-EGFP in the endfeet of the astrocytes, at their contact with the capillary basal lamina. Dystrophin expression in the retinal blood vessels needs to be confirmed using improved imaging high resolution light imaging techniques.

As already mentioned in the introduction (sections 4.4.6.2), retinal abnormalities measured *via* the electroretinogram (ERG) have been observed in DMD patients as well as in different animal models (Pillers *et al.*, 1993; Schmitz and Drenckhahn, 1997). In mice that lack the full-length dystrophin isoform, no changes in the ERG were observed, but changes appeared, when deleting the shorter isoform (Pillers *et al.*, 1999). The changes in the b-wave, observed in under scotopic conditions, measures signals from the inner nuclear layer, suggesting alterations at the synapses between the rod photoreceptors and the ON bipolar cells. At the inner nuclear layer bipolar and horizontal cells receive signals from the photo-terminals. The

synapses are located in the OPL, where dystrophin expression was attributed to the photoreceptors. However, it remains to be shown whether the b-wave changes at the synapse are caused by pre- or postsynaptical changes.

Recently, authors performed more detailed in depth analysis of the dystrophin isoform distribution in the OPL of the retina using a combination of transcriptomic analysis and immunostaining. Dystrophin mRNA expression was detected at the inner nuclear layer. Using immunofluorescence, dystrophin expression was found also in the post-synapse of ON rod and cone bipolar cells, although at lower levels than in the surrounding photoreceptor elements, whereby the authors could not exclude artifacts through fluorescent signals from neighboring regions (Wersinger *et al.*, 2011). Thus using the *Dmd*^{EGFP} mice a better characterization of this region can be performed without the use of antibodies and potential associated staining artifacts.

On the other hand, Müller cell mediated signaling has been proposed to contribute to b-wave generation which suggests a role for Dp71 in the ERG changes observed (Dalloz, 2003; Newman and Odette, 1984). Further evidence is necessary to prove this. Finally, the color blindness observed in some DMD patients (Costa *et al.*, 2007) requires better characterization of dystrophin in cone signaling. Hence, the function and distribution of dystrophin isoforms in the retina remain to be better characterized in order to understand the visual impairment observed in DMD patients.

8.2.5. Dystrophin-EGFP expression in single fibers and in myotubes *in vitro*

We were interested to see, whether the EGFP signal would be strong enough, even on the single myofiber level, to distinguish between the wildtype and the *Dmd*^{EGFP} mouse.

Indeed, in fixed as well as in living single fibers (floating culture, not shown) the EGFP fluorescence was strong enough to distinguish between the two genotypes (Figure 27A). Moreover, a clear enrichment of EGFP fluorescence could be observed around the NMJ. We show co-localization of dystrophin with acetylcholine receptors *via* staining of the fibers with α-bungarotoxin (BTX). Fortunately, the natural EGFP signal was much stronger on the single fibers that were **not** processed for immune staining (Figure 27, compare B and C). This observation confirms that our *Dmd*^{EGFP} model can be used to study the *in vivo* dynamics of dystrophin at the NMJ based on its natural EGFP signal. NMJ alterations have been observed

in dystrophin deficient *mdx* mice where the lack of dystrophin and subsequently also of members from the DAPC cause morphologic changes of the motor endplate and possibly also of synaptic transmission (Kitaoka *et al.*, 1997; Lyons and Slater, 1991). Changes at the post-synaptic membrane have been mostly attributed to the lack of dystrophin *via* a disturbance in the distribution of acetylcholine receptors (Shiao *et al.*, 2004).

Another line of investigation we followed was to find out, whether *ex vivo* isolated satellite cells growing *in vitro* would express dystrophin once they form myotubes in culture. Unfortunately, the native EGFP signal in the myotubes after 8 days of culture was too weak to be picked up by fluorescence microscopy, possibly due to the still low absolute number of dystrophin molecules available. Interestingly, using a well-established anti-GFP antibody, the dystrophin-EGFP fusion protein was detected with a much stronger signal then using any of the anti-dystrophin antibodies. This further confirms the usefulness of our animal model to study dystrophin expression during myogenesis. The ability of *ex vivo* satellite cells from *Dmd*^{EGFP} reporter mice to produce dystrophin-EGFP provides a valuable tool to be used for transplantation and cell-tracing experiments.

8.2.6. *Dmd*^{EGFP} reporter mice: which dystrophin isoforms express the fluorescent tag?

The aim of our study was to generate a reporter mouse, in which dystrophin expression can be visualized and traced in different tissues by means of EGFP fluorescence. Dystrophin and its numerous isoforms and splice variants have pleiotropic functions throughout the body.

Almost all dystrophin isoforms share the C-terminal domain, which is very important for the function of the protein. It includes the dystroglycan, syntrophin and dystrobrevin binding sites. In two isoforms, Dp71c and Dp71$_{\Delta110}$, the syntrophin binding domain is removed. This isoforms are expressed during neural development in humans (Ceccarini *et al.*, 1997). In mice expression of these embryonic variants could be only confirmed on the mRNA level (Bies *et al.*, 1992).

Dmd^{EGFP} reporter mice express EGFP fused to the last exon 79 of dystrophin. Theoretically all isoforms expressing exon 79 should be tagged. These include: Dp427 (M, B, P), Dp260, Dp140, Dp116, Dp71d and Dp71c. The alternatively spliced hydrophobic C-terminus observed in Dp71f and Dp71$_{\Delta110}$ cannot be targeted in our model since skipping of exon 78 shifts the reading frame of the last exon 79. In humans these C-terminally altered isoforms were shown

109

to be involved in early embryonic development, but are also expressed in adult brain, albeit to a lesser extent (Austin *et al.*, 1995, 2000; Feener *et al.*, 1989). In mice, these isoforms have only recently been identified on the protein level in the adult mouse brain (Daoud *et al.*, 2009).

Figure 29 shows a scheme of the different dystrophin isoforms, their theoretical tagging with EGFP and the isoforms we confirmed to be expressed in the reporter mice.

We observed EGFP tagged full-length dystrophin in skeletal, heart and smooth muscle as well as in the retina. These isoforms are transcribed from the muscle and brain specific promoters. The expression of full-length dystrophin in the brain is driven by the Brain and Purkinje promoter. Unfortunately, using EGFP fluorescence and Western blot analysis, we were not able to detect this Dp427 isoform. No EGFP signal was detected in neurons in the cerebellum or hippocampus or cortex of *Dmd*^{EGFP} mice, regions where Dp427 expression was reported previously (Huard and Tremblay, 1992; Jancsik and Hajós, 1998). Most likely the methods we used to investigate the Dp427 expression in the brain were not sensitive enough. Experiments are on the way to show its expression in the reporter mice.

The tagging of the retinal isoform Dp260 was successfully identified by natural EGFP signal in the outer plexiform layer of the retina, where it is expressed next to the Dp427 dystrophin isoform.

Furthermore, we confirmed the successful targeting of Dp71 (i) by Western blot analysis as well as (ii) by immunofluorescence in the brain and retina. Dp71 is expressed in glia cells at the glial-vascular interface, surrounding the endothelial cells. Using fluorescence microscopy, we detected the EGFP signal at the endfeet of the Bergman glia in the *cerebellum*, at the endfeet of the astrocytes of the *hippocampus*, and in the Müller glia of the retina.

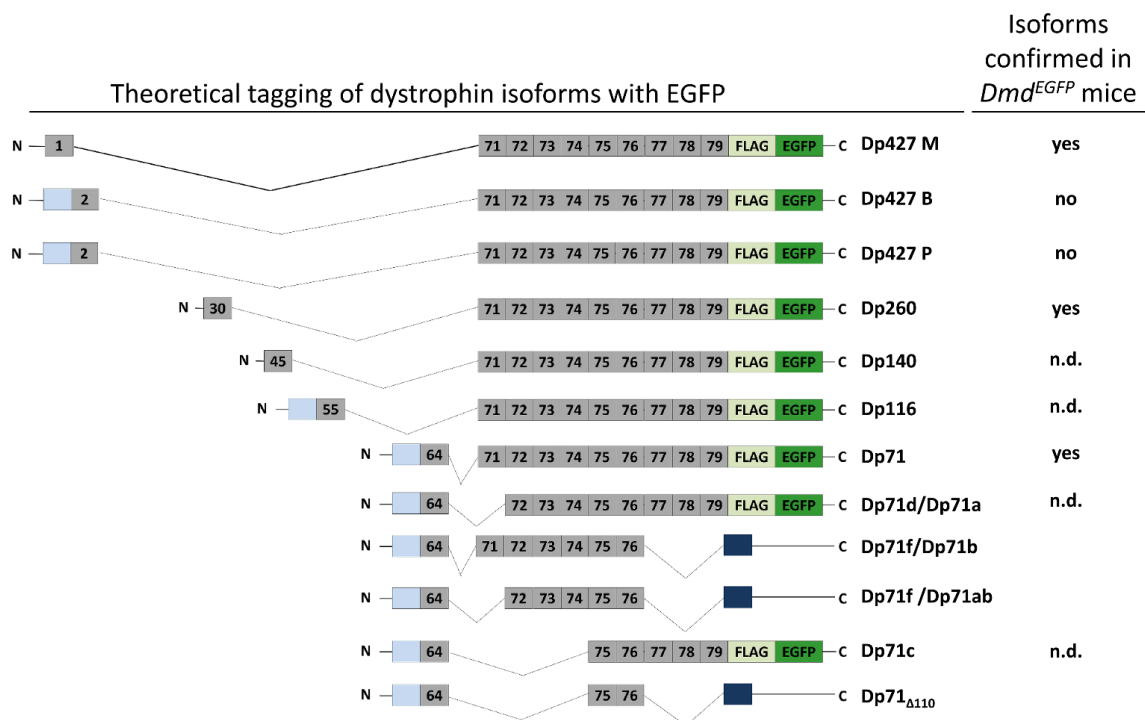The targeting of Dp116 and Dp140 isoforms remains to be analyzed.

Figure 29: Targeting of various dystrophin isoforms in *Dmd^EGFP* reporter mice.
A schematic representation of known dystrophin isoforms and splice variants and their alternative C-termini. In *Dmd^EGFP* mice the FLAG-EGFP sequence is fused to the exon 79 coding sequence of *Dmd*. Theoretically we expected successful targeting of the following isoforms Dp427 (M, B, P), Dp260, Dp140, Dp116, Dp71, Dp71d and Dp71c. The alternatively spliced variants of Dp71: Dp71f and Dp71$_{\Delta110}$ contain an alternative C-terminus that shifts the original reading frame of exon 79 and hence cannot be tagged with EGFP. We confirmed the expression of dystrophin-EGFP fusion protein in Dp427 (M), Dp260, Dp71, but could not detect Dp427 (B, P). Light blue squares represent alternative exons at the N-terminus of some isoforms. Dark blue squares show the alternative C-terminal sequence generated by exon 78 skipping. M: Muscle specific promoter, B: brain specific promoter, P: Purkinje cell promoter, n.d.: not determined, N: N-terminus, C: C-terminus.

8.3. Future applications of the *Dmd^EGFP* reporter mouse

In this work we investigated the main features of the *Dmd^EGFP* model, confirming the correct expression of the dystrophin-EGFP fusion protein at known tissues and sites throughout the murine body. The model we have developed can now be applied to answer biological questions concerning the expression, localization as well as the function of dystrophin, which seem to be more diverse than initially thought. Several questions could be addressed using common and well established techniques like fluorescence, confocal, two-photon, and FRET (Fluorescence Resonance Energy Transfer) microscopy. Moreover, dystrophin-EGFP expression in the reporter mice could also be studied with a combination of novel imaging techniques. Live confocal imaging, live two-photon, light-sheet microscopy, STORM (stochastic optical reconstruction microscopy), and PALM (photoactivated localization

111

microscopy) are newly developed imaging techniques that enable us to identify individual subcellular structures at high resolution so that their distributions and dynamics can be analyzed. Spatial differences in dense populations of molecules can be resolved.

I would now like to discuss possible future applications of the *Dmd*^{EGFP} reporter model to solve biological questions that would have been difficult to take up with standard immunohistological techniques. These are the study of **(i)** the dystrophin expression and subcellular localization during development and in living animals, **(ii)** dystrophin expression patterns in adult muscle and especially in non-muscle tissues, **(iii)** dystrophin expression patterns during satellite cell activation, differentiation and fusion, **(iv)** the regenerative capability of satellite cells after *Dmd*^{EGFP} satellite cell transplantation into dystrophic mice, **(v)** the dystrophin expression in revertant fibers, and **(vi)** the development of exon skipping approaches.

8.3.1. Dystrophin expression during mouse development

Dystrophin plays an important role during development and the expression of different specific isoforms has been reported. Their precise function still remains to be clarified. In humans, the Dp140 and Dp71 isoforms were shown to be expressed during development and neurogenesis. In DMD patients, mutations affecting these isoforms have been linked to cognitive impairment and mental retardation (Lidov *et al.*, 1995; Morris *et al.*, 1995). This underlines the importance of a better characterization of their role. Furthermore, a role of dystrophin during myogenesis has been postulated in studies conducted in *mdx* mice. It has been shown that dystrophin would be essential for correct fiber-type specification and stem cell function (Merrick *et al.*, 2009). However, the native spacial and temporal expression pattern of dystrophin during development remains to be determined.

This question could be addressed using the *Dmd*^{EGFP} reporter mice. First, however, we would have to confirm whether our model was suitable to study the expression of dystrophin based on its natural EGFP fluorescence during embryogenesis. If this is the case one could use live-cell confocal microscopy of the developing embryo. Another new exiting approach was developed allowing the observation of the normal development of mouse embryos between E6.5 and E8.5 for up to 24 h using light-sheet microscopy (Lopez *et al.*, 2015; Udan *et al.*, 2014).

8.3.2. Dystrophin expression in adult muscle and non-muscle tissue

The subsarcolemmal expression of dystrophin in muscle tissue was clearly seen in the *Dmd*^{EGFP} reporter mice. Yet, a more "mobile" dystrophin population has been recently observed in the muscle cells of zebrafish (Bajanca *et al.*, 2015). Whether such a population exists in mice could be analyzed using our model in combination with FRET and two-photon confocal live-cell imaging techniques as described by the group of Bajanca.

In non-muscle tissues, we observed strong EGFP expression in the photoreceptor terminals of the retina. In this region, the distribution of Dp427/Dp260 isoforms are not clearly defined. Moreover, dystrophin was suggested to be expressed in ON bipolar cells (Wersinger *et al.*, 2011). The *Dmd*^{EGFP} reporter mice are suitable to address these questions using advanced imaging techniques.

The strong EGFP signal of Dp71, which we observed at the glial-vascular interface in the brain and retina of the *Dmd*^{EGFP} mice, could be exploited to study the role and dynamics of dystrophin at the blood-brain barrier and blood-retina barrier. In combination with advanced super resolution imaging techniques like STORM and PALM the expression of dystrophin could be better characterized at the subcellular or even compartmental level.

Finally, the expression of dystrophin mRNA coding for different dystrophin isoforms has been confirmed in non-muscle tissues i.e. lung, liver, kidney, thymus, spleen, *testis*, and *uterus* (Tokarz *et al.*, 1998). The dystrophin EGFP fluorescence in the *Dmd*^{EGFP} reporter mice will facilitate the investigation of the dystrophin protein expression in these organs and help to find out whether isoform-specific mRNA copy numbers really reflect the magnitude of expression of the respective isoforms.

8.3.3. Dystrophin expression in satellite cells

It has recently been discovered that dystrophin plays a role in the regulation of asymmetric division and polarity of satellite cells (Dumont *et al.*, 2015). This opens a whole new avenue of research into dystrophinopathies. Natural EGFP expression on activated satellite cells, from single fibers should first be confirmed in our model, since the expression could be weak and below background fluorescence. If the EGFP expression was strong enough, live-cell imaging of freshly isolated single fibers with their attached satellite cells could be done in order to

follow up on the exact mechanism of dystrophin expression during asymmetric division. Furthermore, we could characterize the satellite cell population expressing dystrophin by inducing injury *via* cardiotoxin in the *Dmd*^{EGFP} mice in order to activate the satellite cells followed by FACS sorting of the EGFP expressing population. Subsequently, RNA sequencing as well as functional experiments with the cells could be performed. Furthermore, *Dmd*^{EGFP} reporter mice could be cardiotoxin-injured and the muscles screened by live-cell imaging for the expression of dystrophin-EGFP in activated satellite cells.

8.3.4. Studying satellite cell function

Transplantation experiments using satellite cells from the *Dmd*^{EGFP} mice could be conducted to understand the decline in functions of satellite cells with age and their role in sarcopenia as well as muscle degeneration after acute or chronic injury. Many factors contributing to satellite cell exhaustion during aging and dystrophic process are still not well defined. The ability of young *versus* old satellite cells to proliferate and repair a dystrophic or injured muscle could be studied. This would help to elucidate the contribution of cues from a young *versus* an aged satellite cell niche in the regenerative process. Transplanted cells could be easily traced by their EGFP fluorescence.

8.3.5. Studying dystrophin positive revertant fibers

An important topic to be investigated with the *Dmd*^{EGFP} mouse, and the initial idea for creating this model, will be the enigma of dystrophin positive revertant fibers. The revertant fibers have been discovered in the late 80ies shortly after the *DMD* gene was found and after the first antibodies had been produced.

To generate such a disease model, the *Dmd*^{EGFP} allele has first to be crossed into the *mdx* background in *cis*. This aim could be achieved through the natural recombination in female F1 mice that are heterozygous for the *Dmd*^{EGFP} as well as the *mdx* allele. Crossing over and recombination during meiosis between *Dmd* exon 23 bearing the *mdx* nonsense mutation on one and the exon 79-EGFP sequence on the other X chromosome corresponds to a hypothetic recombination frequency of ≈1 centiMorgan (cM) (≈1%), since both exons are separated by ≈1 Mio bp. For this, one would expect one crossing over in ≈100 litters. A successful crossing over and the position of both *mdx* mutation and EGFP-tag in *cis* could then be detected in the

114

male progeny of the F2 generation by genotyping. If the exon 23 *mdx* nonsense mutation and the EGFP-tag are on one allele in *cis* in a male mouse, those mice will not express the EGFP-tag due to the intervening premature termination codon, at least not the full-length muscle isoform. Only in revertant dystrophin positive fibers the EGFP tag will be (re)expressed if the reading frame of exon 79 is maintained or reconstituted. Usually regions in the central rod domain surrounding the mutation are skipped in those fibers and the last exon 79 would be present (Lu *et al.*, 2000). The *Dmd^mdx-EGFP^* model will facilitate the study of dystrophin positive revertant fibers and will enable their tracing as well as extraction and analyses of their attached satellite cells.

In preparation for such an experiment, we were able to show that EGFP expression on the level of single fibers can be clearly distinguished from non-EGFP expressing fibers. These results suggest that single fibers with a dystrophin positive revertant region could be distinguished from non-revertant ones (dystrophin negative). Hence, their attached satellite cells that are located close to the region where the revertant event had taken place, could be isolated, multiplied in culture and analyzed on the mRNA or protein level. Furthermore, using laser capture microdissection an area of revertant fibers can be directly dissected from muscle cross sections (without prior staining), RNA isolated and sequenced. This experiment will give us insights into whether such revertant events occur on the genomic level (by somatic deletions) or on the mRNA level (by alternative splicing patterns). The splicing pattern can be then compared between clusters of the same muscle as well as between different muscles. Moreover, using the RNA-seq technology other genes that are upregulated or down-regulated and might play an important role in revertant fiber formation can be identified if compared to non-revertant fiber regions.

8.3.6. The use of *Dmd^EGFP^* reporter mice in exon skipping approaches for DMD

Once the *Dmd^mdx-EGFP^* model is established, it will be very useful to test and to improve various exon skipping approaches against DMD. Successful restoration of dystrophin expression was reported after the use of a novel antisense oligonucleotides the tricycle-DNA (tcDNA) oligomers, leading to an improvement of brain, heart, and skeletal muscle function (Goyenvalle *et al.*, 2015). Use of the *Dmd^mdx-EGFP^* mouse will facilitate and aid optimization experiments with tcDNA-AON since dystrophin restoration can be confirmed and analyzed in

muscle and in non-muscle tissues by direct EGFP fluorescence. Measurement of the *in vivo* fluorescent signal will be much more accurate than using dystrophin antibodies and will enable serial investigations (time series) in the same mouse. Moreover, the *Dmd*^{EGFP} mice or their ES cells could be used to introduce other dystrophin mutations *via* the CRISPR/Cas9 system (Jinek *et al.*, 2012; Wang *et al.*, 2013) followed by screening of exon skipping molecules that are relevant to the treatment of characteristic human *DMD* deletion patterns.

In conclusion the *Dmd*^{EGFP} mouse model will be a very useful tool to further analyze and understand the role of dystrophin and thus the pathology of DMD and will aid the development of exon skipping approaches.

8.4. Conclusion

In the present work, we describe the first dystrophin-reporter mouse model, in which the endogenous dystrophin protein was tagged with the fluorescent EGFP-protein. The generation and characterization of the *Dmd*^{EGFP} reporter mice was described in detail and the application of the model especially in novel super resolution and live-cell imaging techniques discussed. We were able to confirm that the introduction of the EGFP-tag did not have any harmful influence on the expression, distribution and function of the native dystrophin protein. The fusion protein is expressed and can be detected *in vivo* based on its natural green fluorescence in skeletal muscle, heart, and smooth muscle as well as in CNS, as shown for brain and retina. The reporter mice were healthy, viable with normal litter sizes and without any changes of muscle architecture or expression of DAPC components. In the past 28 years after the discovery of the *DMD* gene and its protein product dystrophin many advances have been made to unravel the function of dystrophin in skeletal and heart muscle, the tissues mostly affected in DMD patients. More recently studies on the role of dystrophin in the CNS and its implication on cognitive development have emerged. Not much is known about the function of dystrophin during embryonic development or its role in smooth muscle tissue, and in non-muscle tissues such as liver, spleen, thymus, kidney, and uterus. In our reporter mouse model, dystrophin-EGFP expression can be visualized and followed on the level of single isolated muscle fibers and in satellite cell derived myotubes. The recent discovery of the function of dystrophin in the satellite cells points out that there are still unknown functions to be discovered (Dumont *et al.*, 2015) . Another recent study by Bajanca *et al.*,

(2015) using a human dystrophin cDNA-reporter in the zebrafish model showed that there is a subgroup of dystrophin molecules that are more mobile within the muscle cell than others, a phenomenon not yet understood.

Our model provides a very promising experimental system to study dystrophin in a non-artificial system exploiting the natural EGFP-fluorescence produced from the natural promoters of mouse dystrophin. Dynamic processes can be investigated using recently developed imaging techniques *in vivo* and *ex vivo* that will contribute to a better understanding of the role of dystrophin in normal conditions as well as in disease states. Crossing the *Dmd*^{EGFP} reporter allele into different *mdx*-dystrophic backgrounds or introducing a desired mutation/deletion into the ES-cells of the *Dmd*^{EGFP} reporter mice could be a way to develop a promising model to test different exon skipping approaches or to study revertant dystrophin fibers. Overall, the *Dmd*^{EGFP} reporter mouse has a great potential to unravel unknown functions of dystrophin, to aid the visualization of its precise localization and to discover novel interaction partners.

9. BIBLIOGRAPHY

Alberts B, Johnson A, Lewis J, Raff M, Roberts K, Walter P. General Recombination [Internet]. 2002[cited 2015 Nov 16] Available from: http://www.ncbi.nlm.nih.gov/books/NBK26898/

Amann KJ, Renley BA, Ervasti JM. A cluster of basic repeats in the dystrophin rod domain binds F-actin through an electrostatic interaction. J. Biol. Chem. 1998; 273: 28419–28423.

Anderson JL, Head SI, Morley JW. Altered inhibitory input to Purkinje cells of dystrophin-deficient mice. Brain Res. 2003; 982: 280–283.

Anderson JL, Head SI, Morley JW. Long-term depression is reduced in cerebellar Purkinje cells of dystrophin-deficient mdx mice. Brain Res. 2004; 1019: 289–292.

Anderson JL, Morley JW, Head SI. Enhanced homosynaptic LTD in cerebellar Purkinje cells of the dystrophic MDX mouse. Muscle Nerve 2010; 41: 329–334.

Anderson JT, Rogers RP, Jarrett HW. Ca2+-calmodulin binds to the carboxyl-terminal domain of dystrophin. J. Biol. Chem. 1996; 271: 6605–6610.

Aoki Y, Yokota T, Nagata T, Nakamura A, Tanihata J, Saito T, et al. Bodywide skipping of exons 45-55 in dystrophic mdx52 mice by systemic antisense delivery. Proc. Natl. Acad. Sci. 2012; 109: 13763–13768.

Araki E, Nakamura K, Nakao K, Kameya S, Kobayashi O, Nonaka I, et al. Targeted disruption of exon 52 in the mouse dystrophin gene induced muscle degeneration similar to that observed in Duchenne muscular dystrophy. Biochem. Biophys. Res. Commun. 1997; 238: 492–497.

Arechavala-Gomeza V, Kinali M, Feng L, Guglieri M, Edge G, Main M, et al. Revertant fibres and dystrophin traces in Duchenne muscular dystrophy: implication for clinical trials. Neuromuscul. Disord. NMD 2010; 20: 295–301.

Armstrong SC, Latham CA, Shivell CL, Ganote CE. Ischemic Loss of Sarcolemmal Dystrophin and Spectrin: Correlation with Myocardial Injury. J. Mol. Cell. Cardiol. 2001; 33: 1165–1179.

Austin RC, Howard PL, D'Souza VN, Klamut HJ, Ray PN. Cloning and characterization of alternatively spliced isoforms of Dp71. Hum. Mol. Genet. 1995; 4: 1475–1483.

Austin RC, Morris GE, Howard PL, Klamut HJ, Ray PN. Expression and synthesis of alternatively spliced variants of Dp71 in adult human brain. Neuromuscul. Disord. NMD 2000; 10: 187–193.

Badorff C, Lee GH, Lamphear BJ, Martone ME, Campbell KP, Rhoads RE, et al. Enteroviral protease 2A cleaves dystrophin: evidence of cytoskeletal disruption in an acquired cardiomyopathy. Nat. Med. 1999; 5: 320–326.

Bajanca F, Gonzalez-Perez V, Gillespie SJ, Beley C, Garcia L, Theveneau E, et al. In vivo dynamics of skeletal muscle Dystrophin in zebrafish embryos revealed by improved FRAP analysis. eLife 2015; 4

Bardoni A, Felisari G, Sironi M, Comi G, Lai M, Robotti M, et al. Loss of Dp140 regulatory sequences is associated with cognitive impairment in dystrophinopathies. Neuromuscul. Disord. 2000; 3: 194–199.

Barohn RJ, Levine EJ, Olson JO, Mendell JR. Gastric hypomotility in Duchenne's muscular dystrophy. N. Engl. J. Med. 1988; 319: 15–18.

Bar S, Barnea E, Levy Z, Neuman S, Yaffe D, Nudel U. A novel product of the Duchenne muscular dystrophy gene which greatly differs from the known isoforms in its structure and tissue distribution. Biochem. J. 1990; 272: 557–560.

Becker PE, Kiener F. [A new x-chromosomal muscular dystrophy]. Arch. Für Psychiatr. Nervenkrankh. Ver. Mit Z. Für Gesamte Neurol. Psychiatr. 1955; 193: 427–448.

Bies RD, Phelps SF, Cortez MD, Roberts R, Caskey CT, Chamberlain JS. Human and murine dystrophin mRNA transcripts are differentially expressed during skeletal muscle, heart, and brain development. Nucleic Acids Res. 1992; 20: 1725–1731.

Billard C, Gillet P, Barthez M, Hommet C, Bertrand P. Reading ability and processing in Duchenne muscular dystrophy and spinal muscular atrophy. Dev. Med. Child Neurol. 1998; 40: 12–20.

Billard C, Gillet P, Signoret JL, Uicaut E, Bertrand P, Fardeau M, et al. Cognitive functions in Duchenne muscular dystrophy: a reappraisal and comparison with spinal muscular atrophy. Neuromuscul. Disord. NMD 1992; 2: 371–378.

Birnboim HC, Doly J. A rapid alkaline extraction procedure for screening recombinant plasmid DNA. Nucleic Acids Res. 1979; 7: 1513–1523.

Bischoff R. Regeneration of single skeletal muscle fibers in vitro. Anat. Rec. 1975; 182: 215–235.

Bischoff R. Analysis of Muscle Regeneration Using Single Myofibers in Culture. Med. Sci. Sports Exerc. 1989; 21: S164–S172.

Blake DJ, Hawkes R, Benson MA, Beesley PW. Different Dystrophin-like Complexes Are Expressed in Neurons and Glia. J. Cell Biol. 1999; 147: 645–658.

Blake DJ, Kröger S. The neurobiology of duchenne muscular dystrophy: learning lessons from muscle? Trends Neurosci. 2000; 23: 92–99.

Blake DJ, Nawrotzki R, Loh NY, Górecki DC, Davies KE. beta-dystrobrevin, a member of the dystrophin-related protein family. Proc. Natl. Acad. Sci. U. S. A. 1998; 95: 241–246.

Blake DJ, Weir A, Newey SE, Davies KE. Function and Genetics of Dystrophin and Dystrophin-Related Proteins in Muscle. Physiol. Rev. 2002; 82: 291–329.

Bodyak N, Kang PM, Hiromura M, Sulijoadikusumo I, Horikoshi N, Khrapko K, et al. Gene expression profiling of the aging mouse cardiac myocytes. Nucleic Acids Res. 2002; 30: 3788–3794.

Boldrin L, Neal A, Zammit PS, Muntoni F, Morgan JE. Donor Satellite Cell Engraftment Is SignificantlyAugmented When the Host Niche Is Preserved and Endogenous Satellite Cells Are Incapacitated. STEM CELLS 2012; 30: 1971–1984.

Bork P, Sudol M. The WW domain: a signalling site in dystrophin? Trends Biochem. Sci. 1994; 19: 531–533.

Bostick B, Yue Y, Long C, Marschalk N, Fine DM, Chen J, et al. Cardiac expression of a mini-dystrophin that normalizes skeletal muscle force only partially restores heart function in aged Mdx mice. Mol. Ther. J. Am. Soc. Gene Ther. 2009; 17: 253–261.

Brack AS, Conboy MJ, Roy S, Lee M, Kuo CJ, Keller C, et al. Increased Wnt signaling during aging alters muscle stem cell fate and increases fibrosis. Science 2007; 317: 807–810.

Bradley A, Evans M, Kaufman MH, Robertson E. Formation of germ-line chimaeras from embryo-derived teratocarcinoma cell lines. Nature 1984; 309: 255–256.

Brenman JE, Chao DS, Gee SH, McGee AW, Craven SE, Santillano DR, et al. Interaction of nitric oxide synthase with the postsynaptic density protein PSD-95 and alpha1-syntrophin mediated by PDZ domains. Cell 1996; 84: 757–767.

Brenman JE, Chao DS, Xia H, Aldape K, Bredt DS. Nitric oxide synthase complexed with dystrophin and absent from skeletal muscle sarcolemma in Duchenne muscular dystrophy. Cell 1995; 82: 743–752.

Bresolin N, Castelli E, Comi GP, Felisari G, Bardoni A, Perani D, et al. Cognitive impairment in Duchenne muscular dystrophy. Neuromuscul. Disord. NMD 1994; 4: 359–369.

Brünig I, Suter A, Knuesel I, Lüscher B, Fritschy J-M. GABAergic terminals are required for postsynaptic clustering of dystrophin but not of GABA(A) receptors and gephyrin. J. Neurosci. Off. J. Soc. Neurosci. 2002; 22: 4805–4813.

Bulfield G, Siller WG, Wight PA, Moore KJ. X chromosome-linked muscular dystrophy (mdx) in the mouse. Proc. Natl. Acad. Sci. 1984; 81: 1189–1192.

Bushby KMD. Genetic and clinical correlations of Xp21 muscular dystrophy. J. Inherit. Metab. Dis. 1992; 15: 551–564.

Bushby KM, Gardner-Medwin D. The clinical, genetic and dystrophin characteristics of Becker muscular dystrophy. I. Natural history. J. Neurol. 1993; 240: 98–104.

Byers TJ, Kunkel LM, Watkins SC. The subcellular distribution of dystrophin in mouse skeletal, cardiac, and smooth muscle. J. Cell Biol. 1991; 115: 411–421.

Byers T, Lidov HG, Kunkel LM. An alternative dystrophin transcript specific to peripheral nerve. Nat. Genet. 1993; 4: 77–81.

Campos EC, Romano MMD, Prado CM, Rossi MA. Isoproterenol induces primary loss of dystrophin in rat hearts: correlation with myocardial injury. Int. J. Exp. Pathol. 2008; 89: 367–381.

Carlson ME, Hsu M, Conboy IM. Imbalance between pSmad3 and Notch induces CDK inhibitors in old muscle stem cells. Nature 2008; 454: 528–532.

Ceccarini M, Rizzo G, Rosa G, Chelucci C, Macioce P, Petrucci TC. A splice variant of Dp71 lacking the syntrophin binding site is expressed in early stages of human neural development. Brain Res. Dev. Brain Res. 1997; 103: 77–82.

Chalfie M, Tu Y, Euskirchen G, Ward WW, Prasher DC. Green fluorescent protein as a marker for gene expression. Science 1994; 263: 802–805.

Chamberlain JS, Metzger J, Reyes M, Townsend D, Faulkner JA. Dystrophin-deficient mdx mice display a reduced life span and are susceptible to spontaneous rhabdomyosarcoma. FASEB J. 2007; 21: 2195–2204.

Chan YM, Bönnemann CG, Lidov HG, Kunkel LM. Molecular organization of sarcoglycan complex in mouse myotubes in culture. J. Cell Biol. 1998; 143: 2033–2044.

Chapman VM, Miller DR, Armstrong D, Caskey CT. Recovery of induced mutations for X chromosome-linked muscular dystrophy in mice. Proc. Natl. Acad. Sci. U. S. A. 1989; 86: 1292–1296.

Chelly J, Hamard G, Koulakoff A, Kaplan JC, Kahn A, Berwald-Netter Y. Dystrophin gene transcribed from different promoters in neuronal and glial cells. Nature 1990; 344: 64–65.

Chiyoko H, Akihiko I, Toshiaki N. The Response of Tibialis Anterior Muscle Fibers in Mice to IncreasedMuscle Activity. Acta Med. Biol. (Niigata) 2001; 49: 5–10.

Christov C, Chrétien F, Abou-Khalil R, Bassez G, Vallet G, Authier F-J, et al. Muscle Satellite Cells and Endothelial Cells: Close Neighbors and Privileged Partners. Mol. Biol. Cell 2007; 18: 1397–1409.

Chung BC, Park HJ, Yoon SB, Lee HW, Kim KW, Lee SI, et al. Acute gastroparesis in Duchenne's muscular dystrophy. Yonsei Med. J. 1998; 39: 175–179.

Cibis GW, Fitzgerald KM, Harris DJ, Rothberg PG, Rupani M. The effects of dystrophin gene mutations on the ERG in mice and humans. Invest. Ophthalmol. Vis. Sci. 1993; 34: 3646–3652.

Ciotta G, Hofemeister H, Maresca M, Fu J, Sarov M, Anastassiadis K, et al. Recombineering BAC transgenes for protein tagging. Methods 2011; 53: 113–119.

Cirak S, Arechavala-Gomeza V, Guglieri M, Feng L, Torelli S, Anthony K, et al. Exon skipping and dystrophin restoration in patients with Duchenne muscular dystrophy after systemic phosphorodiamidate morpholino oligomer treatment: an open-label, phase 2, dose-escalation study. Lancet 2011; 378: 595–605.

Cisneros B, Rendon A, Genty V, Aranda G, Marquez F, Mornet D, et al. Expression of dystrophin Dp71 during PC12 cell differentiation. Neurosci. Lett. 1996; 213: 107–110.

Clerk A, Morris GE, Dubowitz V, Davies KE, Sewry CA. Dystrophin-related protein, utrophin, in normal and dystrophic human fetal skeletal muscle. Histochem. J. 1993; 25: 554–561.

Conboy IM, Conboy MJ, Wagers AJ, Girma ER, Weissman IL, Rando TA. Rejuvenation of aged progenitor cells by exposure to a young systemic environment. Nature 2005; 433: 760–764.

Connors NC, Adams ME, Froehner SC, Kofuji P. The potassium channel Kir4.1 associates with the dystrophin-glycoprotein complex via alpha-syntrophin in glia. J. Biol. Chem. 2004; 279: 28387–28392.

Copeland NG, Jenkins NA, Court DL. MOUSE GENOMIC TECHNOLOGIES: RECOMBINEERING: A POWERFUL NEW TOOL FOR MOUSE FUNCTIONAL GENOMICS. Nat. Rev. Genet. 2001; 2: 769–779.

Cosgrove BD, Gilbert PM, Porpiglia E, Mourkioti F, Lee SP, Corbel SY, et al. Rejuvenation of the muscle stem cell population restores strength to injured aged muscles. Nat. Med. 2014; 20: 255–264.

Costa MF, Oliveira AGF, Feitosa-Santana C, Zatz M, Ventura DF. Red-Green Color Vision Impairment in Duchenne Muscular Dystrophy. Am. J. Hum. Genet. 2007; 80: 1064–1075.

Costantini F, Lacy E. Introduction of a rabbit beta-globin gene into the mouse germ line. Nature 1981; 294: 92–94.

Cox GA, Sunada Y, Campbell KP, Chamberlain JS. Dp71 can restore the dystrophin-associated glycoprotein complex in muscle but fails to prevent dystrophy. Nat. Genet. 1994a; 8: 333–339.

Cox GA, Sunada Y, Campbell KP, Chamberlain JS. Dp71 can restore the dystrophin-associated glycoprotein complex in muscle but fails to prevent dystrophy. Nat. Genet. 1994b; 8: 333–339.

Craig SW, Pardo JV. Gamma actin, spectrin, and intermediate filament proteins colocalize with vinculin at costameres, myofibril-to-sarcolemma attachment sites. Cell Motil. 1983; 3: 449–462.

Crosbie RH, Heighway J, Venzke DP, Lee JC, Campbell KP. Sarcospan, the 25-kDa transmembrane component of the dystrophin-glycoprotein complex. J. Biol. Chem. 1997; 272: 31221–31224.

Culligan K, Ohlendieck K. Diversity of the Brain Dystrophin-Glycoprotein Complex. J. Biomed. Biotechnol. 2002; 2: 31–36.

Dalloz C. Targeted inactivation of dystrophin gene product Dp71: phenotypic impact in mouse retina. Hum. Mol. Genet. 2003; 12: 1543–1554.

Danialou G, Comtois AS, Dudley R, Karpati G, Vincent G, Des Rosiers C, et al. Dystrophin-deficient cardiomyocytes are abnormally vulnerable to mechanical stress-induced contractile failure and injury. FASEB J. Off. Publ. Fed. Am. Soc. Exp. Biol. 2001; 15: 1655–1657.

Danko I, Chapman V, Wolff J. The frequency of revertants in mdx mouse genetic models for Duchenne muscular dystrophy. Pediatr. Res. 1992; 32: 128–31.

Daoud F, Angeard N, Demerre B, Martie I, Benyaou R, Leturcq F, et al. Analysis of Dp71 contribution in the severity of mental retardation through comparison of Duchenne and Becker patients differing by mutation consequences on Dp71 expression. Hum. Mol. Genet. 2009; 18: 3779–3794.

Davies KE, Nowak KJ. Molecular mechanisms of muscular dystrophies: old and new players. Nat. Rev. Mol. Cell Biol. 2006; 7: 762–773.

Deconinck AE, Rafael JA, Skinner JA, Brown SC, Potter AC, Metzinger L, et al. Utrophin-dystrophin-deficient mice as a model for Duchenne muscular dystrophy. Cell 1997; 90: 717–727.

D'Souza VN, thi Man N, Morris GE, Karges W, Pillers D-AM, Ray PN. A novel dystrophin isoform is required for normal retinal electrophysiology. Hum. Mol. Genet. 1995; 4: 837–842.

Dubowitz V, Crome L. The central nervous system in Duchenne muscular dystrophy. Brain J. Neurol. 1969; 92: 805–808.

Duchenne GBA. Recherches sur la paralysie musculaire pseudohypertrophique ou paralysie myo-sclérosique. 1868

Dumont NA, Wang YX, von Maltzahn J, Pasut A, Bentzinger CF, Brun CE, et al. Dystrophin expression in muscle stem cells regulates their polarity and asymmetric division. Nat. Med. 2015

Dunckley MG, Manoharan M, Villiet P, Eperon IC, Dickson G. Modification of splicing in the dystrophin gene in cultured Mdx muscle cells by antisense oligoribonucleotides. Hum. Mol. Genet. 1998; 7: 1083–1090.

Dupont-Versteegden EE, McCarter RJ. Differential expression of muscular dystrophy in diaphragm versus hindlimb muscles of mdx mice. Muscle Nerve 1992; 15: 1105–1110.

Echigoya Y, Lee J, Rodrigues M, Nagata T, Tanihata J, Nozohourmehrabad A, et al. Mutation Types and Aging Differently Affect Revertant Fiber Expansion in Dystrophic Mdx and Mdx52 Mice. PLoS ONE 2013; 8: e69194.

Ehmsen J, Poon E, Davies KE. The dystrophin-associated protein complex. J. Cell Sci. 2002; 115: 2801–2803.

Ehrig K, Leivo I, Argraves WS, Ruoslahti E, Engvall E. Merosin, a tissue-specific basement membrane protein, is a laminin-like protein. Proc. Natl. Acad. Sci. U. S. A. 1990; 87: 3264–3268.

Emery AE. Abnormalities of the electrocardiogram in hereditary myopathies. J. Med. Genet. 1972; 9: 8–12.

Emery AEH. The muscular dystrophies. BMJ 1998; 317: 991–995.

Emery A, Muntoni F. Duchenne muscular dystrophy. 3rd ed. Oxford University Press; 2003.

Enger R, Gundersen GA, Haj-Yasein NN, Eilert-Olsen M, Thoren AE, Vindedal GF, et al. Molecular scaffolds underpinning macroglial polarization: an analysis of retinal Müller cells and brain astrocytes in mouse. Glia 2012; 60: 2018–2026.

England SB, Nicholson LV, Johnson MA, Forrest SM, Love DR, Zubrzycka-Gaarn EE, et al. Very mild muscular dystrophy associated with the deletion of 46% of dystrophin. Nature 1990; 343: 180–182.

Ervasti JM. Costameres: the Achilles' heel of Herculean muscle. J. Biol. Chem. 2003; 278: 13591–13594.

Ervasti JM, Campbell KP. A role for the dystrophin-glycoprotein complex as a transmembrane linker between laminin and actin. J. Cell Biol. 1993; 122: 809–823.

Evans MJ, Kaufman MH. Establishment in culture of pluripotential cells from mouse embryos. Nature 1981; 292: 154–156.

Fanchaouy M, Polakova E, Jung C, Ogrodnik J, Shirokova N, Niggli E. Pathways of abnormal stress-induced Ca2+ influx into dystrophic mdx cardiomyocytes. Cell Calcium 2009; 46: 114–121.

Feener CA, Koenig M, Kunkel LM. Alternative splicing of human dystrophin mRNA generates isoforms at the carboxy terminus. Nature 1989; 338: 509–511.

Fletcher S, Honeyman K, Fall AM, Harding PL, Johnsen RD, Steinhaus JP, et al. Morpholino Oligomer–Mediated Exon Skipping Averts the Onset of Dystrophic Pathology in the mdx Mouse. Mol. Ther. 2007; 15: 1587–1592.

Fletcher S, Honeyman K, Fall AM, Harding PL, Johnsen RD, Wilton SD. Dystrophin expression in the mdx mouse after localised and systemic administration of a morpholino antisense oligonucleotide. J. Gene Med. 2006; 8: 207–216.

Friedrich O, von Wegner F, Chamberlain JS, Fink RHA, Rohrbach P. L-type Ca2+ channel function is linked to dystrophin expression in mammalian muscle. PloS One 2008; 3: e1762.

Fry CS, Lee JD, Mula J, Kirby TJ, Jackson JR, Liu F, et al. Inducible depletion of satellite cells in adult, sedentary mice impairs muscle regenerative capacity without affecting sarcopenia. Nat. Med. 2015; 21: 76–80.

Gaedigk R, Law DJ, Fitzgerald-Gustafson KM, McNulty SG, Nsumu NN, Modrcin AC, et al. Improvement in survival and muscle function in an mdx/utrn(-/-) double mutant mouse using a human retinal dystrophin transgene. Neuromuscul. Disord. NMD 2006; 16: 192–203.

Garcia RA, Vasudevan K, Buonanno A. The neuregulin receptor ErbB-4 interacts with PDZ-containing proteins at neuronal synapses. Proc. Natl. Acad. Sci. U. S. A. 2000; 97: 3596–3601.

Gebski BL, Mann CJ, Fletcher S, Wilton SD. Morpholino antisense oligonucleotide induced dystrophin exon 23 skipping in mdx mouse muscle. Hum. Mol. Genet. 2003; 12: 1801–1811.

Gee SH, Madhavan R, Levinson SR, Caldwell JH, Sealock R, Froehner SC. Interaction of Muscle and Brain Sodium Channels with Multiple Members of the Syntrophin Family of Dystrophin-Associated Proteins. J. Neurosci. 1998; 18: 128–137.

Gilbert R, Nalbantoglu J, Petrof BJ, Ebihara S, Guibinga GH, Tinsley JM, et al. Adenovirus-mediated utrophin gene transfer mitigates the dystrophic phenotype of mdx mouse muscles. Hum. Gene Ther. 1999; 10: 1299–1310.

Goemans NM, Tulinius M, van den Akker JT, Burm BE, Ekhart PF, Heuvelmans N, et al. Systemic administration of PRO051 in Duchenne's muscular dystrophy. N. Engl. J. Med. 2011; 364: 1513–1522.

Gopinath SD, Rando TA. Stem Cell Review Series: Aging of the skeletal muscle stem cell niche. Aging Cell 2008; 7: 590–598.

Gordon JW, Ruddle FH. Integration and stable germ line transmission of genes injected into mouse pronuclei. Science 1981; 214: 1244–1246.

Górecki DC, Monaco AP, Derry JMJ, Walker AP, Barnard EA, Barnard PJ. Expression of four alternative dystrophin transcripts in brain regions regulated by different promoters. Hum. Mol. Genet. 1992; 1: 505–510.

Gorza L. Identification of a novel type 2 fiber population in mammalian skeletal muscle by combined use of histochemical myosin ATPase and anti-myosin monoclonal antibodies. J. Histochem. Cytochem. 1990; 38: 257–265.

Gowers WR. Clinical lecture on pseudohypertrophic muscular paralysis. Lancet 1878

Goyenvalle A, Babbs A, van Ommen G-JB, Garcia L, Davies KE. Enhanced Exon-skipping Induced by U7 snRNA Carrying a Splicing Silencer Sequence: Promising Tool for DMD Therapy. Mol. Ther. 2009; 17: 1234–1240.

Goyenvalle A, Griffith G, Babbs A, El Andaloussi S, Ezzat K, Avril A, et al. Functional correction in mouse models of muscular dystrophy using exon-skipping tricyclo-DNA oligomers. Nat. Med. 2015; 21: 270–275.

Goyenvalle A, Seto JT, Davies KE, Chamberlain J. Therapeutic approaches to muscular dystrophy. Hum. Mol. Genet. 2011; 20: R69–R78.

Goyenvalle A, Vulin A, Fougerousse F, Leturcq F, Kaplan J-C, Garcia L, et al. Rescue of Dystrophic Muscle Through U7 snRNA-Mediated Exon Skipping. Science 2004; 306: 1796–1799.

Graciotti L, Minelli A, Minciacchi D, Procopio A, Fulgenzi G. GABAergic miniature spontaneous activity is increased in the CA1 hippocampal region of dystrophic mdx mice. Neuromuscul. Disord. NMD 2008; 18: 220–226.

Grady RM, Grange RW, Lau KS, Maimone MM, Nichol MC, Stull JT, et al. Role for alpha-dystrobrevin in the pathogenesis of dystrophin-dependent muscular dystrophies. Nat. Cell Biol. 1999; 1: 215–220.

Greenberg DS, Sunada Y, Campbell KP, Yaffe D, Nudel U. Exogenous Dp71 restores the levels of dystrophin associated proteins but does not alleviate muscle damage in mdx mice. Nat. Genet. 1994; 8: 340–344.

Greener MJ, Sewry CA, Muntoni F, Roberts RG. The 3'-untranslated region of the dystrophin gene - conservation and consequences of loss. Eur. J. Hum. Genet. EJHG 2002; 10: 413–420.

Haenggi T, Soontornmalai A, Schaub MC, Fritschy J-M. The role of utrophin and Dp71 for assembly of different dystrophin-associated protein complexes (DPCS) in the choroid plexus and microvasculature of the brain. Neuroscience 2004; 129: 403–413.

Hakim CH, Duan D. Truncated dystrophins reduce muscle stiffness in the extensor digitorum longus muscle of mdx mice. J. Appl. Physiol. 2013; 114: 482–489.

Harbers K, Jähner D, Jaenisch R. Microinjection of cloned retroviral genomes into mouse zygotes: integration and expression in the animal. Nature 1981; 293: 540–542.

Harper SQ, Hauser MA, DelloRusso C, Duan D, Crawford RW, Phelps SF, et al. Modular flexibility of dystrophin: Implications for gene therapy of Duchenne muscular dystrophy. Nat. Med. 2002; 8: 253–261.

Hasegawa M, Cuenda A, Spillantini MG, Thomas GM, Buée-Scherrer V, Cohen P, et al. Stress-activated Protein Kinase-3 Interacts with the PDZ Domain of α1-Syntrophin A MECHANISM FOR SPECIFIC SUBSTRATE RECOGNITION. J. Biol. Chem. 1999; 274: 12626–12631.

Hasty P, Rivera-Pérez J, Bradley A. The length of homology required for gene targeting in embryonic stem cells. Mol. Cell. Biol. 1991; 11: 5586–5591.

Heemskerk HA, de Winter CL, de Kimpe SJ, van Kuik-Romeijn P, Heuvelmans N, Platenburg GJ, et al. In vivo comparison of 2'-O-methyl phosphorothioate and morpholino antisense oligonucleotides for Duchenne muscular dystrophy exon skipping. J. Gene Med. 2009; 11: 257–266.

Helliwell TR, Man NT, Morris GE, Davies KE. The dystrophin-related protein, utrophin, is expressed on the sarcolemma of regenerating human skeletal muscle fibres in dystrophies and inflammatory myopathies. Neuromuscul. Disord. NMD 1992; 2: 177–184.

Hemler ME. Dystroglycan Versatility. Cell 1999; 97: 543–546.

Heuer J, Bremer S, Pohl I, Spielmann H. Development of an in vitro embryotoxicity test using murine embryonic stem cell cultures. Toxicol. Vitro Int. J. Publ. Assoc. BIBRA 1993; 7: 551–556.

Hoffman EP, Brown Jr. RH, Kunkel LM. Dystrophin: The protein product of the duchenne muscular dystrophy locus. Cell 1987; 51: 919–928.

Hoffman EP, Hudecki MS, Rosenberg PA, Pollina CM, Kunkel LM. Cell and fiber-type distribution of dystrophin. Neuron 1988; 1: 411–420.

Hoffman EP, Morgan JE, Watkins SC, Partridge TA. Somatic reversion/suppression of the mouse mdx phenotype in vivo. J. Neurol. Sci. 1990; 99: 9–25.

Holt KH, Campbell KP. Assembly of the sarcoglycan complex. Insights for muscular dystrophy. J. Biol. Chem. 1998; 273: 34667–34670.

Hopp TP, Prickett KS, Price VL, Libby RT, March CJ, Pat Cerretti D, et al. A Short Polypeptide Marker Sequence Useful for Recombinant Protein Identification and Purification. Nat. Biotechnol. 1988; 6: 1204–1210.

Howard PL, Dally GY, Wong MH, Ho A, Weleber RG, Pillers DA, et al. Localization of dystrophin isoform Dp71 to the inner limiting membrane of the retina suggests a unique functional contribution of Dp71 in the retina. Hum. Mol. Genet. 1998; 7: 1385–1391.

Howard PL, D'Souza VN, Klamut HJ, Ray PN, others, Austin. Cloning and characterization of alternatively spliced isoforms of Dp71. Hum. Mol. Genet. 1995; 4: 1475–1483.

Huard J, Fortier L-P, Labrecque C, Dansereau G, Tremblay JP. Is dystrophin present in the nerve terminal nat the neuromuscular junction? An immunoshistochemical study of the heterozygote dystrophic (mdx) mouse. Synapse 1991; 7: 135–140.

Huard J, Tremblay JP. Localization of dystrophin in the Purkinje cells of normal mice. Neurosci. Lett. 1992; 137: 105–108.

Huxley AF, Niedergerke R. Structural changes in muscle during contraction; interference microscopy of living muscle fibres. Nature 1954; 173: 971–973.

Ibraghimov-Beskrovnaya O, Ervasti JM, Leveille CJ, Slaughter CA, Sernett SW, Campbell KP. Primary structure of dystrophin-associated glycoproteins linking dystrophin to the extracellular matrix. Nature 1992; 355: 696–702.

Jaffe KM, McDonald CM, Ingman E, Haas J. Symptoms of upper gastrointestinal dysfunction in Duchenne muscular dystrophy: case-control study. Arch. Phys. Med. Rehabil. 1990; 71: 742–744.

Jagadha V, Becker LE. Brain morphology in Duchenne muscular dystrophy: a Golgi study. Pediatr. Neurol. 1988; 4: 87–92.

Jancsik V, Hajós F. Differential distribution of dystrophin in postsynaptic densities of spine synapses. Neuroreport 1998; 9: 2249–2251.

Janssen I, Heymsfield SB, Wang Z, Ross R. Skeletal muscle mass and distribution in 468 men and women aged 18–88 yr. J. Appl. Physiol. 2000; 89: 81–88.

Jejurikar SS, Kuzon WM. Satellite cell depletion in degenerative skeletal muscle. Apoptosis Int. J. Program. Cell Death 2003; 8: 573–578.

Jinek M, Chylinski K, Fonfara I, Hauer M, Doudna JA, Charpentier E. A Programmable Dual-RNA–Guided DNA Endonuclease in Adaptive Bacterial Immunity. Science 2012; 337: 816–821.

Judge LM. Dissecting the signaling and mechanical functions of the dystrophin-glycoprotein complex. J. Cell Sci. 2006; 119: 1537–1546.

Kanagawa M, Toda T. The genetic and molecular basis of muscular dystrophy: roles of cell-matrix linkage in the pathogenesis. J. Hum. Genet. 2006; 51: 915–926.

Katz B. The Terminations of the Afferent Nerve Fibre in the Muscle Spindle of the Frog. Philos. Trans. R. Soc. Lond. B. Biol. Sci. 1961; 243: 221–240.

Kim TW, Wu K, Xu JL, Black IB. Detection of dystrophin in the postsynaptic density of rat brain and deficiency in a mouse model of Duchenne muscular dystrophy. Proc. Natl. Acad. Sci. U. S. A. 1992; 89: 11642–11644.

Kitaoka K, Matsuda Y, Desaki J, Oki S, Nagano Y, Shibata T. Topographic comparison of subneural apparatuses at neuromuscular junctions in normal and dystrophic [mdx] mice: a scanning electron microscope study. J. Electron Microsc. (Tokyo) 1997; 46: 193–197.

Klietsch R, Ervasti JM, Arnold W, Campbell KP, Jorgensen AO. Dystrophin-glycoprotein complex and laminin colocalize to the sarcolemma and transverse tubules of cardiac muscle. Circ. Res. 1993; 72: 349–360.

Kneussel M, Brandstätter JH, Laube B, Stahl S, Müller U, Betz H. Loss of postsynaptic GABA(A) receptor clustering in gephyrin-deficient mice. J. Neurosci. Off. J. Soc. Neurosci. 1999; 19: 9289–9297.

Koenig M, Beggs AH, Moyer M, Scherpf S, Heindrich K, Bettecken T, et al. The molecular basis for Duchenne versus Becker muscular dystrophy: correlation of severity with type of deletion. Am. J. Hum. Genet. 1989; 45: 498–506.

Koenig M, Hoffman EP, Bertelson CJ, Monaco AP, Feener C, Kunkel LM. Complete cloning of the duchenne muscular dystrophy (DMD) cDNA and preliminary genomic organization of the DMD gene in normal and affected individuals. Cell 1987; 50: 509–517.

Koenig M, Kunkel LM. Detailed analysis of the repeat domain of dystrophin reveals four potential hinge segments that may confer flexibility. J. Biol. Chem. 1990; 265: 4560–4566.

Koenig M, Monaco AP, Kunkel LM. The complete sequence of dystrophin predicts a rod-shaped cytoskeletal protein. Cell 1988; 53: 219–228.

Konigsberg UR, Lipton BH, Konigsberg IR. The regenerative response of single mature muscle fibers isolated in vitro. Dev. Biol. 1975; 45: 260–275.

Koppanati BM, Li J, Reay DP, Wang B, Daood M, Zheng H, et al. Improvement of the mdx mouse dystrophic phenotype by systemic in utero AAV8 delivery of a minidystrophin gene. Gene Ther. 2010; 17: 1355–1362.

Kornegay JN, Li J, Bogan JR, Bogan DJ, Chen C, Zheng H, et al. Widespread Muscle Expression of an AAV9 Human Mini-dystrophin Vector After Intravenous Injection in Neonatal Dystrophin-deficient Dogs. Mol. Ther. 2010; 18: 1501–1508.

Krivov LI, Stenina MA, Yarygin VN, Polyakov AV, Savchuk VI, Obrubov SA, et al. A new genetic variant of mdx mice: study of the phenotype. Bull. Exp. Biol. Med. 2009; 147: 625–629.

Kueh S, Head S, Morley J. GABAA RECEPTOR EXPRESSION AND INHIBITORY POST-SYNAPTIC CURRENTS IN CEREBELLAR PURKINJE CELLS IN DYSTROPHIN-DEFICIENT mdx MICE. Clin. Exp. Pharmacol. Physiol. 2008; 35: 207–210.

Kyoi S, Otani H, Hamano A, Matsuhisa S, Akita Y, Fujiwara H, et al. Dystrophin is a possible end-target of ischemic preconditioning against cardiomyocyte oncosis during the early phase of reperfusion. Cardiovasc. Res. 2006; 70: 354–363.

Lai Y, Thomas GD, Yue Y, Yang HT, Li D, Long C, et al. Dystrophins carrying spectrin-like repeats 16 and 17 anchor nNOS to the sarcolemma and enhance exercise performance in a mouse model of muscular dystrophy. J. Clin. Invest. 2009; 119: 624–635.

Larsen CA, Howard MT. Conserved regions of the DMD 3' UTR regulate translation and mRNA abundance in cultured myotubes. Neuromuscul. Disord. NMD 2014; 24: 693–706.

Lederfein D, Levy Z, Augier N, Mornet D, Morris G, Fuchs O, et al. A 71-kilodalton protein is a major product of the Duchenne muscular dystrophy gene in brain and other nonmuscle tissues. Proc. Natl. Acad. Sci. U. S. A. 1992; 89: 5346–5350.

Lederfein D, Yaffe D, Nudel U. A housekeeping type promoter, located in the 3'region of the Duchenne muscular dystrophy gene, controls the expression of Dp71, a major product of the gene. Hum. Mol. Genet. 1993; 2: 1883–1888.

Lees D, Fabbrizio E, Mornet D, Harricane M-C, Travo P. Dystrophin (Xp21), a New Phenotype Marker of Cultured Rat Aortic Myocytes. Exp. Cell Res. 1994; 210: 230–235.

Lees D, Fabbrizio E, Mornet D, Pugnère D, Travo P. Parallel expression level of dystrophin and contractile performances of rat aortic smooth muscle. Exp. Cell Res. 1995; 218: 401–404.

Lemaire C, Heilig R, Mandel JL. The chicken dystrophin cDNA: striking conservation of the C-terminal coding and 3' untranslated regions between man and chicken. EMBO J. 1988; 7: 4157–4162.

Lenk U, Hanke R, Thiele H, Speer A. Point mutations at the carboxy terminus of the human dystrophin gene: implications for an association with mental retardation in DMD patients. Hum. Mol. Genet. 1993; 2: 1877–1881.

Leon SH, Schuffler MD, Kettler M, Rohrmann CA. Chronic intestinal pseudoobstruction as a complication of Duchenne's muscular dystrophy. Gastroenterology 1986; 90: 455–459.

Li D, Bareja A, Judge L, Yue Y, Lai Y, Fairclough R, et al. Sarcolemmal nNOS anchoring reveals a qualitative difference between dystrophin and utrophin. J. Cell Sci. 2010; 123: 2008–2013.

Lidov HG, Byers TJ, Watkins SC, Kunkel LM. Localization of dystrophin to postsynaptic regions of central nervous system cortical neurons. Nature 1990; 348: 725–728.

Lidov HG, Selig S, Kunkel LM. Dp140: a novel 140 kDa CNS transcript from the dystrophin locus. Hum. Mol. Genet. 1995; 4: 329–335.

Limaye A, Hall B, Kulkarni AB. Manipulation of Mouse Embryonic Stem Cells for Knockout Mouse Production. Curr. Protoc. Cell Biol. Editor. Board Juan Bonifacino Al 2009; CHAPTER: Unit–19.1324.

Lipton BH, Schultz E. Developmental fate of skeletal muscle satellite cells. Science 1979; 205: 1292–1294.

Li S, Kimura E, Ng R, Fall BM, Meuse L, Reyes M, et al. A highly functional mini-dystrophin/GFP fusion gene for cell and gene therapy studies of Duchenne muscular dystrophy. Hum. Mol. Genet. 2006; 15: 1610–1622.

Liu P, Jenkins NA, Copeland NG. A highly efficient recombineering-based method for generating conditional knockout mutations. Genome Res. 2003; 13: 476–484.

Lopez AL, Garcia MD, Dickinson ME, Larina IV. Live confocal microscopy of the developing mouse embryonic yolk sac vasculature. Methods Mol. Biol. Clifton NJ 2015; 1214: 163–172.

Lorain S, Gross D-A, Goyenvalle A, Danos O, Davoust J, Garcia L. Transient immunomodulation allows repeated injections of AAV1 and correction of muscular dystrophy in multiple muscles. Mol. Ther. J. Am. Soc. Gene Ther. 2008; 16: 541–547.

Love DR, Byth BC, Tinsley JM, Blake DJ, Davies KE. Dystrophin and dystrophin-related proteins: a review of protein and RNA studies. Neuromuscul. Disord. NMD 1993; 3: 5–21.

Lu QL, Mann CJ, Bou-Gharios G, Morris GE, Xue SA, Fletcher S, et al. Functional amounts of dystrophin produced by skipping the mutated exon in the mdx dystrophic mouse. Nat. Med. 2003; 9: 1009–14.

Lu QL, Morris GE, Wilton SD, Ly T, Artem'yeva OV, Strong P, et al. Massive Idiosyncratic Exon Skipping Corrects the Nonsense Mutation in Dystrophic Mouse Muscle and Produces Functional Revertant Fibers by Clonal Expansion. J. Cell Biol. 2000; 148: 985–996.

Lyons PR, Slater CR. Structure and function of the neuromuscular junction in young adult mdx mice. J. Neurocytol. 1991; 20: 969–981.

Maffioletti SM, Noviello M, English K, Tedesco FS. Stem cell transplantation for muscular dystrophy: the challenge of immune response. BioMed Res. Int. 2014; 2014: 964010.

Man N thi, Cartwright AJ, Morris GE, Love DR, Bloomfield JF, Davies KE. Monoclonal antibodies against defined regions of the muscular dystrophy protein, dystrophin. FEBS Lett. 1990; 262: 237–240.

Matsumura K, Ervasti JM, Ohlendieck K, Kahl SD, Campbell KP. Association of dystrophin-related protein with dystrophin-associated proteins in mdx mouse muscle. Nature 1992; 360: 588–591.

Matsuo M, Masumura T, Nishio H, Nakajima T, Kitoh Y, Takumi T, et al. Exon skipping during splicing of dystrophin mRNA precursor due to an intraexon deletion in the dystrophin gene of Duchenne muscular dystrophy kobe. J. Clin. Invest. 1991; 87: 2127–2131.

Mauro A. Satellite cell of skeletal muscle fibers. J. Biophys. Biochem. Cytol. 1961; 9: 493–495.

McDouall RM, Dunn MJ, Dubowitz V. Nature of the mononuclear infiltrate and the mechanism of muscle damage in juvenile dermatomyositis and Duchenne muscular dystrophy. J. Neurol. Sci. 1990; 99: 199–217.

McGreevy JW, Hakim CH, McIntosh MA, Duan D. Animal models of Duchenne muscular dystrophy: from basic mechanisms to gene therapy. Dis. Model. Mech. 2015; 8: 195–213.

Mehler MF. Brain dystrophin, neurogenetics and mental retardation. Brain Res. Brain Res. Rev. 2000; 32: 277–307.

Mehler MF, Haas KZ, Kessler JA, Stanton PK. Enhanced sensitivity of hippocampal pyramidal neurons from mdx mice to hypoxia-induced loss of synaptic transmission. Proc. Natl. Acad. Sci. U. S. A. 1992; 89: 2461–2465.

Mendell JR, Rodino-Klapac LR, Sahenk Z, Roush K, Bird L, Lowes LP, et al. Eteplirsen for the treatment of Duchenne muscular dystrophy. Ann. Neurol. 2013; 74: 637–647.

Merrick D, Stadler LKJ, Larner D, Smith J. Muscular dystrophy begins early in embryonic development deriving from stem cell loss and disrupted skeletal muscle formation. Dis. Model. Mech. 2009; 2: 374–388.

Monaco AP, Bertelson CJ, Liechti-Gallati S, Moser H, Kunkel LM. An explanation for the phenotypic differences between patients bearing partial deletions of the DMD locus. Genomics 1988; 2: 90–95.

Monaco AP, Neve RL, Colletti-Feener C, Bertelson CJ, Kurnit DM, Kunkel LM. Isolation of candidate cDNAs for portions of the Duchenne muscular dystrophy gene. Nature 1986; 323: 646 – 650.

Monaco AP, Neve RL, Colletti-Feener C, Bertelson CJ, Kurnit DM, Kunkel LM. Isolation of candidate cDNAs for portions of the Duchenne muscular dystrophy gene. Nature 1986; 323: 646–650.

Moore SA, Saito F, Chen J, Michele DE, Henry MD, Messing A, et al. Deletion of brain dystroglycan recapitulates aspects of congenital muscular dystrophy. Nature 2002; 418: 422–425.

Morris GE, Simmons C, Man NT. Apo-Dystrophins (DP140 and DP71) and Dystrophin-Splicing Isoforms in Developing Brain. Biochem. Biophys. Res. Commun. 1995; 215: 361–367.

Muntoni F, Mateddu A, Serra G. Passive avoidance behaviour deficit in the mdx mouse. Neuromuscul. Disord. NMD 1991; 1: 121–123.

Murphy KC. Use of Bacteriophage λ Recombination Functions To Promote Gene Replacement in Escherichia coli. J. Bacteriol. 1998; 180: 2063–2071.

Muyrers JP, Zhang Y, Stewart AF. Techniques: Recombinogenic engineering--new options for cloning and manipulating DNA. Trends Biochem. Sci. 2001; 26: 325–331.

Nakamura A, Harrod GV, Davies KE. Activation of calcineurin and stress activated protein kinase/p38-mitogen activated protein kinase in hearts of utrophin-dystrophin knockout mice. Neuromuscul. Disord. NMD 2001; 11: 251–259.

Newey SE, Benson MA, Ponting CP, Davies KE, Blake DJ. Alternative splicing of dystrobrevin regulates the stoichiometry of syntrophin binding to the dystrophin protein complex. Curr. Biol. CB 2000; 10: 1295–1298.

Newman EA, Odette LL. Model of electroretinogram b-wave generation: a test of the K+ hypothesis. J. Neurophysiol. 1984; 51: 164–182.

Nguyen H, Ostendorf AP, Satz JS, Westra S, Ross-Barta SE, Campbell KP, et al. Glial scaffold required for cerebellar granule cell migration is dependent on dystroglycan function as a receptor for basement membrane proteins. Acta Neuropathol. Commun. 2013; 1: 1–19.

Nicchia GP, Cogotzi L, Rossi A, Basco D, Brancaccio A, Svelto M, et al. Expression of multiple AQP4 pools in the plasma membrane and their association with the dystrophin complex. J. Neurochem. 2008; 105: 2156–2165.

Nicholson LV. The 'rescue' of dystrophin synthesis in boys with Duchenne muscular dystrophy. Neuromuscul. Disord. 1993; 3: 525–31.

Nicholson LV, Davison K, Johnson MA, Slater CR, Young C, Bhattacharya S, et al. Dystrophin in skeletal muscle. II. Immunoreactivity in patients with Xp21 muscular dystrophy. J. Neurol. Sci. 1989; 94: 137–146.

Nico B, Frigeri A, Nicchia GP, Corsi P, Ribatti D, Quondamatteo F, et al. Severe alterations of endothelial and glial cells in the blood-brain barrier of dystrophic mdx mice. Glia 2003; 42: 235–251.

Nico B, Mangieri D, Crivellato E, Longo V, De Giorgis M, Capobianco C, et al. HIF activation and VEGF overexpression are coupled with ZO-1 up-phosphorylation in the brain of dystrophic mdx mouse. Brain Pathol. Zurich Switz. 2007; 17: 399–406.

Nico B, Paola Nicchia G, Frigeri A, Corsi P, Mangieri D, Ribatti D, et al. Altered blood-brain barrier development in dystrophic MDX mice. Neuroscience 2004; 125: 921–935.

Nigro G, Comi LI, Politano L, Bain RJI. The incidence and evolution of cardiomyopathy in Duchenne muscular dystrophy. Int. J. Cardiol. 1990; 26: 271–277.

Noordeen MH, Haddad FS, Muntoni F, Gobbi P, Hollyer JS, Bentley G. Blood loss in Duchenne muscular dystrophy: vascular smooth muscle dysfunction? J. Pediatr. Orthop. Part B 1999; 8: 212–215.

North AJ, Galazkiewicz B, Byers TJ, Glenney JR, Small JV. Complementary distributions of vinculin and dystrophin define two distinct sarcolemma domains in smooth muscle. J. Cell Biol. 1993; 120: 1159–1167.

Norwood FL, Sutherland-Smith AJ, Keep NH, Kendrick-Jones J. The structure of the N-terminal actin-binding domain of human dystrophin and how mutations in this domain may cause Duchenne or Becker muscular dystrophy. Structure 2000; 8: 481–491.

Nowak TV, Ionasescu V, Anuras S. Gastrointestinal manifestations of the muscular dystrophies. Gastroenterology 1982; 82: 800–810.

Nudel U, Zuk D, Einat P, Zeelon E, Levy Z, Neuman S, et al. Duchenne muscular dystrophy gene product is not identical in muscle and brain. Nture 1989; 337: 76–8.

Ogasawara A. Downward shift in IQ in persons with Duchenne muscular dystrophy compared to those with spinal muscular atrophy. Am. J. Ment. Retard. AJMR 1989; 93: 544–547.

Ohlendieck K, Ervasti JM, Matsumura K, Kahl SD, Leveille CJ, Campbell KP. Dystrophin-related protein is localized to neuromuscular junctions of adult skeletal muscle. Neuron 1991; 7: 499–508.

Okabe M, Ikawa M, Kominami K, Nakanishi T, Nishimune Y. 'Green mice' as a source of ubiquitous green cells. FEBS Lett. 1997; 407: 313–319.

Ong S-E, Blagoev B, Kratchmarova I, Kristensen DB, Steen H, Pandey A, et al. Stable Isotope Labeling by Amino Acids in Cell Culture, SILAC, as a Simple and Accurate Approach to Expression Proteomics. Mol. Cell. Proteomics 2002; 1: 376–386.

Palmer E, Freeman T. Investigation into the use of C- and N-terminal GFP fusion proteins for subcellular localization studies using reverse transfection microarrays. Comp. Funct. Genomics 2004; 5: 342–353.

Palmiter RD, Brinster RL, Hammer RE, Trumbauer ME, Rosenfeld MG, Birnberg NC, et al. Dramatic growth of mice that develop from eggs microinjected with metallothionein–growth hormone fusion genes. Nature 1982; 300: 611–615.

Pardo JV, Siliciano JD, Craig SW. A vinculin-containing cortical lattice in skeletal muscle: transverse lattice elements ('costameres') mark sites of attachment between myofibrils and sarcolemma. Proc. Natl. Acad. Sci. 1983; 80: 1008–1012.

Partridge TA. The mdx mouse model as a surrogate for Duchenne muscular dystrophy. FEBS J. 2013; 280: 4177–4186.

Pasternak C, Wong S, Elson EL. Mechanical function of dystrophin in muscle cells. J. Cell Biol. 1995; 128: 355–361.

Pastoret C, Sebille A. mdx mice show progressive weakness and muscle deterioration with age. J. Neurol. Sci. 1995; 129: 97–105.

Pasut A, Jones AE, Rudnicki MA. Isolation and Culture of Individual Myofibers and their Satellite Cells from Adult Skeletal Muscle [Internet]. J. Vis. Exp. 2013[cited 2015 Jun 6] Available from: http://www.jove.com/video/50074/isolation-culture-individual-myofibers-their-satellite-cells-from

Patterson GH, Knobel SM, Sharif WD, Kain SR, Piston DW. Use of the green fluorescent protein and its mutants in quantitative fluorescence microscopy. Biophys. J. 1997; 73: 2782–2790.

Patton BL, Miner JH, Chiu AY, Sanes JR. Distribution and function of laminins in the neuromuscular system of developing, adult, and mutant mice. J. Cell Biol. 1997; 139: 1507–1521.

Perloff JK, Roberts WC, de Leon AC, O'Doherty D. The distinctive electrocardiogram of Duchenne's progressive muscular dystrophy. An electrocardiographic-pathologic correlative study. Am. J. Med. 1967; 42: 179–188.

Perriard J-C, Hirschy A, Ehler E. Dilated Cardiomyopathy. Trends Cardiovasc. Med. 2003; 13: 30–38.

Perronnet C, Vaillend C, Perronnet C, Vaillend C. Dystrophins, Utrophins, and Associated Scaffolding Complexes: Role in Mammalian Brain and Implications for Therapeutic Strategies, Dystrophins, Utrophins, and Associated Scaffolding Complexes: Role in Mammalian Brain and Implications for Therapeutic Strategies. BioMed Res. Int. BioMed Res. Int. 2010; 2010, 2010: e849426.

Peters MF, O'Brien KF, Sadoulet-Puccio HM, Kunkel LM, Adams ME, Froehner SC. beta-dystrobrevin, a new member of the dystrophin family. Identification, cloning, and protein associations. J. Biol. Chem. 1997; 272: 31561–31569.

Peters MF, Sadoulet-Puccio HM, Grady RM, Kramarcy NR, Kunkel LM, Sanes JR, et al. Differential Membrane Localization and Intermolecular Associations of α-Dystrobrevin Isoforms in Skeletal Muscle. J. Cell Biol. 1998; 142: 1269–1278.

Petrof BJ, Shrager JB, Stedman HH, Kelly AM, Sweeney HL. Dystrophin protects the sarcolemma from stresses developed during muscle contraction. Proc. Natl. Acad. Sci. 1993; 90: 3710–3714.

Phelps SF, Hauser MA, Cole NM, Rafael JA, Hinkle RT, Faulkner JA, et al. Expression of full-length and truncated dystrophin mini-genes in transgenic mdx mice. Hum. Mol. Genet. 1995; 4: 1251–1258.

Pigozzo SR, Da Re L, Romualdi C, Mazzara PG, Galletta E, Fletcher S, et al. Revertant Fibers in the mdx Murine Model of Duchenne Muscular Dystrophy: An Age- and Muscle-Related Reappraisal. PLoS ONE 2013; 8: e72147.

Pillers DA, Bulman DE, Weleber RG, Sigesmund DA, Musarella MA, Powell BR, et al. Dystrophin expression in the human retina is required for normal function as defined by electroretinography. Nat. Genet. 1993; 4: 82–86.

Pillers D-AM, Weleber RG, Green DG, Rash SM, Dally GY, Howard PL, et al. Effects of Dystrophin Isoforms on Signal Transduction through Neural Retina: Genotype–Phenotype Analysis of Duchenne Muscular Dystrophy Mouse Mutants. Mol. Genet. Metab. 1999; 66: 100–110.

Pons F, Robert A, Fabbrizio E, Hugon G, Califano JC, Fehrentz JA, et al. Utrophin localization in normal and dystrophin-deficient heart. Circulation 1994; 90: 369–374.

Ponting CP, Blake DJ, Davies KE, Kendrick-Jones J, Winder SJ. ZZ and TAZ: new putative zinc fingers in dystrophin and other proteins. Trends Biochem. Sci. 1996; 21: 11–13.

Poon E, Howman EV, Newey SE, Davies KE. Association of syncoilin and desmin: linking intermediate filament proteins to the dystrophin-associated protein complex. J. Biol. Chem. 2002; 277: 3433–3439.

Porter GA, Dmytrenko GM, Winkelmann JC, Bloch RJ. Dystrophin colocalizes with beta-spectrin in distinct subsarcolemmal domains in mammalian skeletal muscle. J. Cell Biol. 1992; 117: 997–1005.

Porter GA, Scher MG, Resneck WG, Porter NC, Fowler VM, Bloch RJ. Two populations of β-spectrin in rat skeletal muscle. Cell Motil. Cytoskeleton 1997; 37: 7–19.

Poteete AR. What makes the bacteriophage λ Red system useful for genetic engineering: molecular mechanism and biological function. FEMS Microbiol. Lett. 2001; 201: 9–14.

Pramono ZAD, Takeshima Y, Alimsardjono H, Ishii A, Takeda S, Matsuo M. Induction of Exon Skipping of the Dystrophin Transcript in Lymphoblastoid Cells by Transfecting an Antisense Oligodeoxynucleotide Complementary to an Exon Recognition Sequence. Biochem. Biophys. Res. Commun. 1996; 226: 445–449.

Prasher DC, Eckenrode VK, Ward WW, Prendergast FG, Cormier MJ. Primary structure of the Aequorea victoria green-fluorescent protein. Gene 1992; 111: 229–233.

Pratt SJP, Valencia AP, Le GK, Shah SB, Lovering RM. Pre- and postsynaptic changes in the neuromuscular junction in dystrophic mice. Striated Muscle Physiol. 2015: 252.

Quinlan JG, Hahn HS, Wong BL, Lorenz JN, Wenisch AS, Levin LS. Evolution of the mdx mouse cardiomyopathy: physiological and morphological findings. Neuromuscul. Disord. NMD 2004; 14: 491–496.

Rando TA. The dystrophin-glycoprotein complex, cellular signaling, and the regulation of cell survival in the muscular dystrophies. Muscle Nerve 2001; 24: 1575–1594.

Rapaport D, Passos-Bueno MR, Brandão L, Love D, Vainzof M, Zatz M. Apparent association of mental retardation and specific patterns of deletions screened with probes cf56a and cf23a in Duchenne muscular dystrophy. Am. J. Med. Genet. 1991; 39: 437–441.

Rau F, Lainé J, Ramanoudjame L, Ferry A, Arandel L, Delalande O, et al. Abnormal splicing switch of DMD's penultimate exon compromises muscle fibre maintenance in myotonic dystrophy. Nat. Commun. 2015; 6: 7205.

Relaix F, Zammit PS. Satellite cells are essential for skeletal muscle regeneration: the cell on the edge returns centre stage. Dev. Camb. Engl. 2012; 139: 2845–2856.

Rivier F, Robert A, Hugon G, Mornet D. Different utrophin and dystrophin properties related to their vascular smooth muscle distributions. FEBS Lett. 1997; 408: 94–98.

Roberts RG, Bobrow M. Dystrophins in Vertebrates and Invertebrates. Hum. Mol. Genet. 1998; 7: 589–595.

Rodríguez M, Cai W-J, Kostin S, Lucchesi BR, Schaper J. Ischemia depletes dystrophin and inhibits protein synthesis in the canine heart: mechanisms of myocardial ischemic injury. J. Mol. Cell. Cardiol. 2005; 38: 723–733.

Ruf-Zamojski F, Trivedi V, Fraser SE, Trinh LA. Spatio-Temporal Differences in Dystrophin Dynamics at mRNA and Protein Levels Revealed by a Novel FlipTrap Line. PloS One 2015; 10: e0128944.

Rybakova IN, Humston JL, Sonnemann KJ, Ervasti JM. Dystrophin and utrophin bind actin through distinct modes of contact. J. Biol. Chem. 2006; 281: 9996–10001.

Sacco P, Jones DA, Dick JR, Vrbová G. Contractile properties and susceptibility to exercise-induced damage of normal and mdx mouse tibialis anterior muscle. Clin. Sci. Lond. Engl. 1979 1992; 82: 227–236.

Sakamoto M, Yuasa K, Yoshimura M, Yokota T, Ikemoto T, Suzuki M, et al. Micro-dystrophin cDNA ameliorates dystrophic phenotypes when introduced into mdx mice as a transgene. Biochem. Biophys. Res. Commun. 2002; 293: 1265–1272.

Sanger F, Nicklen S, Coulson AR. DNA sequencing with chain-terminating inhibitors. Proc. Natl. Acad. Sci. U. S. A. 1977; 74: 5463–5467.

Sarig R, Mezger-Lallemand V, Gitelman I, Davis C, Fuchs O, Yaffe D, et al. Targeted inactivation of Dp71, the major non-muscle product of the DMD gene: differential activity of the Dp71 promoter during development. Hum. Mol. Genet. 1999; 8: 1–10.

Sasaki T, Giltay R, Talts U, Timpl R, Talts JF. Expression and distribution of laminin alpha1 and alpha2 chains in embryonic and adult mouse tissues: an immunochemical approach. Exp. Cell Res. 2002; 275: 185–199.

Schatzberg SJ, Anderson LVB, Wilton SD, Kornegay JN, Mann CJ, Solomon GG, et al. Alternative dystrophin gene transcripts in golden retriever muscular dystrophy. Muscle Nerve 1998; 21: 991–998.

Schiaffino S, Reggiani C. Fiber types in mammalian skeletal muscles. Physiol. Rev. 2011; 91: 1447–1531.

Schmidt WM, Uddin MH, Dysek S, Moser-Thier K, Pirker C, Höger H, et al. DNA Damage, Somatic Aneuploidy, and Malignant Sarcoma Susceptibility in Muscular Dystrophies [Internet]. PLoS Genet. 2011; 7[cited 2015 Nov 14] Available from: http://www.ncbi.nlm.nih.gov/pmc/articles/PMC3077392/

Schmitz F, Drenckhahn D. Dystrophin in the retina. Prog. Neurobiol. 1997; 53: 547–560.

Schofield JN, Blake DJ, Simmons C, Morris GE, Tinsley JM, Davies KE, et al. Apo-dystrophin-1 and apo-dystrophin-2, products of the Duchenne muscular dystrophy locus: expression during mouse embryogenesis and in cultured cell lines. Hum. Mol. Genet. 1994; 3: 1309–1316.

Schöler HR, Hatzopoulos AK, Balling R, Suzuki N, Gruss P. A family of octamer-specific proteins present during mouse embryogenesis: evidence for germline-specific expression of an Oct factor. EMBO J. 1989; 8: 2543–2550.

Schoonjans L, Kreemers V, Danloy S, Moreadith RW, Laroche Y, Collen D. Improved Generation of Germline-Competent Embryonic Stem Cell Lines from Inbred Mouse Strains. STEM CELLS 2003; 21: 90–97.

Schultz J, Hoffmuüller U, Krause G, Ashurst J, Macias MJ, Schmieder P, et al. Specific interactions between the syntrophin PDZ domain and voltage-gated sodium channels. Nat. Struct. Mol. Biol. 1998; 5: 19–24.

Schwenk F, Baron U, Rajewsky K. A cre-transgenic mouse strain for the ubiquitous deletion of loxP-flanked gene segments including deletion in germ cells. Nucleic Acids Res. 1995; 23: 5080–5081.

Sekiguchi M, Zushida K, Yoshida M, Maekawa M, Kamichi S, Yoshida M, et al. A deficit of brain dystrophin impairs specific amygdala GABAergic transmission and enhances defensive behaviour in mice. Brain 2009; 132: 124–135.

Sene A, Tadayoni R, Pannicke T, Wurm A, El Mathari B, Benard R, et al. Functional implication of Dp71 in osmoregulation and vascular permeability of the retina. PloS One 2009; 4: e7329.

Seto JT, Ramos JN, Muir L, Chamberlain JS, Odom GL. Gene replacement therapies for Duchenne muscular dystrophy using adeno-associated viral vectors. Curr. Gene Ther. 2012; 12: 139–151.

Sharan SK, Thomason LC, Kuznetsov SG, Court DL. Recombineering: a homologous recombination-based method of genetic engineering. Nat. Protoc. 2009; 4: 206–223.

Shavlakadze T, McGeachie J, Grounds MD. Delayed but excellent myogenic stem cell response of regenerating geriatric skeletal muscles in mice. Biogerontology 2009; 11: 363–376.

Shiao T, Fond A, Deng B, Wehling-Henricks M, Adams ME, Froehner SC, et al. Defects in neuromuscular junction structure in dystrophic muscle are corrected by expression of a NOS transgene in dystrophin-deficient muscles, but not in muscles lacking α- and β1-syntrophins. Hum. Mol. Genet. 2004; 13: 1873–1884.

Shiga K, Yoshioka H, Matsumiya T, Kimura I, Takeda S 'ichi, Imamura M. Zeta-sarcoglycan is a functional homologue of gamma-sarcoglycan in the formation of the sarcoglycan complex. Exp. Cell Res. 2006; 312: 2083–2092.

Shimomura O, Johnson FH, Saiga Y. Extraction, purification and properties of aequorin, a bioluminescent protein from the luminous hydromedusan, Aequorea. J. Cell. Comp. Physiol. 1962; 59: 223–239.

Sicinski P, Geng Y, Ryder-Cook AS, Barnard EA, Darlison MG, Barnard PJ. The molecular basis of muscular dystrophy in the mdx mouse: a point mutation. Science 1989; 244: 1578–1580.

Sironi M, Cagliani R, Pozzoli U, Bardoni A, Comi GP, Giorda R, et al. The dystrophin gene is alternatively spliced throughout its coding sequence. FEBS Lett. 2002; 517: 163–166.

Smithies O, Gregg RG, Boggs SS, Koralewski MA, Kucherlapati RS. Insertion of DNA sequences into the human chromosomal β-globin locus by homologous recombination. Nature 1985; 317: 230–234.

Snapp E. Design and Use of Fluorescent Fusion Proteins in Cell Biology. Curr. Protoc. Cell Biol. Editor. Board Juan Bonifacino Al 2005; CHAPTER: Unit–21.4.

Sotgia F, Lee H, Bedford MT, Petrucci T, Sudol M, Lisanti MP. Tyrosine phosphorylation of beta-dystroglycan at its WW domain binding motif, PPxY, recruits SH2 domain containing proteins. Biochemistry (Mosc.) 2001; 40: 14585–14592.

Sotgia F, Lee JK, Das K, Bedford M, Petrucci TC, Macioce P, et al. Caveolin-3 directly interacts with the C-terminal tail of beta -dystroglycan. Identification of a central WW-like domain within caveolin family members. J. Biol. Chem. 2000; 275: 38048–38058.

Spence HJ, Dhillon AS, James M, Winder SJ. Dystroglycan, a scaffold for the ERK-MAP kinase cascade. EMBO Rep. 2004; 5: 484–489.

Spencer MJ, Mellgren RL. Overexpression of a calpastatin transgene in mdx muscle reduces dystrophic pathology. Hum. Mol. Genet. 2002; 11: 2645–2655.

Stahl FW. Recombination in phage λ: one geneticist's historical perspective1. Gene 1998; 223: 95–102.

Stedman HH, Sweeney HL, Shrager JB, Maguire HC, Panettieri RA, Petrof B, et al. The mdx mouse diaphragm reproduces the degenerative changes of Duchenne muscular dystrophy. Nature 1991; 352: 536–539.

Stewart TA, Mintz B. Successive generations of mice produced from an established culture line of euploid teratocarcinoma cells. Proc. Natl. Acad. Sci. U. S. A. 1981; 78: 6314–6318.

Straub V, Bittner RE, Léger JJ, Voit T. Direct visualization of the dystrophin network on skeletal muscle fiber membrane. J. Cell Biol. 1992; 119: 1183–1191.

Takahashi M, Tanonaka K, Yoshida H, Koshimizu M, Daicho T, Oikawa R, et al. Possible involvement of calpain activation in pathogenesis of chronic heart failure after acute myocardial infarction. J. Cardiovasc. Pharmacol. 2006; 47: 413–421.

Thanh LT, Nguyen TM, Helliwell TR, Morris GE. Characterization of revertant muscle fibers in Duchenne muscular dystrophy, using exon-specific monoclonal antibodies against dystrophin. Am. J. Hum. Genet. 1995; 56: 725–731.

Thomas KR, Folger KR, Capecchi MR. High frequency targeting of genes to specific sites in the mammalian genome. Cell 1986; 44: 419–428.

Tinsley J, Deconinck N, Fisher R, Kahn D, Phelps S, Gillis JM, et al. Expression of full-length utrophin prevents muscular dystrophy in mdx mice. Nat. Med. 1998; 4: 1441–1444.

Tinsley JM, Fairclough RJ, Storer R, Wilkes FJ, Potter AC, Squire SE, et al. Daily Treatment with SMTC1100, a Novel Small Molecule Utrophin Upregulator, Dramatically Reduces the Dystrophic Symptoms in the mdx Mouse. PLoS ONE 2011; 6: e19189.

Tinsley JM, Potter AC, Phelps SR, Fisher R, Trickett JI, Davies KE. Amelioration of the dystrophic phenotype of mdx mice using a truncated utrophin transgene. Nature 1996; 384: 349–353.

Tinsley J, Robinson N, Wilson F, Horne G, Davies K. Future Clinical And Biomarker Development For SMT C1100, The First Utrophin Modulator To Enter Clinical Trials For Duchenne Muscular Dystrophy (DMD) (S6.004). Neurology 2014; 82: S6.004.

Tokarz SA, Duncan NM, Rash SM, Sadeghi A, Dewan AK, Pillers DA. Redefinition of dystrophin isoform distribution in mouse tissue by RT-PCR implies role in nonmuscle manifestations of duchenne muscular dystrophy. Mol. Genet. Metab. 1998; 65: 272–281.

Torelli S, Ferlini A, Obici L, Sewry C, Muntoni F. Expression, regulation and localisation of dystrophin isoforms in human foetal skeletal and cardiac muscle. Neuromuscul. Disord. NMD 1999; 9: 541–551.

Townsend D, Blankinship MJ, Allen JM, Gregorevic P, Chamberlain JS, Metzger JM. Systemic administration of micro-dystrophin restores cardiac geometry and prevents dobutamine-induced cardiac pump failure. Mol. Ther. J. Am. Soc. Gene Ther. 2007; 15: 1086–1092.

Toyo-Oka T, Takahashi M, Takeo S, Masui F, Kumagai H. Evidence that Activation of Endogenous Calpain is Responsible for the Pathogenesis of Ischemic Cardiomyopathy via Loss of Dystrophin and its Associated Proteins. J. Card. Fail. 2005; 11: S249.

Tremblay JP, Skuk D, Palmieri B, Rothstein DM. A Case for Immunosuppression for Myoblast Transplantation in Duchenne Muscular Dystrophy. Mol. Ther. 2009; 17: 1122–1124.

Turczyńska KM, Swärd K, Hien TT, Wohlfahrt J, Mattisson IY, Ekman M, et al. Regulation of smooth muscle dystrophin and synaptopodin 2 expression by actin polymerization and vascular injury. Arterioscler. Thromb. Vasc. Biol. 2015; 35: 1489–1497.

Uchino M, Teramoto H, Naoe H, Yoshioka K, Miike T, Ando M. Localisation and characterisation of dystrophin in the central nervous system of controls and patients with Duchenne muscular dystrophy. J. Neurol. Neurosurg. Psychiatry 1994; 57: 426–429.

Udan RS, Piazza VG, Hsu C, Hadjantonakis A-K, Dickinson ME. Quantitative imaging of cell dynamics in mouse embryos using light-sheet microscopy. Development 2014; 141: 4406–4414.

Vaillend C, Billard J-M. Facilitated CA1 hippocampal synaptic plasticity in dystrophin-deficient mice: role for GABAA receptors? Hippocampus 2002; 12: 713–717.

Vaillend C, Billard JM, Claudepierre T, Rendon A, Dutar P, Ungerer A. Spatial discrimination learning and CA1 hippocampal synaptic plasticity in mdx and mdx3cv mice lacking dystrophin gene products. Neuroscience 1998; 86: 53–66.

Vaillend C, Billard J-M, Laroche S. Impaired long-term spatial and recognition memory and enhanced CA1 hippocampal LTP in the dystrophin-deficient Dmd(mdx) mouse. Neurobiol. Dis. 2004; 17: 10–20.

Vaillend C, Rendon A, Misslin R, Ungerer A. Influence of dystrophin-gene mutation on mdx mouse behavior. I. Retention deficits at long delays in spontaneous alternation and bar-pressing tasks. Behav. Genet. 1995; 25: 569–579.

Vaillend C, Ungerer A, Billard JM. Facilitated NMDA receptor-mediated synaptic plasticity in the hippocampal CA1 area of dystrophin-deficient mice. Synap. N. Y. N 1999; 33: 59–70.

Vajda Z, Pedersen M, Füchtbauer E-M, Wertz K, Stødkilde-Jørgensen H, Sulyok E, et al. Delayed onset of brain edema and mislocalization of aquaporin-4 in dystrophin-null transgenic mice. Proc. Natl. Acad. Sci. U. S. A. 2002; 99: 13131–13136.

Voit T, Topaloglu H, Straub V, Muntoni F, Deconinck N, Campion G, et al. Safety and efficacy of drisapersen for the treatment of Duchenne muscular dystrophy (DEMAND II): an exploratory, randomised, placebo-controlled phase 2 study. Lancet Neurol. 2014; 13: 987–996.

Wagner EF, Stewart TA, Mintz B. The human beta-globin gene and a functional viral thymidine kinase gene in developing mice. Proc. Natl. Acad. Sci. U. S. A. 1981; 78: 5016–5020.

Wang H, Yang H, Shivalila CS, Dawlaty MM, Cheng AW, Zhang F, et al. One-step generation of mice carrying mutations in multiple genes by CRISPR/Cas-mediated genome engineering. Cell 2013; 153: 910–918.

Wang Z, Tapscott SJ, Chamberlain JS, Storb R. Immunity and AAV-Mediated Gene Therapy for Muscular Dystrophies in Large Animal Models and Human Trials. Front. Microbiol. 2011; 2: 201.

Warner LE, DelloRusso C, Crawford RW, Rybakova IN, Patel JR, Ervasti JM, et al. Expression of Dp260 in muscle tethers the actin cytoskeleton to the dystrophin–glycoprotein complex and partially prevents dystrophy. Hum. Mol. Genet. 2002; 11: 1095–1105.

Wasala NB, Zhang K, Wasala LP, Hakim CH, Duan D. The FVB Background Does Not Dramatically Alter the Dystrophic Phenotype of Mdx Mice. PLoS Curr. 2015; 7

Watkins SC, Hoffman EP, Slayter HS, Kunkel LM. Immunoelectron microscopic localization of dystrophin in myofibres. Nature 1988; 333: 863–866.

Wersinger E, Bordais A, Schwab Y, Sene A, Bénard R, Alunni V, et al. Reevaluation of Dystrophin Localization in the Mouse Retina. Investig. Opthalmology Vis. Sci. 2011; 52: 7901.

Williamson RA, Henry MD, Daniels KJ, Hrstka RF, Lee JC, Sunada Y, et al. Dystroglycan is essential for early embryonic development: disruption of Reichert's membrane in Dag1-null mice. Hum. Mol. Genet. 1997; 6: 831–841.

Williams RL, Hilton DJ, Pease S, Willson TA, Stewart CL, Gearing DP, et al. Myeloid leukaemia inhibitory factor maintains the developmental potential of embryonic stem cells. Nature 1988; 336: 684–687.

Wilton SD, Dye DE, Blechynden LM, Laing NG. Revertant fibres: a possible genetic therapy for Duchenne muscular dystrophy? Neuromuscul. Disord. 1997; 7: 329–335.

Wilton SD, Dye DE, Laing NG. DYSTROPHIN GENE TRANSCRIPTS SKIPPING THE mdx MUTATION. Muscle Nerve 1997; 20: 728–34.

Winder SJ. The complexities of dystroglycan. Trends Biochem. Sci. 2001; 26: 118–124.

Winkelmann JC, Costa FF, Linzie BL, Forget BG. Beta spectrin in human skeletal muscle. Tissue-specific differential processing of 3' beta spectrin pre-mRNA generates a beta spectrin isoform with a unique carboxyl terminus. J. Biol. Chem. 1990; 265: 20449–20454.

Worton R. Muscular dystrophies: diseases of the dystrophin-glycoprotein complex. Science 1995; 270: 755–756.

Wu B, Lu P, Cloer C, Shaban M, Grewal S, Milazi S, et al. Long-term rescue of dystrophin expression and improvement in muscle pathology and function in dystrophic mdx mice by peptide-conjugated morpholino. Am. J. Pathol. 2012; 181: 392–400.

Yablonka-Reuveni Z. The skeletal muscle satellite cell: still young and fascinating at 50. J. Histochem. Cytochem. Off. J. Histochem. Soc. 2011; 59: 1041–1059.

Yablonka-Reuveni Z, Seger R, Rivera AJ. Fibroblast Growth Factor Promotes Recruitment of Skeletal Muscle Satellite Cells in Young and Old Rats. J. Histochem. Cytochem. 1999; 47: 23–42.

Yamakawa H, Oyama S, Mitsuhashi H, Sasagawa N, Uchino S, Kohsaka S, et al. Neuroligins 3 and 4X interact with syntrophin-gamma2, and the interactions are affected by autism-related mutations. Biochem. Biophys. Res. Commun. 2007; 355: 41–46.

Yang B, Jung D, Motto D, Meyer J, Koretzky G, Campbell KP. SH3 Domain-mediated Interaction of Dystroglycan and Grb2. J. Biol. Chem. 1995; 270: 11711–11714.

Yang F, Moss LG, Phillips Jr. GN. The molecular structure of green fluorescent protein. Nat.Biotechnol. 1996; 14: 1246–1251.

Yasuda S, Townsend D, Michele DE, Favre EG, Day SM, Metzger JM. Dystrophic heart failure blocked by membrane sealant poloxamer. Nature 2005; 436: 1025–1029.

Yokota T, Duddy W, Partridge T. Optimizing exon skipping therapies for DMD. Acta Myol. 2007; 26: 179.

Yokota T, Lu Q-L, Morgan JE, Davies KE, Fisher R, Takeda S 'ichi, et al. Expansion of revertant fibers in dystrophic mdx muscles reflects activity of muscle precursor cells and serves as an index of muscle regeneration. J. Cell Sci. 2006; 119: 2679–2687.

Yokota T, Lu Q-L, Partridge T, Kobayashi M, Nakamura A, Takeda S, et al. Efficacy of systemic morpholino exon-skipping in Duchenne dystrophy dogs. Ann. Neurol. 2009; 65: 667–676.

Yoon JH, Johnson E, Xu R, Martin LT, Martin PT, Montanaro F. Comparative proteomic profiling of dystroglycan-associated proteins in wild type, mdx and Galgt2 transgenic mouse skeletal muscle. J. Proteome Res. 2012; 11: 4413–4424.

Yoshida-Moriguchi T, Yu L, Stalnaker SH, Davis S, Kunz S, Madson M, et al. O-mannosyl phosphorylation of alpha-dystroglycan is required for laminin binding. Science 2010; 327: 88–92.

Yoshida T, Pan Y, Hanada H, Iwata Y, Shigekawa M. Bidirectional signaling between sarcoglycans and the integrin adhesion system in cultured L6 myocytes. J. Biol. Chem. 1998; 273: 1583–1590.

Yoshioka M, Okuno T, Honda Y, Nakano Y. Central nervous system involvement in progressive muscular dystrophy. Arch. Dis. Child. 1980; 55: 589–594.

Zacharias DA, Violin JD, Newton AC, Tsien RY. Partitioning of lipid-modified monomeric GFPs into membrane microdomains of live cells. Science 2002; 296: 913–916.

Zammit PS, Partridge TA, Yablonka-Reuveni Z. The skeletal muscle satellite cell: the stem cell that came in from the cold. J. Histochem. Cytochem. Off. J. Histochem. Soc. 2006; 54: 1177–1191.

Zatz M, Starling A. Calpains and disease. N. Engl. J. Med. 2005; 352: 2413–2423.

Zellweger H, Niedermeyer E. Central nervous system manifestations in childhood muscular dystrophy (CMD). I. Psychometric and electroencephalographic findings. Ann. Paediatr. Int. Rev. Pediatr. 1965; 205: 25–42.

Zhang Y, Buchholz F, Muyrers JP, Stewart AF. A new logic for DNA engineering using recombination in Escherichia coli. Nat. Genet. 1998; 20: 123–128.

Zimprich A, Grabowski M, Asmus F, Naumann M, Berg D, Bertram M, et al. Mutations in the gene encoding epsilon-sarcoglycan cause myoclonus-dystonia syndrome. Nat. Genet. 2001; 29: 66–69.

NCI at Frederick: Protocols [Internet]. [cited 2015 Sep 19] Available from: https://ncifrederick.cancer.gov/research/brb/protocol.aspx

10.   ABBREVIATIONS

Ab	antibody
ACh	acetylcholine
AChR	acetylcholine receptor
AQP4	aquaporin-4
ATP	adenosine triphosphate
Amp	ampicillin resistance
AONs	antisense oligonucleotides
BAC	bacterial artificial chromosome
BMD	Becker muscular dystrophy
bp	base pair
BS	blocking solution
BSA	bovine serum albumin
α-BTX	α-bungarotoxin
cM	centiMorgan
CIP	calf intestine phosphatase
CNS	central nervous system
Cre	Cre-recombinase
Da	Dalton
dH$_2$O	distilled water
DAPC	dystrophin associated protein complex
DIA	diaphragm
DMD	Duchenne muscular dystrophy
DMEM	Dulbecco' s modified Eagle Medium
DMSO	dimethyl sulfoxide
DNA	deoxyribonucleic acid
dNTP	deoxynucleoside triphosphate
ECM	extracellular matrix
EDL	*extensor digitorum longus*
EGFP	enhanced green fluorescent protein
ES cells	embryonic stem cells
for	forward
FRET	fluorescence resonance energy transfer
GABA	γ-aminobutyric acid receptors
GABA$_A$-R	γ-aminobutyric acid A receptors
GAS	*gastrocnemius*
GFP	green fluorescent protein
Grb2	growth factor receptor-bound protein 2
HA	homology arm
H&E	haematoxylin/eosin
HS	horse serum
IF	immunofluorescence
Ig	immunoglobulin
IHC	immunohistochemistry
ILM	inner limiting membrane
INL	Inner nuclear layer
K$^+$	potassium ion
kb	kilo base
kDa	kilo Dalton
Kir4.1	inward rectifier K$^+$ channel-4.1

LIF	leukemia inhibition factor
lox*P*- site	locus of crossing over-site
Mb	mega base pairs
mdx	murine dystrophy X-linked
mRNA	messenger ribonucleic acid
MW	molecular weight
neo	neomycin
NMJ	neuromuscular junction
NO	nitric oxide
nNOS	neuronal nitric oxide synthase
2'OMe-PS	2'-O-methyl phosphorothioate
OPL	outer plexiform layer
Pax7	paired box 7 protein
PBS	phosphate buffered saline
PCR	polymerase chain reaction
PDZ domain	PSD-95, disc-large and ZO-1 domain
PFA	paraformaldehyde
PH	plekstrin homology
PMO	phosphorodiamidate morpholino oligomer
PSD	postsynaptic densities
PSD-95	postsynaptic protein 95
QUAD	*quadriceps*
rev	reverse
SAP	shrimp alkaline phosphatase
SAPK	stress-activated protein kinases
SB	Southern blot
SOL	*soleus*
TA	*tibialis anterior*
Taq	*Thermus acquaticus*
tc-DNA	tricyclo-DNA
TBS	tris buffered saline
Tris	tris(hydroxymethyl)-aminomethane
U	unit
UTR	untranslated region
WB	Western blot
WT	wildtype
ZO-1	zonula occludens-1

11.   LIST OF FIGURES

12.   LIST OF TABLES

Table 1: Plastic material for tissue culture and molecular biology 36

Table 2: Instruments and equipment for molecular biological work 37

Table 3: Instruments and equipment for tissue culture work..38

Table 4: Instruments and equipment for histological work 38

Table 5: Chemicals 38

Table 6: Kits...40

Table 7: Standard markers..40

Table 8: Enzymes..40

Table 9: Nucleotides 40

Table 10: Plasmids 41

Table 11: Bacteria 41

Table 12: Cell lines, primary murine cells and media used for culturing 42

Table 13: Mouse strains...42

Table 14: Software 42
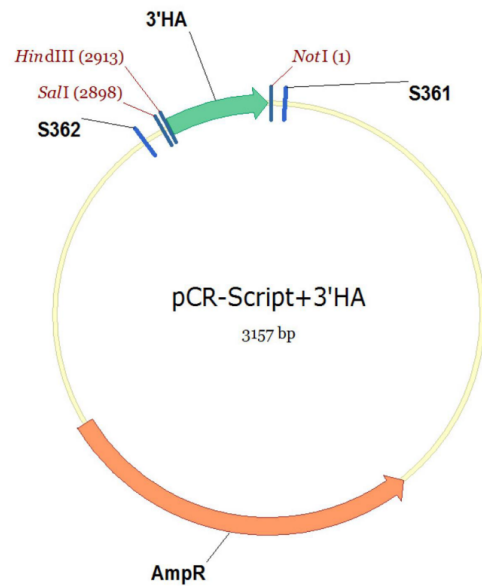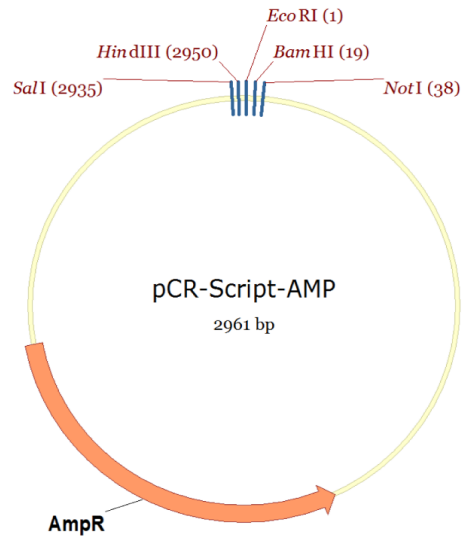
139

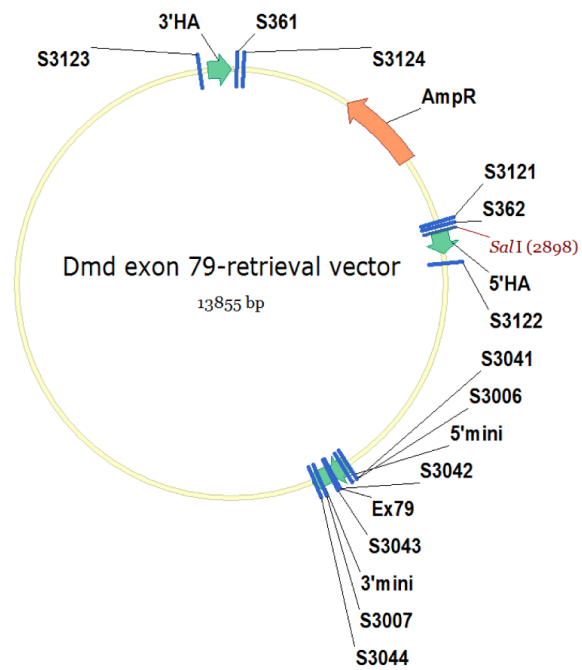## 13. APPENDIX

13.1. List of primers
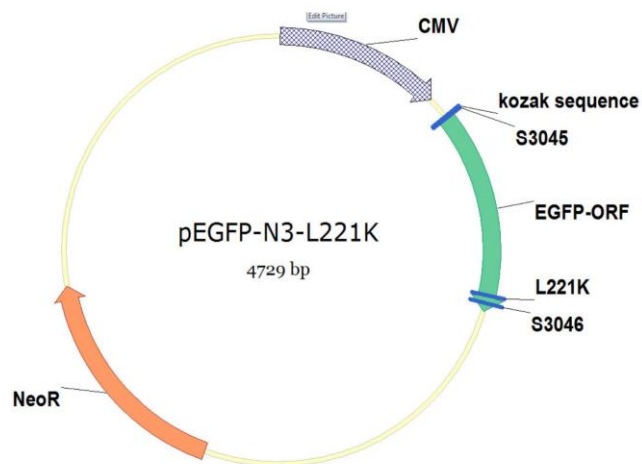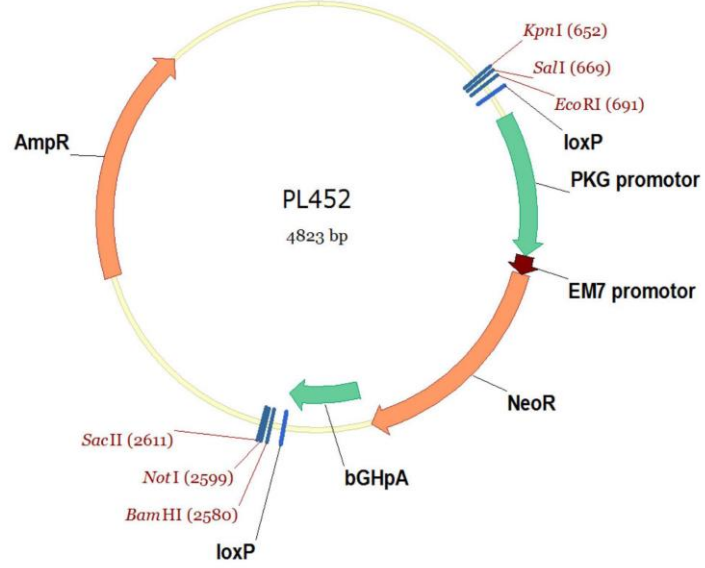
Table A1: List of primers

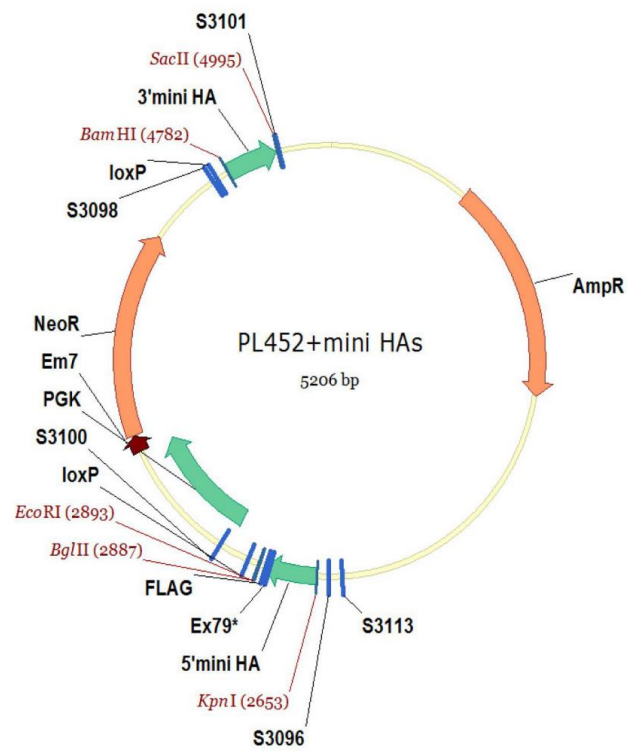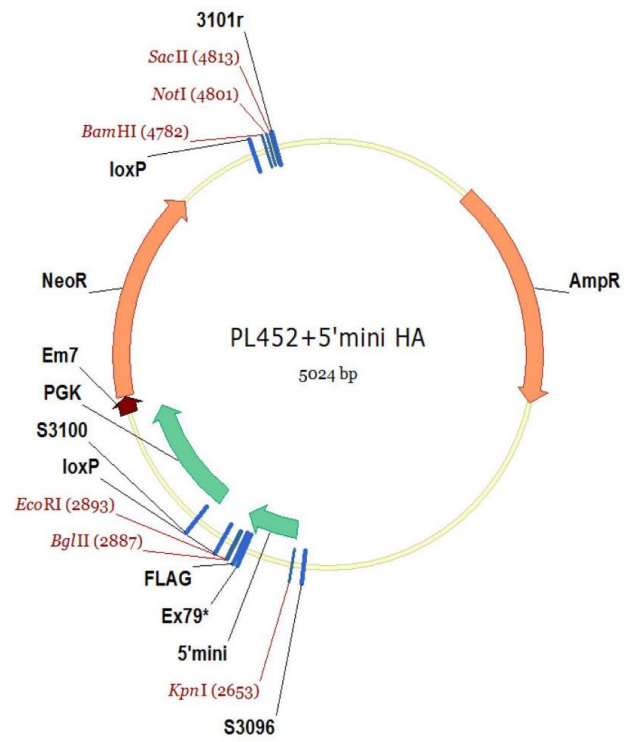| Primer name	for/rev	Sequence 5'->3'	Application
S361	rev	AATTAACCCTCACTAAAGGG	Verification of correct cloning of HAs in PCR-Script
S362	for	GTAATACGACTCACTATAGGGC	Verification of cloning of HAs in PCR-Script Verification of cloning of EGFP into pGEM-Teasy
S395	rev	ATTTAGGTGACACTATAGAATACT	Verification of cloning of EGFP into pGEM-Teasy
S745	rev	CGTCGCCGTCCAGCTCGACCAG	Verification of of EGFP into PL452+mini HAs; Sequencing
S1240	for	GGAGGACTGCAGGACACAATGTTGG AAGCCGATTA	Exon 79*-FLAG-EGFP for cloning into pCMV-3Ataq
S1241	rev	GGAGGAAAGCTTTTACTTGTACAGCT CGTCCATGC	Exon 79*-FLAG-EGFP for cloning into pCMV-3Ataq
S3033	for	GTTGGAGCTCGAGACAAAGG	Amplification of 5'Hybridization probe for cloning into pGEM-T easy
S3034	rev	TCAAGTTTGCCATTCAGTCG	Amplification of 5'Hybridization probe for cloning into pGEM-T easy
S3035	for	TAGCCCCTTTACCTGTGTGG	Amplification of 3'Hybridization probe for cloning into pGEM-T easy
S3036	rev	CTGAGTTCCTGTTTGCGTCA	Amplification of 3'Hybridization probe for cloning into pGEM-T easy
S3041	for	GGAGGAGGTACCCACCATGCAATGCT TCATTA	5'mini HA for cloning into for cloning into PL452
S3042	rev	GTCGAATTCAGATCTCTTATCGTCGTC ATCCTTGTAATCGGCTTCCAACATTGT GTCCTG	Amplification of 5'mini HA (PL452), primer contains modified Ex79* and FLAG sequence
S3043	for	GGAGGAGGATCCTTTTCCACATGGCA GATGA	Amplification of 3' mini HA for cloning into PL452
S3044	rev	GGAGGACCGCGGACAGTATAGTACC ACTACCCTTCACAA	Amplification of 3' mini HA for cloning into PL452
S3045	for	GGAGGAGAATTCATGGTGAGCAAGG GCGAGGA	mEGFP amplification for cloning into PL452+mini HAs
S3046	rev	GGAGGAGAATTCTTACTTGTACAGCT CGTCCATGCCGAGAG	mEGFP amplification for cloning into PL452
S3096	for	ACGCCAAGCTCGAAATTAAC	Verification of 5'mini arm in PL452, Sequencing
S3098	for	GAGCTTGCGGAACCCTTAAT	Verification of 3'mini arm in PL452
S3100	rev	CTAAAGCGCATGCTCCAGAC	Verification of 5'mini arm in PL452, Sequencing
S3101	rev	TCACTATAGGGCGAATTGGA	Verification of 3'mini arm in PL452
S3113	for	GTGGAATTGTGAGCGGATA	Verification of cloning of EGFP into PL452+mini HAs; Sequencing
S3114	for	GACGTAAACGGCCACAAGT	Verification of cloning of EGFP into PL452+mini HAs; Sequencing
S3115	for	ATCCGCCACAACATCGAG	Verification of cloning of EGFP into PL452+mini HAs Sequencing
S3121	for	GTTTTCCCAGTCACGACGTT	Verification of recombineering of genomic *Dmd* exon 79 fragment into PCR-HAs (Retrieval vector), 5'site
S3122	rev	GGGGGTACAGTGAGGTCATTA	Verification of recombineering of genomic *Dmd* exon 79 fragment into PCR-HAs (Retrieval vector), 5'site

S3123	*for*	TTGGGAGTAGCCAACTGAGG	Verification of recombineering of genomic *Dmd* exon 79 fragment into PCR-HAs (Retrieval vector), 3'site
S3124	*rev*	TGTGGAATTGTGAGCGGATA	Verification of recombineering of genomic *Dmd* exon 79 fragment into PCR-HAs (Retrieval vector), 3'site
S3248	*for*	TCTCCCCATCAAATGACACC	Verification of recombineering of mini targeting cassette into retrieval vector (Targeting vector); Sequencing
S3249	*rev*	AAACAACCCAAAATGCGTTC	Verification of recombineering of mini targeting cassette on retrieval vector; Sequencing
S3255	*for*	GGAGGACTGCAGGACACAATGTTGG AAGCCGATTA	exon79*-FLAG-EGFP amplification for cloning into pCMV-3Ataq
S3256	*rev*	GGAGGAAAGCTTTTACTTGTACAGCT CGTCCATGC	exon79*-FLAG-EGFP amplification for cloning into pCMV-tag3A
S3257	*for*	GGAGGAGGATCCCATGTCTGTCCTGA CGCCACT	Cox8a amplification for cloning into pCMV-tag-3A
S3258	*rev*	GGAGGACTGCAGCTCCCGCGCCGGCT TCGAGT	Cox8a amplification for cloning into pCMV-tag-3A
S4228	*for*	GACTCCCAATAGTGGCAACC	Genotyping *Dmd*^{EGFP} mice
S4229	*rev*	CCATGCGGGAATCAGGAGTT	Genotyping *Dmd*^{EGFP} mice
S4269	*for*	GAGCAAAGACCCCAACGAGA	Genotyping *Dmd*^{EGFP} mice
Neo3f	*for*	CAAGCTCTTCAGCAATATCACGGG	Genotyping *Dmd*^{EGFP-Neo} mice
Neo3r	*rev*	CCTGTCCGGTGCCCTGAATGAACT	Genotyping *Dmd*^{EGFP-Neo} mice

13.2. Plasmid maps

PL452
4823 bp

*Kpn*I (652)
*Sal*I (669)
*Eco*RI (691)
loxP
PKG promotor
EM7 promotor
NeoR
bGHpA
loxP
*Sac*II (2611)
*Not*I (2599)
*Bam*HI (2580)
AmpR

pEGFP-N3-L221K
4729 bp

CMV
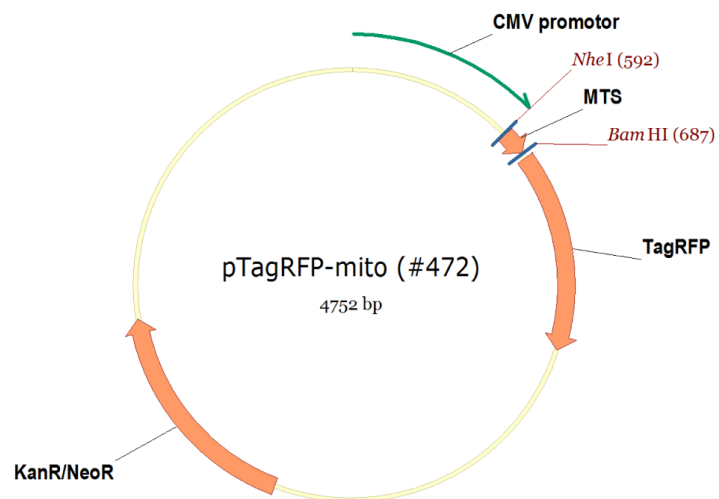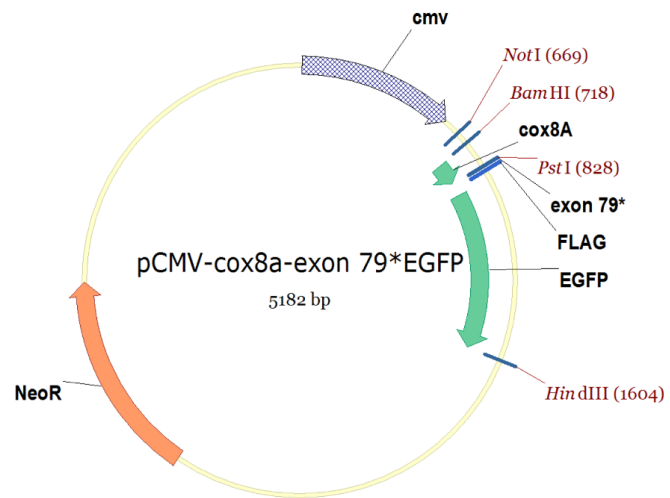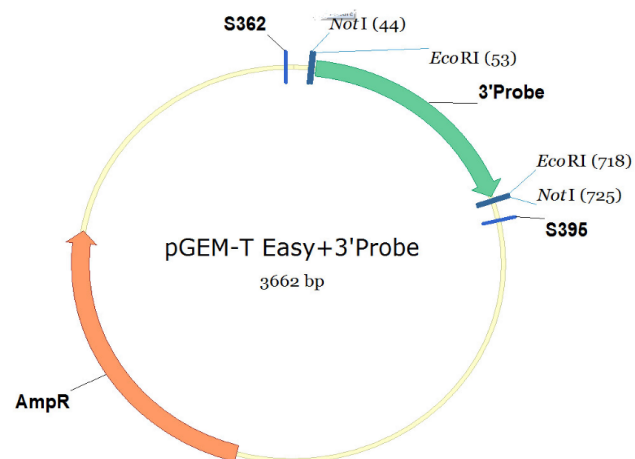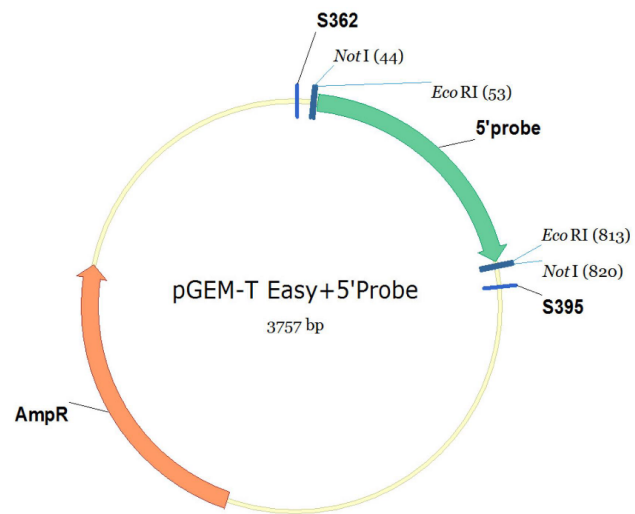kozak sequence
S3045
EGFP-ORF
L221K
S3046
NeoR

144
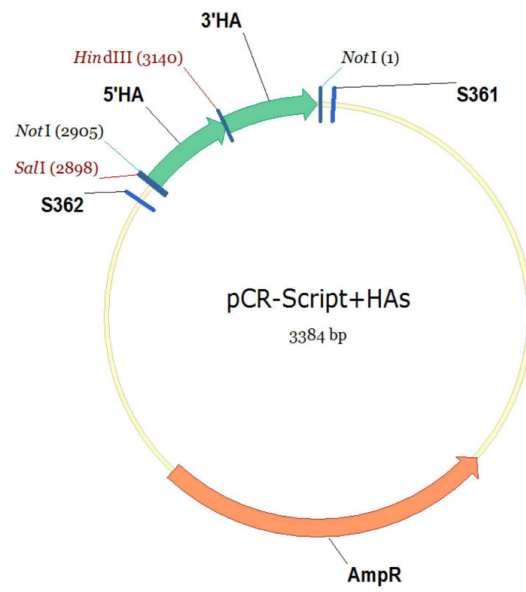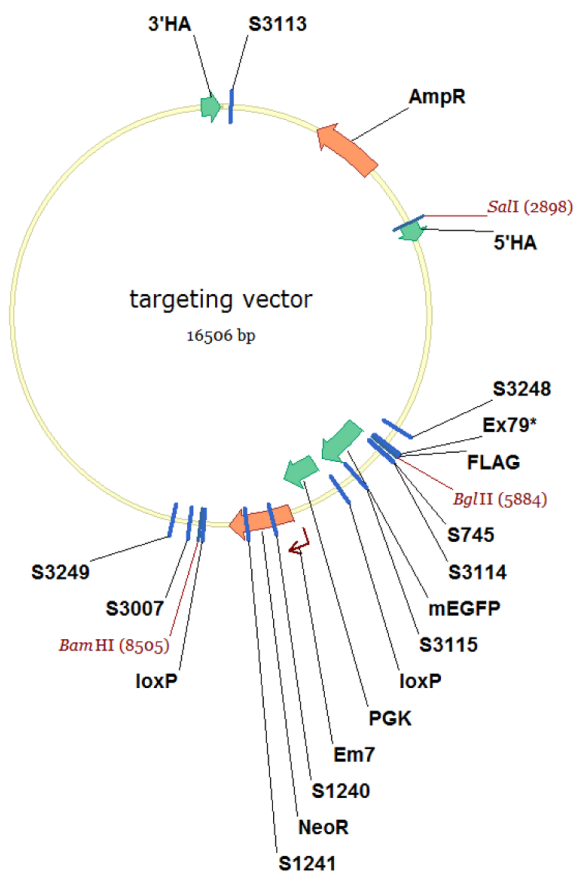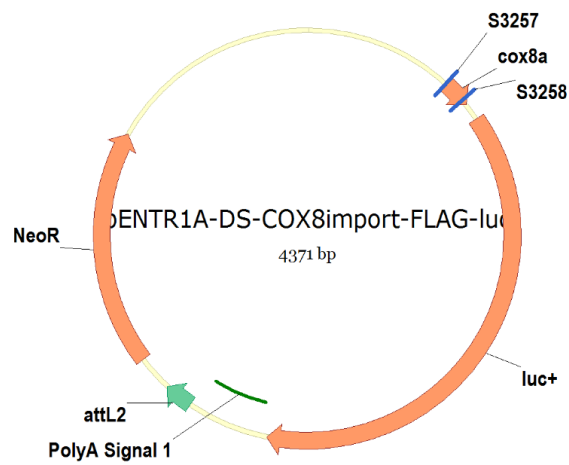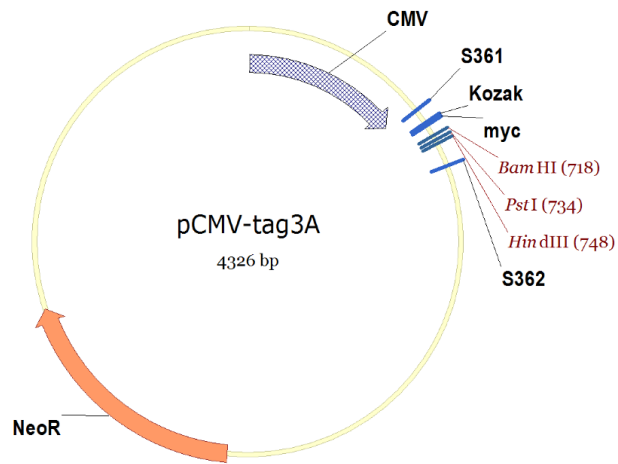
Figure A1: Plasmidmaps
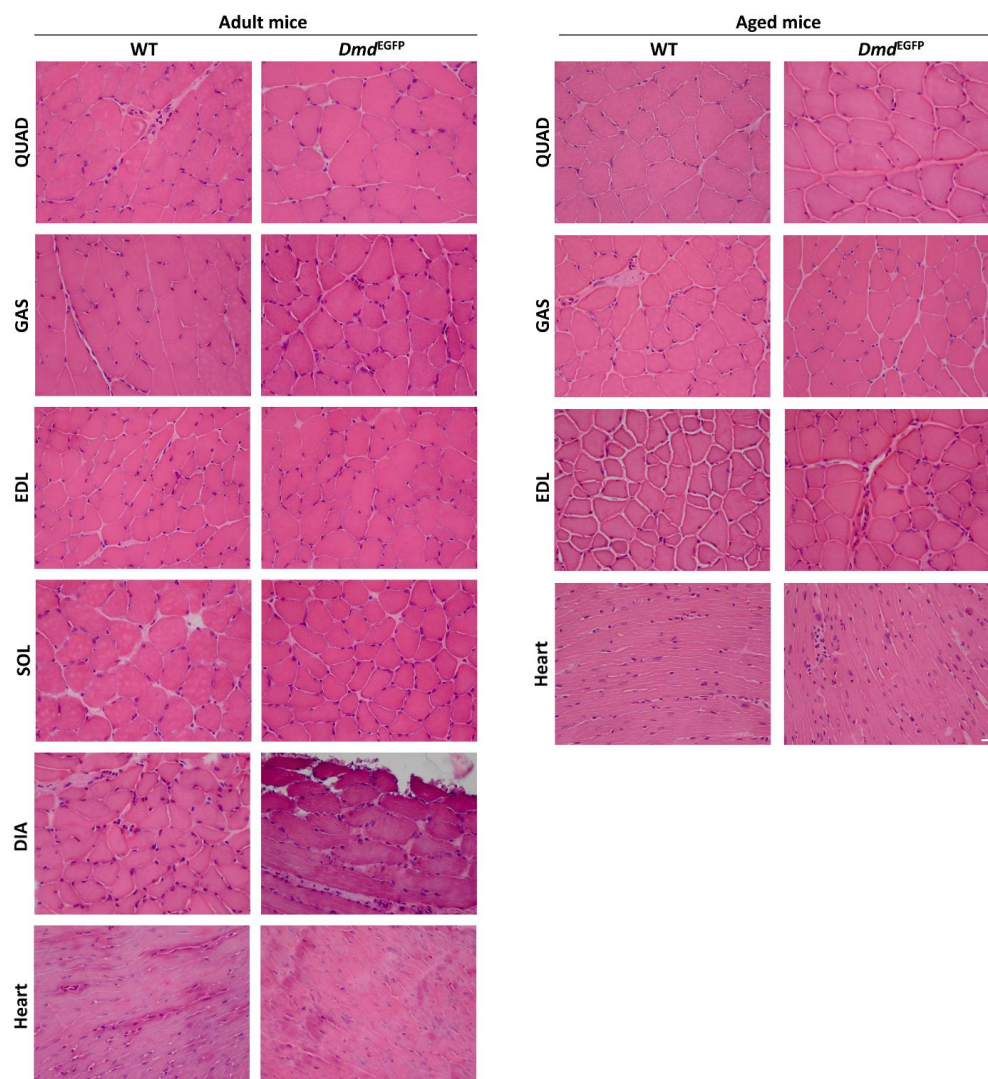
13.3. H&E staining of skeletal and heart muscles

Figure A2: H&E staining of skeletal and heart muscle of adult and aged wildtype (WT) and *Dmd*EGFP mice.
Skeletal muscles *quadriceps* (QUAD), *gastrocnemius* (GAS), *extensor digitorum longus* (EDL), *soleus* (SOL), diaphragm (DIA) and heart muscle from adult wildtype and transgenic mice show normal morphology with consistency in fiber caliber and no evidence of central nuclei. No further changes are observed in aged mice in the QUAD, GAS, EDL and heart muscle. Scale bar = 20 μm.

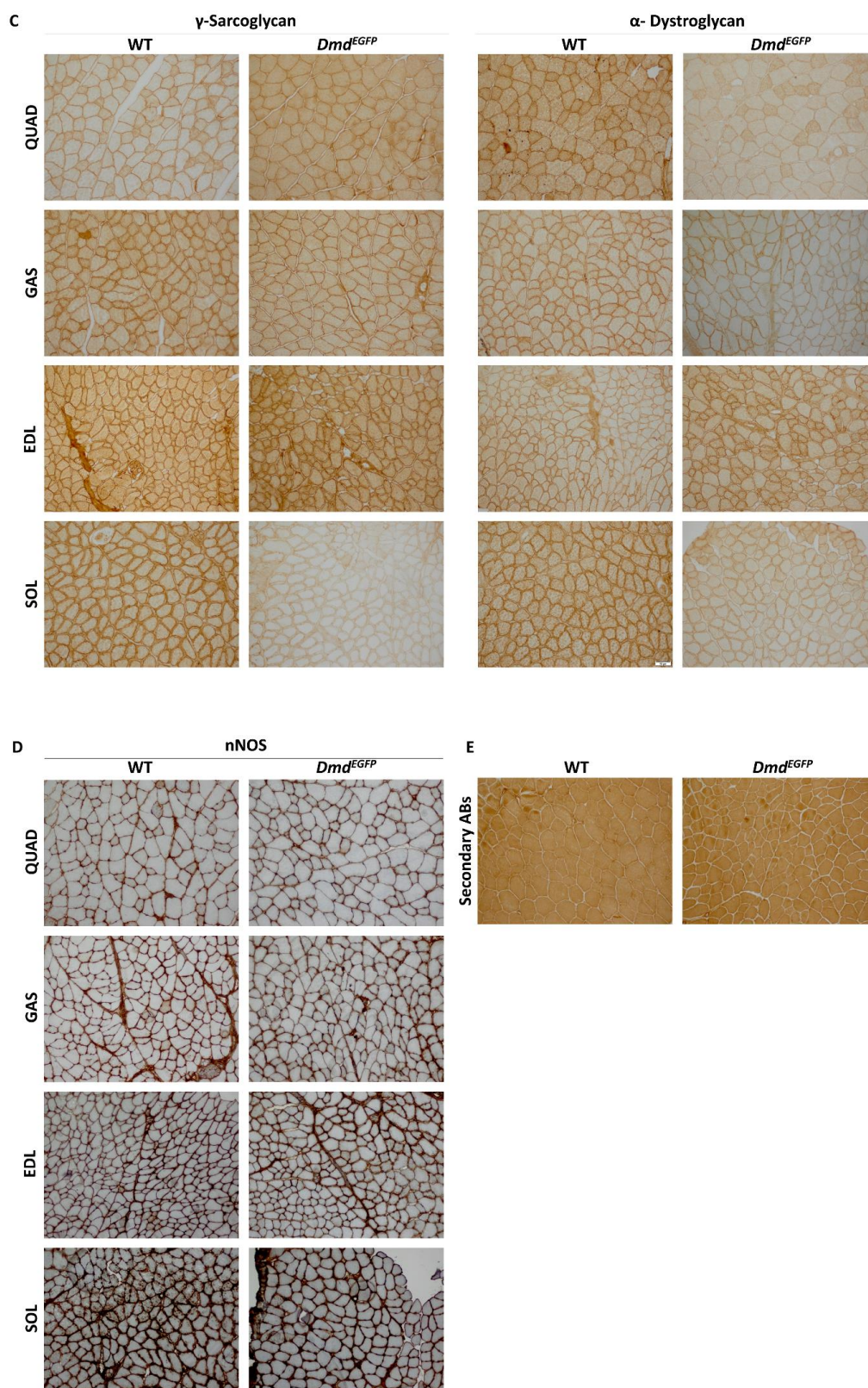## 13.4. IHC of skeletal muscle sections

B
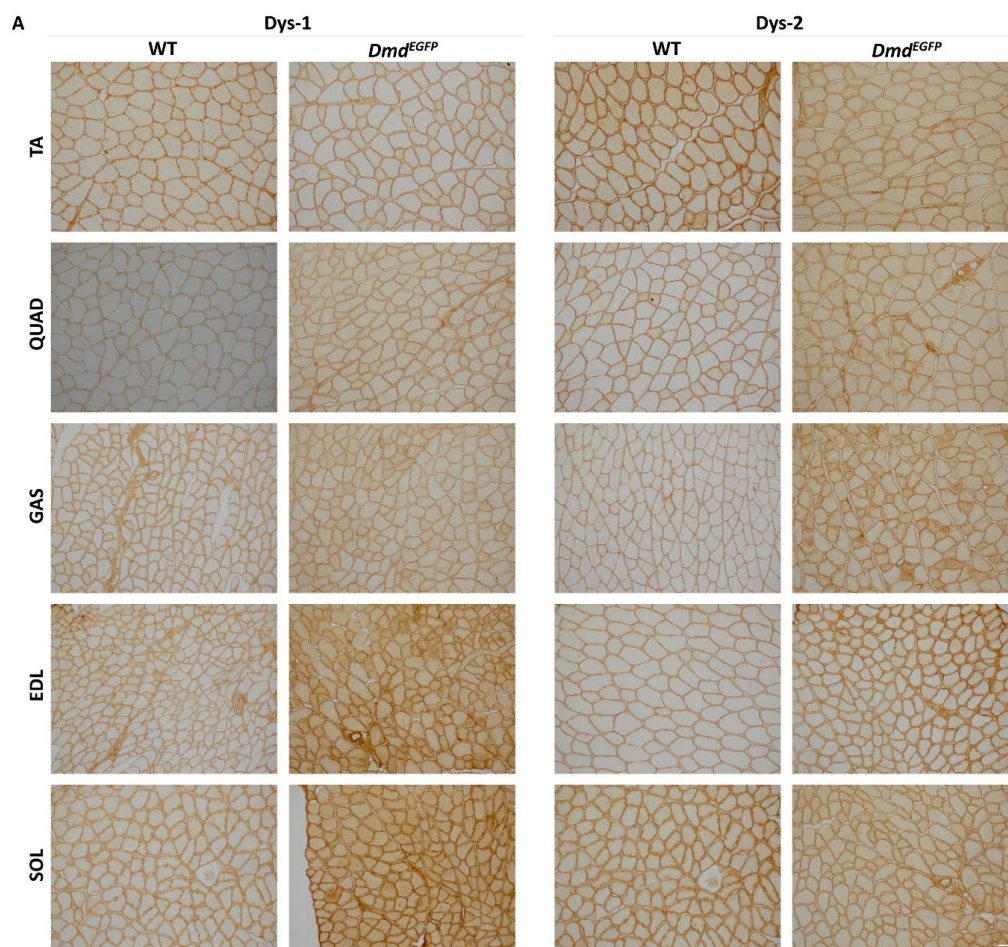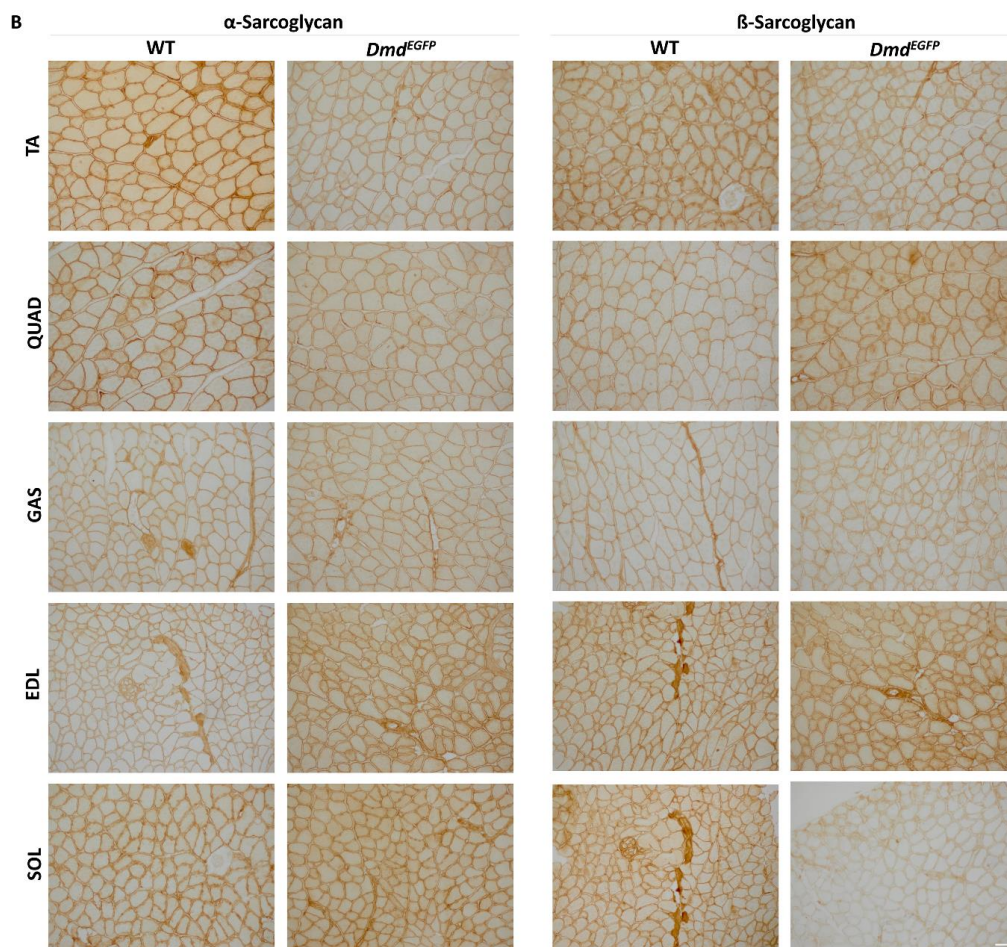
Figure A3: Immunohistochemistry of skeletal muscles of wildtype (WT) and *Dmd^EGFP* mice. Normal sarcolemmal expression of dystrophin, C-terminal (Dys2) and rod domain (Dys1) **(A),** α- ,β- Sarcoglycan **(B),** γ-Sarcoglycan, α-Dystroglycan **(C)**, nNOS **(D)** can be observed in following skeletal muscles *gastrocnemius (GAS), soleus* (SOL), *tibialis anterior* (TA), *quadriceps* (QUAD) and *extensor digitorum longus* (EDL). Staining of a TA section only with secondary anti-mouse antibodies using the MOM kit shows no background **(E).** Scale bar = 50 μm. AB: antibody.

13.5. Dilution of antibodies used

Table A2: Primary antibodies

Antigen	Isotype	Clone	Species reactivity	WB	IF	IHC	Supplier
α-actinin-2	Rabbit IgG		Human, mouse, chicken, cow	1:2000			Abcam, UK
α –bungarotoxin-CF™568					1:500		Biotium, Hayward, CA, USA
α-dystroglycan	Mouse IgM	IIH6C4	Human, guinea pig, canine, rabbit, mouse, rat			1:10	Millipore, Darmstadt, Germany
CD31	Rabbit IgG		mouse, human, pig		1:25		Abcam, UK
dystrophin, C-terminal	Rabbit IgG		Mouse, rat, human		1:100		Thermoscientific, Wuppertal, Germany
Dystrophin, rod domain (Dys1)	Mouse IgG2a	Dy4/6D3	Human, mouse, rat, rabbit, dog, chicken and hamster	1:100 1:50		1:10	Novocastra/Leica, Wetzlar, Germany
Dystrophin, C-terminal (Dys2)	Mouse IgG1	Dy8/6C5		1:100	1:10	1:10	Novocastra/Leica, Wetzlar, Germany
dystrophin, C-terminal (H4)	Mouse IgG1			1:200			gift from Cyrille Vailland
dystrophin, rod-domain (MANDYS19)	Mouse IgG1	86F	Human, mouse		1:10		DSHB, IO, USA
FLAG	Rabbit IgG						Sigma-Aldrich, Taufenkirchen, Germany
GFAP	Mouse IgG1		Pig, rat, human		1:400		Sigma-Aldrich, Taufenkirchen, Germany
GFP	Mouse IgG1	7.1 and 13.1		1:1000	1:500		Roche, Grenzach-Wyhlen, Germany
laminin	Rabbit IgG				1:500		Sigma-Aldrich, Taufenkirchen, Germany
nNOS	Rabbit IgG		Human, rat, mouse			1:1000	Upstate/ Millipore, Darmstadt, Germany
α-sarcoglycan	Mouse IgG1	Ad1/20A6	Human, mouse			1:100	Novocastra, Leica, Wetzlar, Germany

β-sarcoglycan	Mouse IgG1	β-Sarc/5B1	Human, mouse			1:100	Novocastra Leica, Wetzlar, Germany
γ-sarcoglycan	Mouse IgG2b, kappa	35DAG/21B5	Human, mouse			1:100	Novocastra Leica, Wetzlar, Germany
β-spectrin	Mouse IgG1	RBC1/5B1	Human, rat mouse rabbit		1:25		Novocastra Leica, Wetzlar, Germany
utrophin	Mouse IgG1	DRP3/20C5	Human rat dog		1:10		Novocastra Leica, Wetzlar, Germany
vinculin	Mouse IgG1		Mouse, rat, hamster, human	1:10000			Abcam, UK

Table A3: Secondary antibodies

Antigen	Conjugate	WB	IF	IHC	Supplier
Goat-α-mouse IgG	HRP	1:2000		1:2000	Calbiochem/Merck, Darmstadt, Germany
Goat-α-mouse IgG1	Alexa-488		1:400		LifeTechnologies, Darmstadt, Germany
Goat-α-mouse IgG1	Alexa-568		1:400		LifeTechnologies, Darmstadt, Germany
Goat-α-mouse IgG	Alexa-700	1:2000			LifeTechnologies, Darmstadt, Germany
Goat-α-rabbit IgG	HRP	1:2000		1:2000	Calbiochem/Merck, Darmstadt, Germany
Goat-α-rabbit IgG	Alexa-568		1:400		LifeTechnologies, Darmstadt, Germany
Goat-α-rabbit IgG	Alexa-800	1:2000			LifeTechnologies, Darmstadt, Germany